$\mathcal{O}\alpha_s^1$ and $\mathcal{O}\alpha_s^2$ RADIATIVE CORRECTIONS FOR W-BOSON PRODUCTION AT THE TEVATRON AND ATLAS EXPERIMENT

by

Matthew Teel, B.S.

THESIS

Presented to the Faculty of

The University of Houston-Clear Lake

In Partial Fulfillment

Of the Requirements

For the Degree

MASTER OF SCIENCE

in Physics

THE UNIVERSITY OF HOUSTON-CLEAR LAKE

MAY, 2022

$\mathcal{O}\alpha_s^1$ and $\mathcal{O}\alpha_s^2$ RADIATIVE CORRECTIONS FOR W-BOSON PRODUCTION AT THE TEVATRON AND ATLAS EXPERIMENT

by

Matthew Teel

APPROVED BY

_____

Samina Masood, Ph.D, Chair

_____

David Garrison, Ph.D, Committee Member

_____

Paul Withey, Ph.D, Committee Member

APPROVED/RECEIVED BY THE COLLEGE OF SCIENCE AND ENGINEERING:

_____

David Garrison, Ph.D.

Interim Associate Dean

_____

Miguel Gonzales, Ph.D.

Dean

Dedication

This is dedicated to my family and dearest friends, thesis committee, professors, and teachers and mentors alike. Your patience, unconditional love, generous support during downs and ups, inspiration and doubt, and times woven in failures and success have empowered expeditions through subject matters dear to my heart. I believe the pursuit of curiosity, with revelings amongst deeper consideration, accompanied by admiration toward beauty and awe, renders invariant our inner child-like wonder. And to acknowledge the universe for in some way managing an arrangement possible for self-examination.

Acknowledgements

I want to thank my advisor, Dr. Samina Masood, for her invaluable guidance, support, intuition, and wisdom. Additionally, for the occasional redirection during my stretches of chronic intellectual wander. I am grateful for the many insightful discussions along this path, I can say with confidence that this has been gratifying in both the pursuit of knowledge and life. Additionally, I would like to express my wealth of appreciation and gratitude toward the rest of the committee. I am indebted to the invaluable series of interactions and insights transpiring both through class and personal discussion. Thank you for the inspiration, wisdom, and perspective-shifting considerations. Moreover, I would like to give my appreciation for the guidance of Dr. Eric Van Mayes, who today is no longer with us, early on motivating and directing my intrigue toward the Standard Model and Quantum Field Theory, which I continue to build upon today.

ABSTRACT

$\mathcal{O}\alpha_s^1$ and $\mathcal{O}\alpha_s^2$ RADIATIVE CORRECTIONS FOR W-BOSON PRODUCTION AT THE TEVATRON AND ATLAS EXPERIMENT

Matthew Teel

University of Houston-Clear Lake, 2022

Thesis Chair: Samina Masood, PhD

In this thesis we propose an approach for calculating W-Boson Transverse Momentum Dependent (TMD) distributions using the LHAPDF library with nCTEQ15, MSTW2008 and CT10 Parton Distribution Functions (PDF). We utilize ManeParse as a PDF reader in the Mathematica framework for importing and computing relevant cross sections, luminosity functions and error analysis, and additionally allow cross check with a number of sum rules. A proper description of TMD distributions requires resummation of large logarithms responsible for divergence of the perturbation series in the strong coupling α_s. Our proposed calculation is for next-to-leading-order $(\mathcal{O}\alpha_s^1)$ and next-to-next-to-leading-order $(\mathcal{O}\alpha_s^2)$ large logarithmic perturbative corrections for the differential $W^{\pm}$ p_T partonic cross-sections for processes of the form $pp \to W^{\pm} + X$. The goal of large logarithmic corrections with threshold resummation is to improve accuracy of the p_T distribution thus reducing dependence of the cross-section on renormalization (μ_R) and factorization (μ_F) scales, and plays a role in Higgs searches, precision measurement of the W-boson mass, as well as for testing perturbative QCD.

Table of Contents

List of Figures

This is a general fact of life, in theoretical physics, when I use the word dumb, it is not a pejorative, dumb is good, okay, clever and ingenious is bad, dumb is good. And this is a deep fact about our field, when you're too clever and too ingenious, its you as a human being who's entering the fray, you as a human being suck, whats really great is the universe and the structure of the laws out there. You might go some distance because you're very clever and ingenious and smart, but trust me, youre nothing compared to the vast greatness of the laws that are out there, and at some point, your cleverness and ingenuity will fail you. That's not the point of physics, to be clever and ingenious, the point of physics is to discover simple and deep laws, and to exploit simple and deep laws, so simple and deep, and dumb is good. And you always learn something when you do the dumbest thing first, because 80% of the time it works, and 20% of the time it doesn't work, and you learn something very valuable, which is why the dumbest thing didn't work, so then you know what the second dumbest thing is, and typically you dont have to go past the second or third dumbest thing until something actually works…

-Nima Arkani-Hamed

Chapter 1

Introduction

Determining the underlying mechanism for the W-boson mass is essential in our understanding of the Standard Model (SM), as well as its validity. Implications surrounding ongoing efforts for a more precise measurement either extends our understanding, or breaks it entirely potentially revealing new physics and sending theoreticians back to the drawing board. Perturbation theory in QCD, being the theory of the strong interaction of the hadrons, becomes extremely limited in the light quark sector due to their nonperturbatively acquired mass as a consequence of spontaneous chiral symmetry breaking [1–3]. This manifests through quark (q) antiquark $(\overline{q})$ vacuum fluctuations [4]. In doing so, various conservation laws for the strong and electromagnetic interaction become spontaneously broken during weak decay processes. Furthermore, it is due to the weak interaction that stable matter contains up (u) and down (d) flavour quarks, whereas heavier quark families are energetically unfavorable. The $\pi^0 \rightarrow \gamma\gamma$ transition undergoes $SU(2)_L \otimes SU(2)_R$ chiral symmetry breaking in the electroweak sector of the SM in which we naively expect three resulting massless bosons in the process, however, long range vector fields present in the theory have identical quantum numbers as the otherwise would be observable Goldstone bosons [5]. The massless Goldstone bosons contribute additional longitudinal degrees of freedom rendering the vector fields massive [6, 7]. An introduction in name of brevity introduces a quadratic vector field for the Lagrangian density, $\mathcal{L}_M$,

$$\mathcal{L}_M = \frac{v^2}{8}\Big[(g_w W_\mu^3 - g_w^{'} B_\mu)(g_w W^{3\mu} - g_w^{'} B^\mu) + 2g^2 w W_\mu^- W^{+\mu}\Big] \tag{1.1}$$

where $g_W^{'}$ is the $U(1)$ gauge coupling, and g_W is the $SU(2)$ gauge coupling. The propagator for the B and W^3 fields are not diagonal, so new fields, A_μ, and Z_μ, are introduced to propagate independently

$$\begin{pmatrix} W_\mu^3 \\ B_\mu \end{pmatrix} = \begin{pmatrix} cos\theta_W & -sin\theta_W \\ sin\theta_W & cos\theta_W \end{pmatrix} \begin{pmatrix} Z_\mu \\ A_\mu \end{pmatrix}, \tag{1.2}$$

θ_W is the Weinberg electroweak mixing angle by which the spontaneous symmetry breaking process rotates the original W and B vector boson plane, thus producing the weak neutral current (nc), Z^0, and γ. θ_W becomes fixed by relative coupling strengths of the coupling constants, additionally, it is worth noting this value can vary slightly dependent on the particles momentum

$$sin^2\theta_W = \frac{g_W^{'}}{g_W^2 + g_{W^2}^{'}} \simeq 0.23. \tag{1.3}$$

We rotate the quadratic terms in the vector boson fields arriving at

$$\mathcal{L}_M = \frac{g_{W^{v^2}}^2}{4} W_\mu^+ W^{-\mu} + \frac{(g_W^2 + g_W^{'2})v^2}{8} Z_\mu Z^\mu, \tag{1.4}$$

and find that the W and Z bosons have acquired their masses

$$M_W = \frac{1}{2} v g_W, \tag{1.5}$$

with Z in terms of W

$$M_Z = \frac{1}{2} v \sqrt{g_W^2 + g_W^{'2}} \equiv \frac{M_W}{cos\theta_W}. \tag{1.6}$$

We additionally obtain the Fermi constant, G_F,

$$\frac{g_W^2}{8M_W^2} \equiv \frac{1}{2v^2} = \frac{G_F}{\sqrt{2}}, \tag{1.7}$$

$$G_F = 1.166x10^{-5} GeV^{-2},$$

which determines the coupling strength during the weak interaction [6].

Where v is the Higgs vacuum expectation value (vev) and

$$v^2 = \frac{1}{\sqrt{2}G_F}. \tag{1.8}$$

This implies the vev of the Higgs field, v, is 246 GeV, corresponding to the electroweak scale, while the Higgs mass is measured as 125.15 $\pm$0.17 GeV per the Particle Data Group (PDG) [8]. We can from here show W^+ coupling to quarks and leptons, this becomes relevant when calculating its cross section in chapters to come. The coupling

$$\delta Ł = \frac{g_w}{\sqrt{2}} W_\mu^- (\bar{d}\gamma^\mu P_L u + \bar{\ell}\gamma^\mu P_L \nu) + h.c., \tag{1.9}$$

where $P_L = \frac{1-\gamma^5}{2}$, is the left-handed projector, with g_w the gauge coupling, and $h.c.$ the hermitian conjugate. The W^- additionally is responsible for generating the W^+ field. The associated Goldstone longitudinal polarization vector fields are identified as the π^+, π^- and π^0, being responsible for mediating the Yukawa interaction during weak nuclear scale processes [6,7,9].

The pions are addressed in context of matrix elements representing intermediate states. This provides an opportunity for studying interplay between hard and soft QCD processes. Additionally, the $\pi^0 \to \gamma\gamma$ transition confirmed the colour structure of QCD, and its decay width is directly related to the mentioned chiral anomaly.

Starting with the QCD condensate, we can represent hadrons as interpolating currents and employ the operator product expansion (OPE) to separate long and short distance quark and gluon interactions. In *Drell-Yan* [10, 11] scattering processes at low energy, for example, the hadronic tensor $W_{\mu\nu}$ characterizes the non-perturbative nature of the long and short distance interplay. The results of the OPE become expressed as nucleon matrix elements with two current operators sandwiched to then become related structure functions. Relevant PDF's are extracted from the Dokshitser-Gribov-Lipatov-Altarelli-Parisi (DGLAP) evolution equations that will use these structures functions [12]. The $\mathcal{O}\alpha_s^1$ calculation serves to describe production of longitudinally polarized massive vector bosons plus a *jet*. Combining an extra parton gives a final state result which includes contributions from the $\mathcal{O}\alpha_s^1$ expression. To complicate things further, obtaining accurate measurement of the W mass requires knowledge of its p_T spectrum and requires a different approach. Calorimeter towers partially responsible for detecting events at hadron colliders register the contribution in the transverse plane of the center of mass collision region, $\sqrt{s}$, rather than pertinent information registering longitudinally down the beam pipe [13]. With more accurate measurements of the W mass the better we are able to constrain global electroweak parameters [14], thus further constraining CKM quark mixing matrix elements, and in turn helps to further constrain SM parameters. A review of the first calculations for the p_T W-hadroproduction cross section at $\mathcal{O}\alpha_s^1$ can be seen in [15, 16].

We can state with confidence, with the exception of what is partially known about the mass, that we have not yet been able to fully provide an explanation for any of the mentioned quantities from first principles. Why this fundamentally is the case is due to confinement [17]. Understanding QCD and confinement requires intensive study of the inner workings and structure of the nucleon. The gluons are massless, however the strong nuclear

force takes place at short range extending its influence $10^{-15}m$. The photons are massless with influence extending an infinite range. This proved quite puzzling early on. Consider simple wave mechanics, being that if all plane waves are traveling with the same velocity while exhibiting constructive interference behavior within a small region, their group velocity continues this behavior uniformly as the system evolves in time. The only varying parameter being spatial locations with respect to the group velocity. Varying mode velocities cause the wave packet to disperse. In a modern field theory context, the dispersion term represents mass. When considering a mass parameter, m, of a field in question, m determines its correlation length, $\eta \approx \frac{1}{m}$. The correlation length loosely speaking encodes how far a field can spread its influence [18]. It is suffice to say that gluon exchange by this criteria should be long range as well. However, this is not the case, and confinement is essential to explain why the nuclear force has the short range that it does [19]. The gluon is the gauge boson in QCD analogous with the electric charge in quantum electrodynamics (QED), except, in this case, the gluon consists of what is referred to as "colour" charge. Additionally, unlike QED, the gluon self interacts. A more accurate description being the eight resultant generators via spontaneously broken $SU(3) \otimes SU(3)$ gauge symmetry permute through r, g, and b available states The quark-gluon interaction transfers color charge from one quark to another, necessitating gluons carry two color indices, which are parameterized to rows and columns in the Gell-Mann matrices, seen in A.3, and will be addressed further in Chapter 2. The gluons mix in the adjoint representation of this $SU(3)_c$ gauge group, which is absorbed into the gluon field strength tensor $G_{\mu\nu}G^{\mu\nu}$ present in the Lagrangian describing QCD ($\mathcal{L}_{QCD}$). This characteristic non-linear dynamical evolution defines the non-abelian nature of QCD. A true self interaction would imply r mixing with r, and so-forth, however, it is the case that each color represents a separate charge, and not states of one charge present in the theory.

Moreover, the quarks exchange color charge indices with the gluon field due to carrying colour charge of their own. In subsequent chapters we construct these terms through defining a gauge invariant local theory via the $\mathcal{L}_{QCD}$ through the work of C.N. Yang and Robert Mills.

Both the perturbative and non-perturbative regime can be seen in the behavior of the running coupling α_s. Techniques requiring large logarithmic corrections become necessary in regions of space where we no longer have reliable expansion of α_s [20]. QCD's coupling energy spans a range from asymptotic freedom to confinement. The "running" is referring to the coupling strengths variability at different energy scales. To consider its dependence on the energy range probed, we use renormalization schemes, which can be thought of as an argument for α_s. Separate consideration of scattering processes require separate approaches, some of which are not accessible with the path integral. In high energy $p\overline{p}$ collisions, the colliding hadrons involved in the process are not amenable to perturbative techniques in times when it becomes necessary to calculate the distribution of quarks and gluons. One solution is to use the factorization theorem, which introduces methods for dealing with high energy cross sections. This leads us to the implications of the DGLAP equations for PDF's and Efremov and Radyushkin-Brodsky and Lepage (ERBL) kernels for transversity distributions. With the DGLAP equations we can relate different processes at different scales. For example, we can use the evolution equations phenomenologically to predict what partons might look like at any scale when thinking about future experiments [13].

Since the 2015 the Large Hadron Colliders (LHC) 13 TeV run, we have acquired greater detail and measure of new physics, notably, a more extensive study of the Higgs boson, which was discovered on July 4, 2012. Neither Lattice QCD ($LQCD$) nor perturbative QCD ($pQCD$) offers full solutions for QCD at the colliders. What the community has settled on is $pQCD$ inputs plus non-perturbative modeling and factorization from various frameworks

that serve as specific tools and constraints. Meaningful calculations require accurate contributions from both. We discuss event shapes and the importance for infrared safe observables in QCD [21–23] as they describe the energy and momentum flow of final state events. One of the best event shapes is the energy-energy correlation (EEC), which is used quite extensively in e^+e^- annihilation. The determination of inclusive (integrating over all possible final states) $e^+e^- \rightarrow hadrons$ total cross-section measurements has enabled the first three terms in the QCD perturbation expansion to be known to quite an accurate measure [6].

1.0.1 Relevant Insights

Efforts were met with the need to develop a theory properly describing the dynamics of the newly introduced quarks. A necessary condition for the accuracy of the theory was that the interaction amongst the quarks become increasingly weaker at shorter distances. This in part led to asymptotic freedom, later discovered in 1973 by David Gross and Frank Wilczek, as well as by David Politzer in this same year earning them the 2004 Nobel Prize in Physics [24]. This property is responsible for interactions amongst the particles to become asymptotically weaker as the coupling strength increases while the corresponding length scale decreases. The strength of interaction in the IR region is responsible for the confinement of quarks and gluons within hadron bound states, becoming colourless singlets. It is energetically favorable to create quark antiquark pairs from the condensate rather than to continue the elongation of what is refereed to as the color "flux tubes". Instead of detecting individual quarks in detectors, scientists see $Jets$ composed of color-neutral ground states resulting from hadronization, also called fragmentation, and string breaking. The confining phase can be defined by the action using the Wilson loop, which is the path in spacetime that is traced

out by a quark-antiquark pair that follow the creation and annihilation sequence [25]. There is a running scale that characterizes QCD in terms of its coupling parameter. The coupling parameter α_s also is dependent on choice of renormalization scheme. In the $\overline{MS}$ scheme at 4-loop in the running of α_s, the world average in the 3-flavour case is given by

$$\Lambda \frac{(3)}{MS} = (332 \pm 17) MeV, \tag{1.10}$$

as verified in the $e^+e^- \rightarrow hadrons$. Λ is an energy scale used in QCD, and is accessible in the PDG [8].

Being that the $SU(3)$ symmetry group is a non Abelian gauge theory, due to the "self interacting" gluons giving rise to non-commuting matrices, the theory as a result is highly non-linear. Solving QCD directly in an analytical manner has proven difficult. One powerful non-perturbative tool is the $LQCD$ Monte Carlo simulations carrying out first-principle calculation of the strong interaction. The results in some cases remarkably reflect experimental data. Computational interest has found its way to developing jet algorithms to generate events in the interest of phenomenology as well.

Form factors (FF) are powerful tools when probing the structure of the nucleon. They carry direct information regarding substructure and shape. This is analyzed by charge distribution and the magnetization of the quarks within the nucleon. Hadron FF's are defined as Lorentz-invariant functions that serve to parameterize the matrix elements. We referred to the Lorentz-invariant functions as being sandwiched between the operators we obtained from expanding the products of the hadronic tensor. Furthermore, the FF's depend on the flavors of the quarks taking part in the electromagnetic or weak transition. To develop a general conceptual sense early on, the hadron FF's that we will be interested in can be described by any transition between

the initial and final states of a hadron in which is initiated by an electromagnetic or weak interaction of quarks. Moreover, once this quantity is reached, it enters a probability amplitude to quantify the strong interactions contribution while in the transition process. This we discuss in terms of the pion FF [4]. The parton distribution amplitudes play an important role in describing a number of hard processes (high energy scattering) of bound state hadrons by way of the factorization theorem, which lie at the heart of perturbative QCD [26–28]. The distribution amplitudes (DA's) are complementary to the parton distribution functions (PDFs) associated with these inclusive processes, the DA's are longitudinal projections of hadronic wave functions. They are obtained by integrating out the transverse momenta contribution of the partons. TMD in Fig.1.1 are a separate class of PDFs, they are incorporated when calculating $\mathcal{O}\alpha_s^1$ W mass production involving p_T [27].

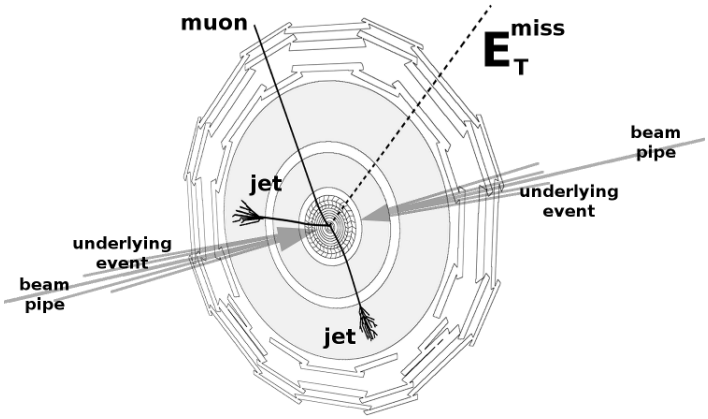

FIGURE 1.1: Transverse momentum is in the direction of the muon line, while the beam pipe represents an example of the longitudinal direction. E_T represents transverse Energy. Underlying events and jets will be discussed in upcoming sections. Image courtesy of [29].

The TMD's produce important results about the QCD bound states. When dealing with large logarithms at $\mathcal{O}\alpha_s^1$ this information will play a pertinent role. Soft gluon resummation techniques become implemented allowing us

to obtain a finite result. It is to be noted that beyond $\mathcal{O}\alpha_s^1$, the theoretical calculation of the vector boson spectrum is still unclear, and the $\mathcal{O}\alpha_s^2$ result is still to be determined. In the absence of this result. We can still improve the $\mathcal{O}\alpha_s^1$ result by adding higher order contributions that still remain incomplete. In the low p_T realm, this becomes critical. Resummation of large logarithms of the form $ln(\frac{p_T}{mV})$ are done to obtain agreement with data. In cases such as inclusive Drell-Yan and Higgs production, where the $\mathcal{O}\alpha_s^2$ corrections are known, it was shown that even in cases such as Higgs production a high percentage of perturbative corrections are influenced through the threshold, giving a good approximation in the result [30]. The resummation at low p_T to next-to-next-to-leading logarithmic level (NNLL) can be seen in this review [31].

This thesis is organized as follows. In *Chapter* 2, we review quantum field theory to distinguish the contributions of C.N. Yang and R. Mills with connection to the applicability of QCD. This theory was adopted by the physics community after Gerard 't Hooft, in 1972, had placed its renormalization on firm footing [32, 33]. This leads naturally to reviewing the SM, followed by renormalization schemes that becomes manifest at infinitely large momenta. We calculate loop diagrams in ultraviolet (UV) divergent calculations, and introduce concepts relevant to *jet* production, where non-perturbative higher order radiative corrections are required for $W^+ + 1$ calculated in the soft IR (infrared) region, . In *Chapter* 3, we incorporate the development of EW theory while drawing from it additional insights on W boson production. In *Chapter* 4 we introduce the parton model beginning with the historical developments that led to its modern implementation. Additionally, the DGLAP evolution equations used for evolving variations of parton distribution functions at their varying process dependent energy scales are motivated here as well. DGLAP evolution equations will be put to use in the context of PDF's. *Chapter* 5 contains relevant experiments at CERN and Fermilab's

CDF collaboration bringing together in clearer focus the development from *Chapters* 2 through 4. In *Chapter* 6, we move to phenomenological inputs and experimental procedure in relevant calculations with resummation of large logarithms concerning high transverse momentum W mass determinations, which include factorization theorems and treating higher order soft gluon contributions.

Chapter 2

Yang-Mills & The Quantum Theory of Fields

"...The difference between a neutron and a proton is then a purely arbitrary process. As usually conceived, however, this arbitrariness is subject to the following limitations: once one chooses what to call a proton, what a neutron, at one space time point, one is then not free to make any choices at other space time points.

It seems, that this is not consistent with the localized field concept that underlies the usual physical theories. In the present paper we wish to explore the possibility of requiring all interaction to be invariant under independent rotations of the isotopic spin at all space time points" [7].

-Yang and Mills (1954)

2.1 Introduction

We have in part taken the title of this chapter from that of Steven Weinberg's *"The Quantum Theory of Fields"*, and to which we refer for a more in-depth study of QFT. [9]. To begin, the traditional formulation of QFT is premised on locality and unitarity, followed by the standard approach of constructing Lagrangians and computing scattering amplitudes via path integrals that rely on the properties of locality and unitarity. Yang-Mills theory was born out of necessity and was needed to establish a local symmetry for

hadronic isospin. This was needed to establish conservation of isotopic spin, which eventually led to non-abelian gauge theory. Robert Mills and Chen Yang developed a foundational paper in 1954 [34] and is known today as a fundamental framework for describing interaction theories, resting upon the axioms developed from Lie groups and associated algebras. The Yang-Mills gauge theories provide a foundation for the SM which gives accurate description for the strong, electromagnetic, and weak interactions [35]. We can refer to $U(1)_Y$ as the gauge invariant symmetry group of quantum electrodynamics. The quantum field theory $SU(2)_L \otimes U(1)_Y$ describes Electroweak and semileptonic processes and are of particular interest for W boson production, additionally involving the $SU(3)_c$ symmetry group for the strong interaction. The $U(1)_Y$ group is abelian, however, the symmetry groups that represent nuclear interaction theories in the real world are all non-abelian.

The $\mathcal{L}_{QCD}$ is expressed in terms of the spinor fields that make up the matter fields of fermions. The quark fields form the fundamental representation of the symmetry group $SU(3)_c$, while the gluon fields are in the adjoint representation of this same group. When we impose gauge invariance to the Dirac Lagrangian, we stumble upon our classical QCD Lagrangian [36].

$$\mathcal{L}_{Dirac} = \overline{\psi}(i\gamma^\mu \partial_\mu - m)\psi \tag{2.1}$$

Where $\overline{\psi} = \psi^\dagger \gamma^0$ with γ^0 being the zeroth Dirac matrix. We will in addition show the formulation of the parton model first from the field theoretic point of view, this will be in order to better facilitate for a time when we do in fact discuss PDFs and the very large role they play in subsequent chapters.

The quarks possess Fermi statistics to account for the spins of the low-mass baryons. These fermions are in a symmetrical state-space, following spin and $SU(3)_f$ degrees of freedom [6]. We have a colour index a with three

possible values running over red, green and blue with $a = 1, 2, 3$ to be carried by each quark. This new index forces the baryon wave function into a totally antisymmetric regime, thus rendering an important mechanical detail defining the representation theory. q_a transforms according to the fundamental 3×3 unitary matrix representation while the antiquarks, $\overline{q}^a$, do so under the complex conjugate representation. The basic colour singlet states are the mesons, $q_a \overline{q}^a$, and the baryons, $\epsilon^{abc} q_a q_b q_c$, where ϵ^{abc} is the total antisymmetric tensor [6, 37].

2.2 The Standard Model and $\mathcal{L}$ Gauge Invariance

We have entered an era of precision tests of the SM, and one objective is the search of new physics. One of central motivation in which tutors this endeavor is to seek out the mechanism of the spontaneous symmetry breaking, which is observed in weak interactions. Ongoing efforts will necessitate aims at future $100TeV$ pp and e^+e^- colliders [38].

The SM, is a gauge field theory based on the symmetry group

$$SU(3)_C \otimes SU(2)_L \otimes U(1)_Y. \tag{2.2}$$

Transformations act on the $SU(2)_L \otimes U(1)_Y$ fields, which become spontaneously broken down to $U(1)_{em}$, being induced by the Higgs vev. The SM contains an $SU(2)$ Higgs doublet [39]

$$\begin{pmatrix} \phi^+ \\ \phi^0 \end{pmatrix} = \begin{pmatrix} (\phi_1 + i\phi_2)/\sqrt{2} \\ (\phi_3 + i\phi_4)/\sqrt{2} \end{pmatrix} \tag{2.3}$$

after SSB, ϕ acquires a vev through $\phi_3 = v$ and $\phi_1 = \phi_2 = \phi_4 = 0$, and now with

$$\phi = \begin{pmatrix} 0 \\ v \end{pmatrix} \rightarrow \begin{pmatrix} 0 \\ v + h \end{pmatrix}, \tag{2.4}$$

resulting in

$$H = \begin{pmatrix} G^+ \\ \frac{1}{\sqrt{2}(v+h+iG^0)}. \end{pmatrix} \tag{2.5}$$

The Higgs is an electroweak doublet and the charge components G^+ and neutral component written G^0 are the goldstone bosons that get "eaten" by the W^+ and 'Z^0 after electroweak symmetry breaking. The h is the physical Higgs with mass $\approx$ 126 GeV, as observed [40]. The g_W term representing the $SU(2)$ doublet is the same doublet scalar field expressed in equation, 1.5, reading

$$M_W = \frac{1}{2} v g_W, \tag{2.6}$$

The Lagrangian comes with global phase invariance preserving quantities such as conserved chargers via Noether's theorem [13]. The gauge principle introduces Lagrangian interactions demanding that the Lagrangian remain invariant under space-time phase changes locally. A consequence is we now have to compensate for an additional term in the derivative. An example being a transformation parameterizing a single real phase θ in Dirac matter fields [7],

$$\not{\partial}\psi' = e^{i\theta(x)}\not{\partial}\psi + e^{i\theta}(i\not{\partial}\theta(x))\psi \neq e^{i\theta(x)}\not{\partial}\psi. \tag{2.7}$$

Equation 2.21 shows the extra derivative showing up and that invariance is not yet established, when constructing gauge invariance the gauge invariant derivative becomes compensated by

$$D_\mu = \partial_\mu - ieA_\mu(x), \tag{2.8}$$

where $A_\mu(x)$ is the new field that now transforms as

$$A_\mu(x) \longrightarrow A'_\mu(x) = A_\mu(x) + \frac{1}{e}\partial_\mu\theta(x). \tag{2.9}$$

These new fields A_μ are the gauge fields and as a result $(\not{D}\psi)' = \not{D}\psi$, with $\not{D} = \gamma_\mu\partial^\mu = \gamma_\mu\frac{\partial}{\partial x_\mu}$. And now a kinematic term needs to be added in order to represent dynamics in our new gauge field A_μ, and is of the form

$$\mathcal{L}_{gauge} = [D_\mu, D_\nu] = (\partial_\mu - \partial_\nu A_\mu)(\partial^\mu A^\nu - \partial^\nu A^\mu) \tag{2.10}$$

and without any additional fields present, we generate mass terms that violate the gauge invariance [13]

$$\mathcal{L}_{gm} = \frac{m^2}{2}A_\mu A^\mu. \tag{2.11}$$

Many of the nineteen parameters and the relations between the parameters involve quantities that participate in the strong interaction. The nineteen parameters in the SM include three generations of leptons containing the electron, muon, tau, and their corresponding neutrinos. These are present in the electroweak interaction, which involves the strong force in many processes. The quark family is amongst these coming in three flavours, and is directly involved for the strong force along with twelve gauge bosons, not including gravity, includes the gauge bosons. Every particle falls into some representation of the groups $SU(3)_c, SU(2)_L, U(1)_Y$. Whereas $SU(2)_L \otimes U(1)_Y$ describes the EW interaction and electric charge Q. The electron is a spinor in spacetime, acting as a singlet under the strong interaction and the role as part of a doublet when participating in the weak interaction, and carries an electromagnetic charge. The quark is a spinor in the fermion field and participates in a triplet representation under the strong interaction and a doublet under the weak interaction, as well as carries electric charge. It turns out

that the gauge fields are spin one fields, fulfilling the Proca equation. The matter particles obey Fermi-Dirac statistics and the Pauli exclusion principle fulfilling the Dirac equation. The Higgs is a spin 0 scalar field fulfilling the Klein-Gordon equation. All gauge bosons generated from gauge fields under local symmetry must be massless. The weak interaction treats fermions with left-handed chirality differently from those with right-handed chirality. The Fermions are, in fact, not massless, and adding the mass terms of the small u and $\overline{d}$ masses spontaneously breaks the symmetry leading to the Higgs mechanism as demonstrated [9].

The theory of the SM contains a Klein-Gordon component due to the Higgs scalar field, and Dirac components for the fermion field, and the Proca equation for the gauge fields and interactions. The Dirac equation in 1928 was a major breakthrough and was followed by the discovery of neutron by Chadwick in 1932. The realization was that the proton and electron model for the nucleus would need to be replaced [41].

2.2.1 Feynman Rules for Non-Abelian Gauge Theories and Greens Functions

Green's theorem relates a line integral along a closed curve with the double integral of a vector field in the plane [42]. It is well known that scattering cross-sections at tree level have classical correspondence to classical theory cross-sections. One effective example being that tree level cross-sections in electron-electron scattering in QED correspond to scattering of the classically represented point charges as represented in classical field theory. The naive explanation for this is that the power of $\hbar$ in terms of its perturbative expansion corresponds to the number of loops in the diagram. In QFT, we calculate the expectation value of the time-ordered product by way of Green's function. This is done over the vacuum fields [43]. They cannot be written

in terms of the standard Feynman diagrams, due to Green functions being more complex than the vacuum.

2.2.2 The QCD Lagrangian

The usual approach is to define a model by writing down its Lagrangian. Each Lagrangian consists of interaction terms as well as the terms that describe the behavior of the fields as they are without including interactions [18]. The QCD Lagrangian has a simple structure while also possessing the dense dynamical interactions responsible for bound states observed. [7]. Additionally, it comes with a highly non trivial topological vacuum structure. [44]. Under further examination, consider the quark fields, $\psi = (\psi_{\alpha i})$

$$\begin{cases} \alpha = d, u, s, c, b, t & N_f = 6 \leftrightarrow SU(N)_f \\ i = 1, 2, 3 & N_c = 3 \leftrightarrow SU(3)_c \end{cases} \tag{2.12}$$

where $\psi_{\alpha i}$ is a 4-component Dirac-spinor. Consider Quark fields with color degree of freedom and their free Lagrangian [45]

$$\psi = \begin{bmatrix} \psi_1 \\ \psi_2 \\ \psi_3 \end{bmatrix} \quad \mathcal{L} = \overline{\psi}[i\gamma_\mu \partial^\mu - m]\psi. \tag{2.13}$$

Local $SU(3)_c$ gauge transformations

$$\psi(x) \longrightarrow \tilde{\psi}(x) = U(x)\psi(x) \tag{2.14}$$

with

$$U(x) = exp[-i\theta_z(x)\frac{\lambda_a}{2}].$$

Physics of strong interaction of quarks is invariant under gauge transformation $\psi(x) \rightarrow U(x)\psi(x)$ $SU(3)_c$ is a non abelian gauge group. The gauge covariant derivative is defined as

$$D_\mu = \partial_\mu - igA_\mu(x), \tag{2.15}$$

where g is a dimensionless coupling strength analogous to e in QED

$$A_\mu(x) = \Sigma_{a=1}^{8} t_a A_\mu^a(x), \quad t_a = \frac{\lambda_a}{2}. \tag{2.16}$$

Introducing $A_\mu^a(x)$ as gauge fields of "gluons" in $SU_c(3)$,

$$\mathcal{L}_1 = \overline{\psi}(x)[i\gamma_\mu D^\mu - m]\psi(x). \tag{2.17}$$

The above Lagrangian is gauge invariant if we define

$$\tilde{D^\mu}\tilde{\psi} \equiv \partial^\mu\tilde{\psi} - ig\tilde{A}^\mu\tilde{\psi} = U(D^\mu U). \tag{2.18}$$

Infinitesimal gauge transformation

$$U = exp[-i\theta_a(x)t_a] \approx 1 - i\theta_a(x)t_a + ..., \tag{2.19}$$

of gauge field linear in $\theta_a(x)$ become

$$A_a^\mu(x) \rightarrow \tilde{A}_a^\mu(x) = A_a^\mu(x) - \frac{1}{g}\partial^\mu\theta_a(x) + f_{abc}\theta_b(x)A_c^\mu(x). \tag{2.20}$$

Gluons have to be massless, otherwise a mass term $m_g A_a^\mu A_\mu^a$ would not remain gauge invariant. Gluonic field tensors can take the form analogous to QED of the form [19, 46]

$$F_{\mu\nu}^a(x) = \partial_\mu A_\nu^a(x) - \partial_\nu A_\mu^a(x). \tag{2.21}$$

Equation 2.21 is not gauge invariant in QCD, so we have to introduce an additional term to obtain gauge invariance. For this purpose Gluonic field tensor is written as

$$G^a_{\mu\nu}(x) = \partial_\mu A^a_\nu(x) - \partial_\nu A^a_\mu(x) + g f_{abc} A^b_\mu(x) A^c_\nu(x) \tag{2.22}$$

with

$$G_{\mu\nu} \equiv t_a G^a_{\mu\nu} = \frac{i}{g}[D_\mu, D_\nu], \tag{2.23}$$

the gluonic contribution to the Lagrangian becomes

$$\mathcal{L}_{glue} = -\frac{1}{4} G^a_{\mu\nu}(x) G^{\mu\nu}_a(x) = -\frac{1}{2} tr\{G_{\mu\nu} G^{\mu\nu}\}, \tag{2.24}$$

and now in context of the full QCD Lagrangian,

$$\mathcal{L}_{QCD} = -\frac{1}{2} Tr[F_{\mu\nu} F^{\mu\nu}] + \sum_{f=1}^{N_f} (\overline{\psi}_f(x)(i\not{D} - m_f)\psi_f(x), \not{D} = \gamma^\mu[\partial_\mu - igA_\mu(x)]. \tag{2.25}$$

This looks similar to the QED Lagrangian, except that there are additional color index terms, and the minus sign indicating the self interacting gauge field giving rise to the nonabelian nature of QCD dynamics. Gluonic field tensors of $\mathcal{L}_{QCD}$ generates non-linear gluon interactions:

The last term in Equation 2.22 corresponds to 3-gluon interaction, and can be seen in Figure 2.1

$$\mathcal{L}^3 = -\frac{g}{2} f_{abc}(\partial^\mu A^\nu_a - \partial^\nu_a) A^b_\mu A^c_\nu. \tag{2.26}$$

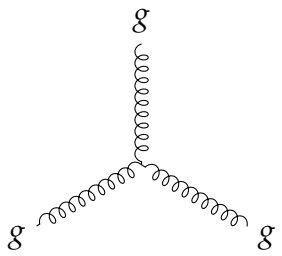

FIGURE 2.1: 3-gluon interaction, denoted g.

the 4-gluon interaction, seen in Figure 2.2 in which the diagrams that represent higher order gluon contributions become increasingly complicated to compute

$$\mathcal{L}^4 = -\frac{g^2}{4} f_{abc} f_{cde} A_{\alpha\mu} A_{b\nu} A_c^\mu A_d^\nu \tag{2.27}$$

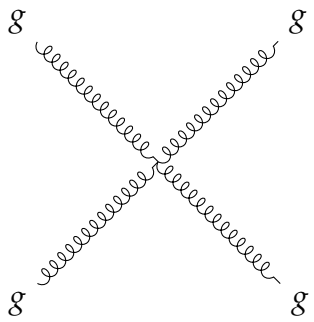

FIGURE 2.2: 4-gluon interaction, denoted g^2.

We now have gauge invariance in the QCD Lagrangian. Since the quarks have three basic color-charge states, they can be labeled as a that can take on *red*, *green*, and *blue*, or assigned 1, 2 and 3. Three color states form a basis in a 3-dimensional vector space being a colorless bound state. A general color state of a quark is then a vector in this space. The color state is rotated by the 3×3 unitary matrices, notably the Gell-Man matrices. All of the unitary transformations have a unit determinant that form a Lie group $SU(3)$ [47]. Gluons are self contained sources of the color field, and are not only color-charged, but additionally produce strong color fields. The quartic terms are proportional to g^2 for Non-Abelian Fields [46, 48]. Furthermore, the Higgs mass ratio to the W mass is the quartic coupling of the Higgs, the mass squared term is the term found in the Lagrangian and determines the *vev*, which determines the W mass.

2.2.3 Quantization of the Path Integral

We an define the quantization for the path integral by beginning with a generating functional [49]

$$\mathcal{Z}[J] = \int \mathcal{D}\phi e^{i\int d^4x(\mathcal{L}+J_a(x)\phi_a(x))} \tag{2.28}$$

where $J_a(x)$ can be an arbitrary external source,

$$\mathcal{D}_\phi \equiv \Pi_{x,a} d\phi(x). \tag{2.29}$$

A quantum field theory is completely determined by its Green's functions. These are defined as

$$G^n_{i_1,...,i_n}(x_1,...,x_n) = \langle 0|T[\hat{\phi}_{i1}(x_1)...\hat{\phi}_{in}(x_n)]|0\rangle \,. \tag{2.30}$$

We compute the Green's functions by differentiating with respect to these external sources [49],

$$< \hat{\phi}_{i1}(x_1)...\hat{\phi}_{in}(x_n) >= \frac{1}{i^n \mathcal{Z}[J]} \frac{\delta^n \mathcal{Z}[J]}{\delta J_{i1}(x_1)...\delta J_{in}(x_n)}|_{J=0}, \tag{2.31}$$

and now the vacuum expectation value becomes [49]

$$< \hat{\phi}_{i1}(x_1)...\hat{\phi}_{in}(x_n) >= \frac{1}{\mathcal{Z}[0]} \int \mathcal{D}\phi(\phi_{i1}(x_1...\hat{\phi}_{i1}(x_n))e^{iS}. \tag{2.32}$$

We are showing here that the Green's function is obtained after computing a weighted average over all of configurations the system can possibly go through. The generating functional involves the integral over the gauge fields $A^a_\mu(x)$. For any field configuration A_μ we can define a gauge orbit to be the set of all fields related to the first by a gauge transformation α. Making a note that all the configurations have the same contribution to the

functional integral giving infinite contributions. We will turn to Faddeev-Popov to achieve a gauge fixing condition of the form $F^a[A] - C^a(x) = 0$[3]. This isolates the contribution over repeated configurations by factorizing it as $\int \mathcal{D}\alpha \int \mathcal{D}A_\mu exp^{iS[A]}$, being eliminated by the normalization [49].

2.2.4 Propagators and Vertices

The correlation functions come by way of Green's function, which are used to calculate scattering matrices pertaining to observables. This allows us to deal with time ordered products in the context of vev's. We cannot compute the correlation functions completely in an analytic way. With perturbation theory we can extract some insightful information regarding the form of the functions however [36]. The gluon propagator comes from the quadratic terms in the gluon fields, which are also to be found in the Lagrangian. We adopt Landau gauge, which corresponds to the limit $\xi \to 0$ and directs the weight aspect of the weight-function on the gauge copy, the key point being that it does not change the result of the physical outcome of the system. This is done through the form of the covariant derivative $\partial^\mu A_\mu$. Following this treatment, the propagator in momentum space looks like

$$D^{ab}_{\mu\nu}(p^2) = \frac{\delta^{ab}}{p^2}[g_{\mu\nu} + (\xi - 1)\frac{p_\mu p_\nu}{p^2}] \tag{2.33}$$

with $\xi = 0$ the Landau gauge as discussed. The ghost fields also have associated Feynman rules. In the Landau gauge the functional derivative obtained

$$A'^a_\mu = A^a_\mu + f^{abc}A^b_\mu \alpha^c + \partial_\mu \alpha^a, \tag{2.34}$$

and now takes on the form $\partial^\mu D_\mu$, giving the Lagrangian contribution now taking on the form [49]

$$\mathcal{L}_{ghost} = -\eta^{-a}\partial_\mu\partial^\mu\eta^a + gf^{abc}\eta^{-a}\partial^\mu(A^b_\mu\eta^c). \tag{2.35}$$

In a non-perturbative framework, we wish to have complete correlation functions with tensor structure that differs from the simple bare vertices that we encounter in zeroth order perturbation theory [50]. We use the Slavnov-Taylor identity to define the tensor structure that represents the gluon propagator associated with the gauge condition. This identity reads

$$\partial^\mu_x\partial^\nu_y < T[A^a_\mu(x)A^b_\nu(y)] >= 0, \tag{2.36}$$

this gives the propagator the orthogonal property needed and using the Landau gauge we have

$$D^{ab}_{\mu\nu}(p) = \delta^{ab}D(p^2)[g_{\mu\nu} - \frac{p_\mu p_\nu}{p^2}]. \tag{2.37}$$

We are then able to extend to higher point correlation functions for the purpose of constructing tensor structures with the established symmetries of the system. This becomes especially important in cases when discretizing the theory for use when frameworks such as Lattice gauge theory become necessary [51].

2.3 Renormalization

2.3.1 Overview

The QCD β function blows up at the Landau pole, and UV divergences at first seems to invalidate our theories. The divergences may be removed for

a renomalizable theory, which requires all couplings to have non-negative energy dimensions, giving finite numbers of divergent amplitudes, thus allowing UV divergent cancellations by a finite set of counterterms, with the caveat of cancellations be done order-by-order in perturbation theory at all orders [52]. For this purpose QFT parameters are redefined and a UV cut-off. Renormalizability is vital to the success of the SM [35, 53].

We begin with a bare electron mass m_0 and associate it to its classical scale down to a radius a. We can consider the observed quantity the bare mass plus the energy in the field, of course divided by c^2. Lets say we have a field energy of $0.7MeV$ when $a = 10^{-15}m$, and it diverges in the limit $a \to 0$. The observed mass of the electron $\approx 0.5MeV$ and is the sum of the large (or infinite) field contribution compensated by the negative and large bare mass. We would need to replace this by a more precise version when going to short distances, but this can serve as a foundation of motivation [53].

2.3.2 Faddeev-Popov and Ghosts

In general, $QFT's$ come with divergences other than ones that can be solved by the Faddeev-Popov method. Calculating radiative corrections in any four dimensional theory will lead you to diverging integrals. We can make a theory finite by means of a technique named as dimensional regularization. We do so by absorbing these divergences that show up in the theory with cleverly chosen parameters. In the perturbative approach we can obtain similar results using techniques for ultraviolet momentum cut-offs or dimensional regularization.

The Slavnov-Taylor identities relate the correlation functions in our path integral to ensure gauge invariance. The integral in our effective Lagrangian remains gauge independent under gauge transformations achieved by adding the Faddeev-Popov ghost fields to the Lagrangian.

2.3.3 The Renormalization Group

The renormalization group came from a need to remedy the problem of infinities in QFT in the quest for finite physical quantities. It was first solved for QED by Julian Schwinger, Richard Feynman, and Shin'ichirō Tomonaga, earning them the Nobel Prize in physics in 1965, for more dedicated reviews consult [51, 54–57]. When referring to the mass of a particular hadron or quark, we need to know what renormalization scheme we are working in. For example, it is common to use the Minimal Subtraction $(\overline{MS})$ scheme, and the renormalization scale is defined through The Lagrangian has terms that are not necessarily related to what is found experimentally regarding coupling strengths in particular. We are working with couplings between particles in the first order approximation. We are interested in the experimental results to choose an appropriate scale. The renormalization group flow of the QCD coupling is governed by

$$\frac{dg}{dt} = \beta(g) = \frac{11}{3} T_2(G) \frac{g^3}{16\pi^2} \tag{2.38}$$

with what is dubbed "the all critical minus sign" [35].

$$T_2(G)\delta_{ab} = f^{acd} f^{bcd} \tag{2.39}$$

being the structure constants we had seen before. When fermions are included in this relation

$$\frac{dg}{dt} = \beta(g) = [-\frac{11}{3} T_2(G) + \frac{4}{3} T_2(F)] \frac{g^3}{16\pi^2} \tag{2.40}$$

where

$$T_2(F)\delta^{ab} = tr[T^a(F) T^b(F)] \tag{2.41}$$

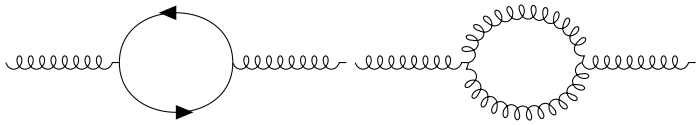

FIGURE 2.3: The Feynman diagram below denotes the leading quantum corrections to the running of the QCD coupling α_s: gluon self energy at one loop order with the ghost diagrams ignored. The left diagram pertains to both QED and QCD rendering the interaction stronger at shorter distance referred to as screening. The second diagram is resultant from nonlinear interaction taking place amongst the gluon field, and this contrarily undergoes an anti-screening effect, thus rendering coupling strength weaker at short distance scales [47].

For $SU(N)T_2(F) = \frac{1}{2}$ and this stands for each fermion in the fundamental representation of our gauge group.

We can now show in analogy with QED for reference, that $\alpha_s(\mu) \equiv g(\mu)^2 4\pi$, which is showing the strong coupling at a momentum scale μ. Now we can show

$$\alpha_s(Q) = \frac{\alpha_s(\mu)}{1 + (1/4\pi)(11 - \frac{2}{3}n_f)\alpha_s(\mu)log(Q^2/\mu^2)} \tag{2.42}$$

This explicitly shows that $\alpha_s(Q) \to 0$ logarithmically as $Q \to \infty$ [35].

2.3.4 The Running Coupling, α_s

The varying scale known as the renormalization scale, μ_R, include these corrections, and denote all couplings in QED as well as QCD in the process with $\alpha = \frac{g^2}{(f\pi)}$. that varies with

$$\mu_R^2 \frac{\partial \alpha(\mu_R^2)}{\partial \mu_R^2} = \beta(\alpha). \tag{2.43}$$

It is convenient to have the β function to expand $\beta(\alpha)$ in a perturbative series and it goes as

$$-\beta(\alpha) = \sum_{n=0}^{\infty} b_n \alpha^{2+n} = \frac{\beta_0}{4\pi}\alpha_s^2 + \frac{\beta_1}{(4\pi)^2}\alpha_s^3 + \dots. \tag{2.44}$$

In $SU(N)$ gauge theories, the first coefficients of β_i in the expansion are as follows [13]

$$\beta_0 = \frac{11}{3}C_A - \frac{4}{3}T_R n_f$$
$$\beta_1 = \frac{34}{3}C_A^2 - \frac{20}{3}C_A T_R n_f - 4C_F T_R n_f \tag{2.45}$$
$$\beta_2 = \frac{2857}{54}C_A^3 + 2C_F^2 T_R n_f - \frac{205}{9}C_F C_A T_R n_f - \frac{1415}{27}C_A^2 T_R n_f \ldots,$$

n_f is the number of active fermions, the Casimir operators come from the gauge group out of the structure constants we computed in *Chapter* 2 and reside in both the fundamental and adjoint representations. We would like to emphasize that the first two coefficients, β_0 and β_1 are renormalization scheme-independent. All of the further terms that contribute to the series beginning with β_2 depend on renormalization scheme. We get β_2 from the $\overline{MS}$ scheme. The running coupling $\alpha_s(Q^2)$ determines the quark and gluon interactions strength dependent on momentum transfer Q [58]. This dependence (Q^2) of the coupling is needed in order to describe the interactions of the hadrons at long and short distance scales. This high Q^2 dependence becomes specific to the renormalization group equation (RGE) in the perturbative approach. The behavior of the QCD coupling especially at low momentum transfers Q is main focus in hadron physics. Schwinger-Dyson equations and light-front holography each uses varying definitions of the coupling strength and effective charges in the IR domain. A further recent review in Reference [58, 59] can be seen. Matching the high and low Q^2 regimes that determines the scale Q_0 allows the setting of the proper interface between perturbative and non-perturbative hadron dynamics. We use Q_0 to set the factorization scale for the DGLAP evolution equations [58]. The hadronic decay rate of the τ lepton additionally serves as one of the most precise determinations of the QCD coupling α_s. The QCD coupling, being dependent on the momentum scale Q^2, exhibits a large coupling at small Q,

being the energy region where quarks and gluons are considered nearly free due to asymptotic freedom. Conversely, at small coupling it thus increases and perturbation theory fails. Protons have an energy $m_p \approx 0.94GeV$, so their coupling is very large. When "new physics" is probed at the colliders, for example, at scales $Q \approx p_t \approx 50GeV - 5TeV$, the coupling is very small.

Chapter 3

Electroweak Theory & the Strong Interaction

This serves as a brief introduction to the Electroweak sector of the SM. Its description is given by a broken $SU(2)_L \otimes U(1)_Y$ gauge group in which represents the massive weak gauge bosons, $W^{\pm}$ and Z^0, and $U(1)_{QED}$. These gauge bosons are the longitudinally polarized vector bosons associated with SSB that we had introduced at the beginning of Chapter 1 beginning with Equation 1.1, where we had arrived at their mass terms, G_F, the vacuum expectation value as well as the value of the Higgs as observed. One consequence of local gauge invariance is an exact symmetry of the $\mathcal{L}_{QCD}$. If we restrict the Lagrangian to the quark sector

$$\mathcal{L} = \sum_{j=u,d} \overline{q}_j (i\not{D} + m) q_j \tag{3.1}$$

which dynamically describes quarks of mass m with $spin$ $\frac{1}{2}$, and consider only first generation light quarks in the u and d fields, we are able to perform a global phase definition of the up and down fields separately while the Lagrangian remains invariant. This is in correspondence with quark number conservation [6, 37]. Matrix notation for the quark field is

$$q = \begin{pmatrix} u \\ d \end{pmatrix}, \tag{3.2}$$

and referring back to Equation 3.1, where

$$m = \begin{pmatrix} m_u & 0 \\ 0 & m_d \end{pmatrix}, \tag{3.3}$$

leads to Lagrangian invariance under 2×2 unitary transformations. Proceeding under the assumption that $m_u - m_d$ is much smaller than the hadronic mass scale, we can represent transformations acting on the quark fields via Pauli matrices. The importance being that an approximate symmetry $SU(2)_V$ is the isospin symmetry in the limit of degenerate mass [6]. Chiral symmetry is not a feature observed in QCD, the u and d quark masses acquired during spontaneous symmetry breaking leads to additional mass terms in the $\mathcal{L}$. The quark condensate in this context, has a non-zero vacuum expectation value of the light-quark operator $q\overline{q}$, and is not invariant under group transformations. the quark condensate connects the left and right-handed fields and eluding to prior becomes spontaneously broken with the small mass terms, u and d, that the quarks in nature do in fact possess [6, 7]. The pions have a very small mass compared to the hadron scale $\approx 1\,GeV$, additionally, the value of the quark masses are deduced from the pions. This is referred to as chiral perturbation theory and it leads to a consistent picture of strong interactions. As we restrict ourselves to the first generation of matter, we will not go into the implications for the heavy quark masses at this time.

3.1 Glashow-Salam-Weinberg Theory of the Electroweak Interaction

The goal of this chapter is to study global spontaneous symmetry breaking. We will at a later time extrapolate some implications of such to situations of physical interest in hadron physics. The Goldstone theorem states

that physical particles in a given theory generate one zero mass term and zero spin for each broken symmetry [9]. Most importantly we begin with $\mathcal{L}_{QCD}$ which describes the theory as symmetric in its degrees of freedom. This however does not represent the real situation in our physical world. Local gauge invariance is a feature which enables the theory to be renormalizable. The QCD vacuum can have non-trivial topological structure. The Ward identities describe the correlation between the global and gauge symmetries. These symmetries are retained after renormalization, and are fundamental to. It would not be possible without the implications of these identities, the QCD equivalent of the Ward ID's are the SlavnovTaylor identities

$$\mathcal{L} = \partial_\mu \phi^* \partial^\mu \phi - m^2 \phi^* \phi - \lambda (\phi^* \phi)^2. \tag{3.4}$$

This Lagrangian is invariant under global $U(1)$ transformation

$$\phi^{i\alpha} \phi, \tag{3.5}$$

where α is an arbitrary real constant. The chiral symmetry present involves hadrons at low energies taking place in the nonperturbative region of QCD. This will carry large implications surrounding global symmetry breaking and the Goldstone bosons. Chiral symmetry breaking provides insight into interactions at low momentum transfer. The chiral perturbation theories that cover some of this ground effectively use the Lagrangian for low energy interactions of the light pseudo-scalars. This effective Lagrangian can then be used as the basis of approach in studying these Nambu-Goldstone modes as a result. Ignoring renormalizability, the mass of the σ is adjusted by making the walls of the double potential well tighter further restricting oscillations, when in the limit of infinitely fast oscillations you end up restricting the π fields to a sphere. This limit is the non-renormalizable non-linear sigma

model in Gell-Mann and Levy's paper [60]. In the nonlinear sigma model, a field theory was constructed where the field values were restricted to a manifold. The term "current algebra" is also sometimes used for a special case when the manifold is a group. The modern version of the current algebra is Chiral Perturbation Theory, (χPT). Naturally, we will start with the chiral anomaly showing up in the Γ_π, namely $\pi^0 \to \gamma\gamma$. The verification of colour charge had been realized by this process as well. Due to the methods of current algebra, the decay rate for $\pi^0 \to \gamma\gamma$ calculated with the small masses of the u and d quarks. It comes into an agreement with the observed decay rate only when each individual flavour quark exists with the possibility to obtain any of the three colour states [44].

3.2 V-A Theory of Charged Currents

It was discovered by Wu in 1957 that helped to discover and establish a parity violation in the weak interaction, namely processes that undergo nuclear β-decay involving a sample of $^{60}Co\,(J = 5)$ at $0.01\,K$ in a solenoid [7]. The experiment established that the conservation of parity is violated in the weak interaction. The alignment of the ^{60}Co had measurements taken from angular distribution of γ-rays from a sample of ^{60}Ni. A way to measure relative intensities of the emitted electrons interacting with the present magnetic field direction was measured, showing consistency via

$$\begin{aligned} I(\theta) &= 1 - < J > \cdot \mathbf{p}/E \\ &= 1 - P_v cos\theta \end{aligned} \tag{3.6}$$

v, $\mathbf{p}$ and E are the speed of the electron, momentum and energy, with P being the polarizations magnitude, while θ is angle of emission of electron with respect to $< J >$. We have to note the angular momentum, $\mathbf{J}$ being an axial

vector operating under the transformation $< \mathbf{J} > \rightarrow < \mathbf{J} >$ under **P,** while **P** is a polar vector under transformation going as $\mathbf{p} \rightarrow \mathbf{p}$. This gives the result in the now parity transformed system [7]

$$I_{\mathbf{p}}(\theta) = 1 + P_v cos\theta. \tag{3.7}$$

When compared to the result in equation (3.10) it shows a sign difference distinguishing separate coordinate systems. We have a pseudoscalar quantity $< \mathbf{J} > \cdot \mathbf{p}$ as well as a scalar quantity '1' [7].

3.3 Spontaneous Symmetry Breaking

3.3.1 The $\pi^0 \rightarrow \gamma\gamma$ Transition

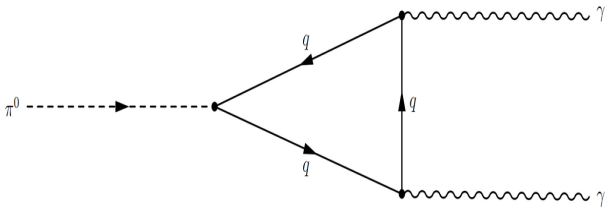

FIGURE 3.1: $\pi^0 \rightarrow \gamma\gamma$ decay additionally is where observed spontaneous symmetry breaking from the chiral anomaly takes place. The goldstone bosons giving rise to vector boson masses as well as the Higgs mechanism are observed in this process [61].

Consider a hadronic process mediated by two local quark currents, we can consider the separation from each other by an average long distance of $\mathcal{O}\frac{1}{\Lambda_{QCD}}$, and this is where we lose the notion of locality [4]. π^0 decay problem proved to unravel a great deal of physics contributing to the SM puzzle. One implication being the decay rate for $\pi^0 \rightarrow 2\gamma$ was only in good agreement with theoretical results $\iff N_c = 3$. This was the first evidence for colour

in quarks [9]. We proceed to obtain the decay rate of the pion from first principles and compare it to the latest experimental data and take note of the accuracy when compared with experimental results. The rate for the above process in 3.1 is determined by

$$\langle 0|\, J_\alpha(x) J_\beta(y)\phi(0)\,|0\rangle = \frac{1}{f_\pi m_\pi^2}\,\langle 0|\, J_\alpha(x) J_\beta(y)\partial_\mu A^\mu(0)\,|0\rangle\,, \tag{3.8}$$

J_α being is the electromagnetic current and is represented by A on the right hand side, giving $f_\pi \approx 93\ MeV$

$$\approx \Gamma_\pi,$$

as measured from $\pi^- \to \mu\bar{\nu}_\mu$

$$\langle 0|\, A^\mu(0)\,|\pi(p)\rangle = i f_\pi p^\mu. \tag{3.9}$$

The rate for the decay is calculable using the diagram shown above in Fig. 3.1. We obtain from this an absolute prediction for the decay rate,

$$\Gamma(\pi^0 \to \gamma\gamma) = \zeta^2(\frac{\alpha}{\pi})^2\frac{1}{64\pi}\frac{m_\pi^3}{f_\pi^2} = 7.6\,\zeta^2\,eV. \tag{3.10}$$

ζ is the color factor for three colours of the fractionally charged quarks. Remarkably the experimentally measured value reads $7.7 \pm 0.6\,eV$ [4,6].

3.3.2 The Yukawa Interaction

The Klein-Gordon equation describes the pion electromagnetic Form Factor where we need to take into account its electromagnetic potential energy. We can calculate matrix elements between states by the following,

$$\langle p|\,(J_\mu - J_{5\mu})\,|n\rangle\,,\ \langle 0|\,(J_\mu - J_{5\mu})\,|\pi^-\rangle\,, \tag{3.11}$$

J_μ and $J_{5\mu}$ being two currents that transform as a Lorentz vector, and axial vector respectively. This corresponds to three semi-leptonic decay processes [35]

$$\begin{aligned} n &\to p + e^- + \overline{\nu} \\ \pi^- &\to e^- + \overline{\nu} \\ \pi^- &\to \pi^0 + e^- + \overline{\nu}^- n \to p + e^- + \overline{\nu}. \end{aligned} \tag{3.12}$$

It was the neutron β decay process $n \to p + e^- + \overline{\nu}$ from which Fermi initially began to construct his theory. He initially added a term in the original Lagrangian as

$$\mathcal{L} = G[\overline{e}\gamma^\mu(1-\gamma_5)\nu][(\overline{p}\gamma_\mu)n], \tag{3.13}$$

where n is a neutron field annihilating a neutron, p a proton field annihilating a proton, ν a neutrino field annihilating a neutrino, and e an electron field annihilating an electron [35]. The strong interaction must be treated to all orders in the strong coupling, the calculation of the matrix elements that we need in this approach introduces a problem in the strong interaction [14]. Fermi did not go on to write separate Lagranians for each nucleus at play. Nuclear theorists at the time proceeded to calculate the matrix element $\langle Z+1, A| \left[\overline{p}\gamma_\mu(1-\gamma_5)n\right] |Z, A\rangle$. This is for the weak interaction, for the strong interaction the theorist calculate the matrix elements that look like $\langle n| \left(J_\mu - J_{5\mu}\right) |n\rangle$. We think of J_μ and $J_{5\mu}$ as the quantum operators, and as mentioned are the two currents transforming as Lorentz vectors [4, 35].

3.4 Non-local Vacuum Condensates

Quark anti-quark and gluon fields fluctuate giving way to a nonvanishing average density vacuum st [4]. Correlation functions interact with the QCD vacuum fields allowing insight to be gained regarding its dynamical

behavior. The distribution amplitude is the fundamental gauge invariant wavefunction which describes the fractional longitudinal momentum distributions of the valence quarks in a hadron integrated over transverse momentum up to the scale Q. The pions electromagnetic FF can be written as [62]

$$F_\pi(Q^2) = \int_0^1 dx \int_0^1 dy \phi_\pi^*(y,Q) T_H(x,y,Q) \phi_\pi(x,Q)(1+\mathcal{O}(\frac{1}{Q})). \quad (3.14)$$

In other words the DA's in our case represent the momentum fraction distributions of partons in the meson that is in a particular Fock state [63,64]. Hard exclusive processes producing pions in the final state with sufficient energy are sensitive to momentum fraction distributions of the valence quarks. This occurs at small transverse separations and is more specifically a descriptor of the pion DA. With this we can define the matrix elements of a non-local light-ray quark anti-quark operator [64, 65]. The distribution amplitude in view of its minimal number of constituents is related to the Bethe-Salpeter wave function. This equation essentially arises from the Dyson-Schwinger equation, and describes the bound states of a two-body system [64]. ϕ_{BS} by

$$\phi x \int^{|k_\perp < \mu|} d^2 k_\perp \phi_{BS}(x, k_\perp). \quad (3.15)$$

$\phi(x)$ represents the DA as a function of the parton, integrated over the parton distribution and the transverse momentum of the constituents. The standard approach to DAs, which is due to Brodsky and Lepage, considers the hadron's parton decomposition in the infinite momentum frame, in other words, very close to c. There is also a mathematically equivalent formalism that requires a differed approach which is the light-cone quantization [66]. Either way, power suppressed contributions to exclusive processes in QCD, which are commonly referred to higher twist corrections, are thought to originate from three different sources, with the list given from [63],

- When bad components in the wave function effect the distribution such as wrong spin projections;
- Quark antiquark p_T contributions in the leading twist components that cause integrals to have additional factors of $k_\perp^2$.
- Higher Fock states that contain a greater number of quark/anti-quark pairs and/or gluons than needed.

The pion DA can be represented as the series in the eigenfunctions of the leading order evolution equation, which is in the form of Gegenbauer polynomials [67], and where we will see a bit more on the resulting Mellin space in *Chapter* 4. It is usually assumed that the series is convergent and doing so necessitates the use of only a finite number of terms to be considered in the series. The pion DA is not directly measurable and has to be calculated from the data or additionally be constructed from nonperturbative models. When analyzing theoretically insights are gained and constructed from the first few moments, [68, 69].

$$< \xi^N >_\pi \equiv \int_0^1 dx (2x-1)^N \phi_\pi^{(2)}(x, \mu^2), \tag{3.16}$$

where $N = 2, 4, ...$, $\xi = 2x - 1 = x - \overline{x}, \overline{x} = 1 - x$, with x being the partial longitudinal momentum of the valence quark in the pion. Lattice results gave a measurement for the second moment $< \xi^2 >_\pi$, as can be seen in [70, 71]. There does not seem to be yet enough data obtained from experiment to constrain the moments above $N = 6$ These techniques are further discussed in [72, 73].

PDFs tell us about the partonic content of hadrons, but as single-particle probabilities they tell us nothing about correlations between quarks and gluons. We can obtain the correlation function in terms of interpolating fields constructed from the quark and gluon fields, and the correlation function

is computed by Wilson's OPE. DAs tell us about hadronic structure at amplitude level. We can expand DAs in Gegenbauer polynomials, and their coefficients are the moments. The main tool for studying DAs is QCD light cone sum rules. The pion DA can be defined through the matrix element of a non-local axial current on the light cone

$$< 0|\bar{d}(z)\gamma_\mu\gamma_5 E(z,0)u(0)|\pi(P) > |_{z^2=0} = if_\pi P_\mu \int_0^1 dx e^{ix(zP)}\phi_\pi(x,\mu^2). \tag{3.17}$$

We achieve gauge invariance for the pion DA expressed in Equation 3.18 through the Fock-Schwinger $E(z,0) = \mathcal{P}e^{ig\int_0^z A_\mu(\tau)d\tau^\mu}$ [74]. The physical meaning of the light cone object is that it is the amplitude for the transition of the physical pion to a pair of valence quarks u and d, separated at light cone. It has momentum fractions xP and $\bar{x}P$. This object includes nonperturbative information about the physical pion. It is important to note and introduce that it obeys the Efremov and Radyushikin-Brodsky and Lepage (ER-BL) evolution equation with respect to μ^2. This ties in with that it is convenient to represent the pion DA as an expansion in terms of Gegenbauer polynomials $C_n^{3/2}(2x-1)$, being the 1-loop eigenfunctions of the ERBL kernel [64, 74],

$$\phi_\pi(x;\mu^2) = \phi^{as}(x)[1 + a_2(\mu^2)C_2^{3/2}(2x-1) + a_4(\mu^2)C_4^{3/2}(2x-1) + ...]. \tag{3.18}$$

This means to transfer all the μ^2 dependence of the pion DA into the Gegenbauer coefficients $a_2(\mu^2), a_4(\mu^2), ...$ We are confined to using the non perturbative approach if we wish to obtain the pion DA in the theory. And the first nontrivial model [75] was constructed using the standard QCD sum rule approach to estimate the first two moments of the pion DA [76]

$$< \zeta^2 >_\pi \text{ and } < \zeta^4 >_\pi . \tag{3.19}$$

The first five moments were obtained for the pion DA from NLC QCD sum rules. $< \zeta^{2N} >_{\pi}$ with $N = 1, ...5$.

Correlation Functions

In upcoming chapters we will discuss an accurate way to calculate how correlation functions are influenced by vacuum-field contributions. At $Q^2 >> \Lambda^2_{QCD}$, the distance between the $\bar{q}$ becomes smaller than the scale of the vacuum fluctuations and treat them as static for the purpose of obtaining the average characteristic of the quark fields. Vacuum gluons are emitted and absorbed virtually interchanging with their vacuum counterparts leading to quark-gluon interactions [19]. We can expand the product of the two currents in a series of local operators as follows

$$i \int d^4x e^{i1\cdot x} T\{\overline{\psi}(x)\gamma_\mu\psi(x), \overline{\psi}(0)\gamma_\nu\psi(0)\} = (q_\mu q_\nu - q^2 g_{\mu\nu}) \sum_d C_d(q^2) O_d, \tag{3.20}$$

representing the vacuum condensates with

$$\Pi(q^2) = \sum_d C_d(q^2) \langle 0| O_d |0\rangle . \tag{3.21}$$

with $d = 0$ being a representation of the unit operator attributed to QCD vacuum fields taking place of quark and gluon fields, $\overline{\psi}$, ψ and $G^a_{\mu\nu}$. The operators are ordered according to their dimension d, with perturbative contribution corresponding to the Wilson coefficient, this is given as

$$C_d(q^2) = \Pi^{pert}(q^2), \ \langle 0| O_0 |0\rangle \equiv 1. \tag{3.22}$$

Further making the point that QCD vacuum condensates violate chiral symmetry and its contribution vanishes in the chiral limit, $m = 0$.

The Wilson coefficient receives dominant contributions from regions undergoing short distance interactions, and we need to take into consideration of the product of the quark currents present concerning their quantum number properties. The interactions dependence is encoded within the Wilson coefficient seen in Equation 3.22. The OPE is an invaluable tool used in high energy QCD phenomenology, it is used to define PDF's that have been extracted from experiments, and the OPE with its renormalization group is an operative part in analyzing DIS experiments in which involve lepton-nucleon scattering. When considering a total cross section for the scattering of a lepton, for instance, by an initial hadron, we rely on unitarity occurring as a linear combination of the amplitude components [4, 6],

$$\int d^4x e^{-ik\cdot x} \langle H| J^\mu(x) J^\nu(0) |H\rangle . \tag{3.23}$$

k represents the four-momentum that transfers from lepton to the hadrons, with H being the hadron in the process. This is seen in DIS experiments where we allow the momentum k to approach infinity while setting the high momentum limit of the Fourier transform. One can derive spectral function sum rules in this high momentum limit when replacing the hadron state $|H\rangle$ replaced with the vacuum. A point to make is when taking a simple case of the operator product, $j^\mu(x)j^\nu(0)$, and analytic in x^μ, the Fourier transform would exponentially decay as the Fourier variable k approaches infinity. This description represents Wilson's attempt to bypass quantum field theory and attempt to formulate additional approaches, while not being a full replacement, the approach led to general results that benefited the understanding of QFT properties [9]. The OPE with regard to spectral function sum rules places constraints on the spectral functions of applicable currents.

3.4.1 Pion Two-Point Correlation Function

The pion two-point correlation function is often used to calculate the pion-nucleon coupling, $g_{\pi N}$, in QCD sum rules. We view a correlation function in terms of interpolating field operators by way of its quark and gluon interpolators, and what follows is the employment of Wilson's OPE to compute corresponding correlation functions [64]. Physical quantity of interest match the two descriptions in the deep Euclidean region $(q^2) = -\infty$ via the dispersion relations, the pion two-point correlation function is as follows

$$\Pi(q,p) = i \int d^4x e^{iq\cdot x} \langle 0| T[J_N(x)\bar{J}_N(0)] |\pi(p)\rangle \tag{3.24}$$

and with it can calculate pion-nucleon coupling, $g_{\pi N}$ in QCD sum rules [64, 77, 78].

General correlations between PDFs and physical observables can be computed within the Monte Carlo approach, and can compute the correlation coefficient

$$\rho[A,B] = \frac{N_{rep}}{(N_{rep}-1)} \frac{< AB >_{rep} - < A >_{rep} < B >_{rep}}{\sigma_A \sigma_B} \tag{3.25}$$

which computes averages over an ensemble of the N_{rep} values corresponding to observables. $\sigma_{A,B}$ are the standard deviations of the ensembles. The quantity ρ characterizes whether two observables (or PDFs) are correlated $(\rho \approx 1)$, anti-correlated $(\rho \approx -1)$, or uncorrelated $(\rho \approx 0)$ [79].

3.4.2 Form Factors

Electroproduction is one of the main ways to access FF using the "pion cloud" of the proton via the $p(e, e^{'}\pi^{+})$ process. Furthermore, the FF play an important role due to being the most convenient link between experimental observation and theoretical analysis, they also serve as the matrix elements

[80]. The pion electromagnetic FF, $F_\pi S$ in the time-like region $q^2 = s > 4m_\pi^2$ is directly accessible measuring the $e^+e^- \to \pi^+\pi^-$ cross section at a given center of mass energy $\sqrt{s}$ of the collision. It can be seen from perturbative QCD the pion FF, F_π, is [81–84]

$$F_\pi(Q^2; \mu_R^2 = F_\pi^{LD}(Q^2) + F_\pi^{Fact-WI}(Q^2; \mu_R^2). \tag{3.26}$$

The kinematics probed in the $CELLO$ and the $CLEO$ experiments involves a quasi-real photon with $q^2 \to 0$ [85,86]. The method of Light-Cone QCD sum rules allows the problem of preventing a straightforward QCD calculation of the FF to be avoided by performing the means of QCD calculations at sufficiently large $q^2(\gamma^*)$. It is then sufficient to use dispersion relations to approach the mass-shell photon with zero virtuality. This calculation scheme was proposed by [87]. Processes with two photons in the initial state, and one far off-shell with the other quasi real is

$$\gamma^* + \gamma \to \pi^0. \tag{3.27}$$

This provides a useful tool to access (after their fusion) the partonic structure of the produced hadronic states, the pseudoscalar mesons. Experimentally the photon-to-pion transition FF of this kind has been measured by $CLEO$ with high precision extending the range of Q^2 up to 9 GeV, as compared to the previous low-momentum $CELLO$ data [88]. To see where both perturbative and non-perturbative QCD play roles in the process, we can look at highly energetic photons, where perturbative QCD works well because of factorization being applicable at some factorization scale μ_F^2, so the process can be put into the form of a convolution as follows,

$$F^{\gamma^*\gamma^*\pi}(Q^2, q^2) = C(Q^2, q^2, \mu_F^2, x) \otimes \phi_\pi(x, \mu_F^2) + \mathcal{O}(Q^{-4}) \tag{3.28}$$

which contains the hard part C, which is calculable within perturbation theory, and a wave-function part ϕ_π that is the (leading) second order pion distribution amplitude and has to be modeled within some nonperturbative framework, or extracted from experiment.

The standard definition of the pion electromagnetic FF in the spacelike region is

$$< \pi^+(p_2)|j_\mu^{em}|\pi^+(p1) >= (p1+p2)_\mu F_\pi(q^2) \tag{3.29}$$

where $j_\mu^{em} = (1/2)(\overline{\mu}\gamma_\mu u - \overline{d}\gamma_\mu d)$ is the isovector component of the quark electromagnetic current, and $q = p_2 - p_1$ is the momentum transfer. The FF obeys the normalization condition $F_\pi(0) = 1$, and represents the electric charge of π^+. The standard dispersion relation [84].

$$F_\pi(q^2) = \frac{1}{\pi}\int_{s_0}^{\infty} ds \frac{ImF_\pi(s)}{s - q^2 - i\epsilon} \tag{3.30}$$

connect the spacelike pion FF $F_\pi(q^2)$ at $|q^2 < 0$ with the imaginary part of the time-like FF $F_\pi(s)$ integrated over s above the two-pion threshold $s_0 \equiv 4m_\pi^2$ [4, 84].

Chapter 4

The Parton Model & Theory of Calculation

4.0.1 Introduction

In this chapter, having now at this point introduced background and tools relevant to the physics in question, it perhaps is appropriate to introduce the calculations in theory before heading into Chapters five and six. Perturbative *QCD* predicts the evolution of the structure functions, accompanied by factorization theorems along with remedies for sources of uncertainty will also be topics of study. TMD distributions are an extension of the concept of PDFs, and provide initial state conditions to make predictions for hadron processes. Introduction to Wigner distributions which when integrated over, and considering all coordinates, will allow us to obtain the TMD distributions. Essentially, we end up with three-dimensional densities in momentum space [17] with the distribution functions are obtained from experiment and theory. Beginning with an example for if we wish to compute the Higgs production cross section (σ) at the LHC, we would then employ

$$\sigma_{pp} \to H = \sum_{a,b} f_{a/P} \otimes f_{b/P} \otimes \omega_{ab} \to H \tag{4.1}$$

where PDFs $f_{a/P}$ and $f_{b/P}$ provide probability densities for partons a and b in the process, and $\omega_{ab} \to H$ is the probability density for partons a and b producing the *Higgs* [89]. Techniques have been and are continuing to be

developed for obtaining information on the dynamical character of the confined dynamics of quarks and gluons within the hadron. They provide additional information for hadrons that complements the accompanying PDFs and GPDs. One small example being the gluons carrying away transverse momentum in a process, more information regarding these details provides a glimpse into this nonperturbative realm. Dedicated studies for low P_T resummation have been carried out [90–93]. To continue, a short introduction to the parton model and the PDF

4.1 An Introduction to The Parton Model

The parton model is scaled with $DGLAP$ evolution equations while leaving room for higher-order corrections to hard scattering processes to be implemented [44]. The parton model applies to any process involving hadronic cross sections with large momentum transfer. The parton model was first introduced by Richard Feynman in 1969 as a way to analyze in more detail the constituents of high-energy collisions. This was additionally applied to electron-proton DIS by Bjorken and Paschos. At high energies hadrons look like they are point-like and nearly free objects that are dubbed partons. The high-energy interactions with the initial state hadrons can be described in terms of these point-like partons. The flux of the incoming partons has to be known, and these can be expressed in terms of PDFs. The PDF is the number density of partons carrying a fraction of the parent hadron momentum. The QCD-improved parton model relies on factorization theorems and provides the framework in which almost all cross sections at current high energy colliders are computed. The PDFs are non-perturbative objects and have to be fixed by experimental information. Additionally, PDFs are determined by a global analysis of all available experimental information. Since the PDFs are connected to each other by evolution equations, leaving out certain data

may bias the PDFs towards a specific experiment leading to inaccurate estimations. Here is a quick primer on a global analysis. First, we should choose suitable input functions such as $f_i(x, Q_0; p_i, 1, p_i, 2, ...)$ for the x-dependence of the various partons $(i = u, d, s, ..., g)$ at some initial scale Q_0, where Q_0 has to lie in the perturbative regime such that the perturbatively known evolution equations are applicable. Typically $Q_0 = 1 - 2GeV$ is used. For each point denoted by k, we run the PDFs up an appropriate scale Q_k by using the $DGLAP$ evolution equations. The corresponding theory value is computed in the parton model using the PDFs at the scale Q_k combined with the hard scattering cross sections for the process to which the data point belongs. For each data point k the χ^2_k between theoretical and the experimental value is calculated. By summing up all χ^2_k one obtains the $\chi^2[p_i, 1, p_i, 2, ...] = \sum_k \chi^2_k$ for a given set of parameters $p_1, 1, p_i, 2, ...$ These parameters are used to find a global minimum of the χ^2 function is found. The optimal fit parameters finally determine the best-fit PDF. A review of some pion PDFs is highlighted with references to associated work [94–98].

In 1984, the idea of pionic global analysis came up to summarize data from several Drell-Yan experiments. It turns out the DY data makes no prediction for momentum fraction $x < 0.2$ which leads to large uncertainties for small x. Additionally, it was not sensitive to the gluon or the sea quarks because the DY process is not dominated by gluon and sea contributions. In 1989, the collaborators used prompt photon production, which is partly dominated by qg scattering. The data was taken from $\pi^+ p$ or $\pi^- p$ scattering experiment helping to constrain better PDFs. The notorious issue of ambiguous sea distributions were still not resolved. In 1991, two new approaches were developed using NLO, while the previous pion PDFs were determined in LO calculations. One approach [94] made good assumption of a valence like parton structure at a low resolution scale Q^2 that determines the gluon and sea distribution. Sea and valence distribution were generated

radiatively from this data evaluated out of the valence distribution from DY data. From [95,96], a new idea came up to constrain the pion PDFs based on nucleonic PDFs while using a constituent quark model. One could determine the valence distribution by DY data, which when combined with nucleonic PDFs shed light to new quark and gluon distributions. Mellin moments are a tool used in describing PDFs. PDFs can be either described directly in the x-space or in the Mellin momentum space. It is defined by the transformation

$$f(N) = \int_0^1 dx x^{N-1} f(x), N_{\in}\mathbb{C}. \tag{4.2}$$

Convolution integrals can now be changed into a simple product. The Mellin space evolution equations can be solved analytically, and to get back to x-space we use

$$f(x) = \frac{1}{w\pi i} \int_C dN x^{-N} f(N) \tag{4.3}$$

Where C is an arbitrary contour in the complex plane which has to lie right of all singularities and extend from $-i\infty$ to $i\infty$.

Early SLAC and Bjorkin Scaling Success of Parton Model

The evidence for quarks as constituents of the nucleon emerged from the pursuit and development of hadron spectroscopy. Confinement, which forbids us from observing free quarks in nature was the hurdle preventing wide acceptance of quarks existing in nature. The Stanford Linear Accelerator Centre (SLAC) in DIS experiments eventually observed Bjorken scaling, and so began the success of Feynman's parton model, in which states quarks are the basis fields describing nucleon structure, and consequently was verified and accepted by the community.

Factorization and evolution equations allow us to derive the parton model in ways enabling computation of scale-breaking effects [6,14]. From the field theory realization of the parton model, factorization permits the separation

of short from long distance dependence, essentially separating perturbative from non-perturbative regions [14, 44, 99].

4.1.1 Parton Distribution Functions

Starting with Deeply Inelastic Scattering, unpolarized and longitudinally-polarization quark densities have simple relations to structure functions, structure functions encase important properties of cross sections in experiments, and rely only on elementary properties of electroweak interactions in order to define them. The parton densities can be defined definitively as solely related to the experiment through factorization theorems we derive in terms of said structure functions and other cross sections available to parton the densities [44]. This becomes necessary in the calculation of particle cross-sections at collider experiments. The master formula for PDF's is given as [13].

$$\sigma_x = \sum_{a,b} \int_0^1 dx_1 dx_2 f_a(x_1, \mu_F^2) f_b(x_2, \mu_F^2) \times \hat{\sigma}_{a,b\to x}(x_1, x_2, \alpha_s(\mu_R^2), \frac{Q^2}{\mu_F}, \frac{Q^2}{\mu_R}). \tag{4.4}$$

$$\hat{\sigma}_{ab\to} x = \sigma_0 + \alpha_s \sigma_1 + \alpha_s^2 \sigma_2 + ... \tag{4.5}$$

Equation 4.4 describes the PDF in terms of the scattering cross section, σ, and summing over the constituents of the parton showers in scattering experiments with x_a and x_b representing the outgoing partons. μ_F is the factorization scale where the DGLAP evolution equations enter, which we discuss in more detail in the next subsection. μ_R is the renormalization scale respectively. In Equation 4.5, σ_0 is leading order, $\alpha_s\sigma_1$ next to leading order, and $\alpha_s^2\sigma_2$ is the next-to-next-to leading order contribution in $QCD's$ coupling expansion. The unpolarized cross-section for DIS with single photon exchange is [100]

$$\frac{d\sigma^\gamma}{dx_A Q^2} = \frac{2\pi\alpha_s^2}{x_A Q^4}\left[\left(1 + (1+y)^2\right) F_2^\gamma(x, Q^2) - y^2 F_L^\gamma(x, Q^2)\right] \tag{4.6}$$

The longitudinally polarized cross-section is

$$\frac{d\delta_L\sigma^\gamma(\lambda)}{dx_A dQ^2} = \frac{4\pi\alpha_e^2}{x_A Q^4}\Big[-2\lambda\Big(1-(1-y)^2\Big)xg_1^\gamma(x,Q^2)+y^2 g_L^\gamma(x,Q^2)\Big] \tag{4.7}$$

The Bjorkin limit, $Q^2, \nu \to \infty \,|\, x =$ fixed comes from J.D. Bjorken's argument in 1968 that in the limit of photons interacting with the target constituents (partons,x) will involve no dimension scale, and so then

$$F_2^\gamma(x,Q^2) \to F_2^\gamma(x) \tag{4.8}$$

This was confirmed at SLAC in 1968 and gave the first evidence toward partons being an object of interest [100].

We can choose a frame with $q_\perp = 0$ and arriving to the photon moment

$$q = \Big[\nu, 0, 0, -\sqrt{\nu^2+Q^2}\Big] \to q = \Big[\nu, 0, 0, -\nu - xM_N\Big] \tag{4.9}$$

, with light cone coordinates

$$q^\pm = \frac{1}{\sqrt{2}(q^0 \pm q^3} \to a\cdot b = a^+b^- + a^-b^+ - \overrightarrow{a_\perp}\cdot\overrightarrow{b_\perp}. \tag{4.10}$$

With the Bjorken limit

$$q^- \to \infty q^+ \to -xM_N/\sqrt{2} \tag{4.11}$$

and

$$x = \frac{Q^2}{2p} = -\frac{q^+q^-}{q^-p^+ + q^+p^-} \to -\frac{q^+}{p^+}. \tag{4.12}$$

With lightcone dispersion relation

$$k^- = \frac{m^2 + \overrightarrow{k}^2}{k^+} \tag{4.13}$$

This is only satisfied for $k^{'} = k + q$ if $k^{'+} = 0$ implying $k^{+} = -q^{+}\, x$ has no a physical meaning in terms of lightcone momentum fraction carried by a struck quark prior to photon collision. giving, [100]

$$x = \frac{k^{+}}{p^{+}}. \tag{4.14}$$

4.1.2 DGLAP Evolution of Hadronic Structure Functions

The evolution equations describing the parton distribution function discussed in the previous subsection contain amplitudes that rely on evolution kernels on a renormalization scale, α_s [13]. The distributions in the proton are changing from one value of Q to another. We first find the proton wave function, obtain a valence distribution including gluon distribution as a function of x, and a sea distribution for quarks and anti-quarks. We then integrate the DGLAP equations from low to high Q. The valence quarks emit gluons with their distributions vary at the varying $Q's$, and eventually split into additional gluons and is where splitting functions are employed. We arrive at $t\bar{c}$, and $s\bar{s}$ represent the initial state of the hard processes. Gluons can split substantially to b quarks, these are considered a substantially heavier third generation quark when compared to the light quarks, d , u , s. It may be interesting to ponder LHC processes using the b partons in the proton to initiate reactions that might occur in the third generation, having said this there is a future planned 100 TeV collider with plans to include t quarks as partons in the proton generated by these evolution equations [38]. This of course is the intuitive way that we might do it. In practice, we make a free model of the PDF, and introduce five or six parameters per distribution. Next we write a paramaterized set of equations that represent the PDF at one value of Q, and use the DGLAP equations to evolve this PDF to any number of values of Q appropriate to a number of experiments we are interested in as seen in the

pion example in subsection 4.1.1, and will define further in coming subsections. One example of flexibility in a sense is we can choose Q at of order one, or three, if we wish to represent the old SLAC data, or order of thirty to represent the muon-proton, or muon-nucleus scattering data at CERN in the 1980's. We could also, for example, scale Q of order one hundred, or even hundred's to represent $e^- p$ data that was generated at the HERA collider. For each data set you would then fit these same parameters, and by doing a global fit we arrive at an understanding of the shape of the parton distributions, which now have to be dynamical in Q^2. What we see with this phenomenological approach is the inputs for what we see in the LHC beam to initiate a hard reaction, and serves as a powerful phenomenological tool [38, 101].

We cannot fully trust calculations of $f(x, Q)$ at low Q in the nonperturbative IR regime, we can however trust large Q calculations of changes in $f(x, Q)$ from Q to $Q + \delta Q$. This translates to us being able to trust evolution equations, which necessitates our returning to experiment for information regarding relevant initial conditions. The $LQCD$ community has many promising insights and approaches to nonperturbative aspects of this approach, and is working at providing more accurate descriptions.

In application of DGLAP equations, the PDFs acquire a factorization scale, μF, being that when momentum is carried away by secondary partons, the scale evolution of the partons are described by the equations and is given as [83, 102–104]

$$Q\frac{d}{dQ}f_i(x,Q) = \frac{\alpha_s(Q)}{\pi}\int_x^1 \frac{dz}{z}(P_{qq}(z)f_i(\frac{x}{z},Q) + P_{qg}(z)f_g(\frac{x}{z},Q))$$

$$Q\frac{d}{dQ}f_{\bar{i}}(x,Q) = \frac{\alpha_s(Q)}{\pi}\int_x^1 \frac{dz}{z}(P_{qq}(z)f_{\bar{i}}(\frac{x}{z},Q) + P_{qg}(z)f_g(\frac{x}{z},Q)) \tag{4.15}$$

$$Q\frac{d}{dQ}f_g(x,Q) = \frac{\alpha_s(Q)}{\pi}\int_x^1 \frac{dz}{z}(P_{gq}(z)\Sigma_i[f_i(\frac{x}{z},Q) + f_{\bar{i}}(\frac{x}{2},Q)] + P_{gg}(z)f_g(\frac{x}{z},Q)).$$

A challenge presented being the self interaction of the colour fields adds a contribution due to their non-linear behavior. We split one gluon into a gluon pair $g \to gg$, and then contributes to the splitting function as P_{gg}. The splitting functions give the colour factors associated with one gluon splitting into additional gluons, and is addressed as

$$
\begin{aligned}
P_{qq}(z) &= \frac{4}{3}\left[\frac{1+z^2}{(1-z)} + \frac{3}{2}\delta(1-z)\right] \\
P_{gq}(z) &= \frac{4}{3}\left[\frac{1+(1-z)^2}{z}\right] \\
P_{qg}(z) &= \frac{1}{2}\left[z^2 + (1-z)^2\right] \\
P_{gg}(z) &= 6\left[\frac{1-z}{z} + \frac{z}{(1-z)} + z(1-z) + (\frac{11}{12} - \frac{n_f}{18})\delta(1-z)\right].
\end{aligned}
\tag{4.16}
$$

As Q increases, additional splitting occurs necessitating the functions to operate in the lower x region. [101]. s

4.1.3 Luminosity Functions

Luminosities provide the link between experimental and theoretical cross section measurements. ManeParse [105] is used through the Mathematica framework to calculate integrated luminosities, which have been written as a convolution of PDFs for this task. Once we have these distributions, we can then try to compile luminosity functions which can be used to estimate reaction rates at the LHC. That is, we can use these equations to describe collisions in terms of luminosity. Luminosity is the proton count per area beam and is obtained from the geometry and number of particles flowing per unit area. Given two protons colliding at a certain energy, we have resultant outgoing quark, gluon and anti-quark jets, we can describe the partons in terms of the luminosity, such as $q, \overline{q}$ collisions, or $q\, g$ collisions in that process.

Cross-section for link between experimental and theoretical measurements

$$\sigma(\hat{s}) = \sum_{ij} \int_{\tau}^{1} \frac{d\mathcal{L}_{ij}}{d\tau} \hat{\sigma}_{ij}(\hat{s}) d\tau. \tag{4.17}$$

This is written as a convolution of PDFs and is easily calculable in ManeParse [105]. One advantage of ManeParse being the speed of the interpolation routine for numerical integration, giving the example from [105]

$$\frac{d\mathcal{L}_{ij}}{d\tau}(\tau, \mu) = \frac{1}{\delta_{ij} + 1} \int_{\tau}^{1} \frac{1}{x} \left[f_i(x, \mu) f_j\left(\frac{\tau}{x}, \mu\right) + f_j(x, \mu) f_i\left(\frac{\tau}{x}, \mu\right) \right] dx \tag{4.18}$$

This can be used to reproduce results and compare to other collaborations' PDF sets. Luminosity at the collider goes by the rate N describing events of any type is determined by the luminosity factor, denoted L, and we multiply L by the scattering process cross section σ.

$$N = L\sigma \tag{4.19}$$

L is fixed in the machines parameters, for $p\overline{p}$ we can consider

$$L = \frac{f}{\pi} \frac{N_p N_{\overline{p}}}{n_b} \frac{\gamma}{\sqrt{\beta_x^* \beta_y^* E_x^* E_y^*}}, \tag{4.20}$$

f is the revolution frequency, n_b is the number of bunches, and $\gamma = E/m$ is the relativistic factor. N_p, ($N_{\overline{p}}$ is the number of protons and (antiprotons), with $E_x^*/, E_y^*$ the transverse emittance of the beams, and $\beta_x^* \beta_y^*$ is the betatron oscillations of the beams [6]. We can factorize the cross-section for multiple jet emission in the collinear limit. The production of additional partons in juxtaposition to a jet direction can be described in a time-ordered probabilistic fashion such as a series of $1 - 2$ splittings, which occur successively one after another [106].

4.1.4 Toy Model cross-sections for $\sigma^{\mathcal{O}\alpha_s^0}$ and $\sigma^{\mathcal{O}\alpha_s^1}$ in the subtraction Formalism

In the next chapter, analysis from data sets containing the data from selected LHC runs, we analyze the cross-section at $\sigma^{\mathcal{O}\alpha_s^0}$ and $\sigma^{\mathcal{O}\alpha_s^1}$.

$$\begin{aligned}
\sigma^{\mathcal{O}\alpha_s^0} &= \int d\phi_{\mathcal{B}} \mathcal{B}_n(\phi_{\mathcal{B}}; \mu_F, \mu_R) \\
\sigma^{\mathcal{O}\alpha_s^0} &= \int d\phi_{\mathcal{B}} \Big[\mathcal{B}_n(\phi_{\mathcal{B}}; \mu_F, \mu_R,) + \mathcal{V}_n(\phi_{\mathcal{B}}; \mu_F, \mu_R) + \mathcal{I}_n^{(\mathcal{S})}(\phi_{\mathcal{B}}; \mu_F, \mu_R) \Big] \\
&\quad + \int d\phi_{\mathcal{B}} \Big[\mathcal{R}_n(\phi_{\mathcal{B}}; \mu_F, \mu_R,) + \mathcal{S}_n(\phi_{\mathcal{B}}; \mu_F, \mu_R) \Big]
\end{aligned} \tag{4.21}$$

$\phi_{\mathcal{B}}$ and $\phi_{\mathcal{R}}$ represent the Born and real-emission phase space, with the accompanying matrix elements for the Born, renormalized virtual, integrated subtraction, real-emission, and real subtraction contributions. With the real and integrated subtractions

$$\pm R_m(0) F_m^J \int_0^1 \frac{dx}{x^{1+\epsilon}}. \tag{4.22}$$

which are combined with the virtual correction $V_m F_m^J / \epsilon$ [13]. We will see how the subtraction method works when looking at W production at NLO in *Chapter* 6.

4.1.5 Jets

In colliders, the production of vector bosons constrains many of the processes in the SM. It also assists with bench marking parton luminosities. We use these to improve parton shower predictions as reconstruction of events and more accurate data becomes available [13]. We additionally have to deal with missing energy in the transverse plane (E_T), and a better understanding of the formation of the observed final states improves predictions and

searches for new physics. In *Chapter* 6, we will make use of these descriptions when reconstructing jet contributions, as well as needing to account for the missing E_T and $P\perp$. At lowest order, a parton is identified with a jet. When situations occur with additional radiation that is liable to fall inside or outside the cone, we have to consider theoretical cross sections taking into account the cone size [6]. We also have to take into account various renormalization and factorization scales, μ. Jet E_T, has the profile $\psi(r, R, E_T)$, and we define this as the average fraction of jet energy in the transverse plane. Figure 4.1 shows $V+$ *jet* processes. V denotes vector boson. We leverage fragmenta-

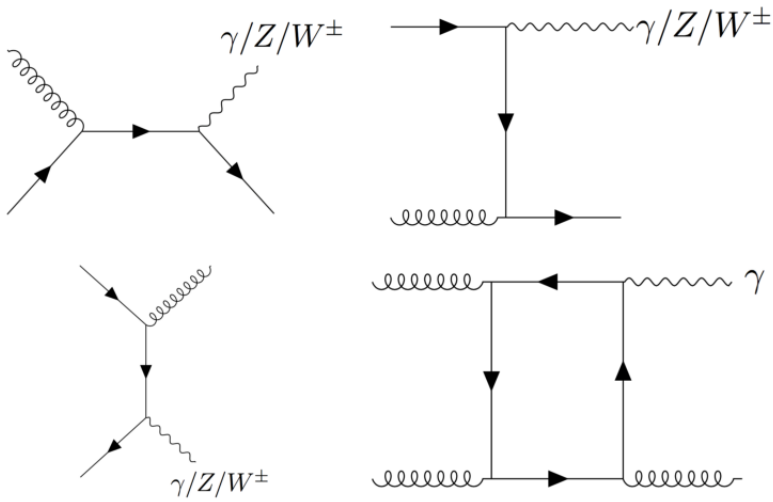

FIGURE 4.1: Feynman diagrams for $V +$ *jet* processes [107].

tion functions, one way is to incorporate DGLAP as well as modified leading logarithms (MLL). This requires the Mellin transforms of the hadron distribution to be expressed in terms of anomalous dimension, being a factor from the interaction, and leads to a perturbative expansion in half powers of α_s. Integer powers of α_s are related to fixed-order corrections. The half integer terms accuracy relies on resummation of soft and collinear logarithms [108].

4.2 *QCD* Sum Rules

Asymptotic freedom is realized when summing whole classes of higher order contributions [7]. *QCD* sum rules is a nonperturbative method to solving *QCD*, and is used to test the validity of interpolations, and the sum of the momentum fractions of the partons in question must equal one. We do this to as accurately as we can account for total momentum of the hadron. Sum rules in our context serve to validate routines that become assigned for the interpolation steps in calculations, in which considers the full momentum range, x for energy, Q [105]. PDF groups that are dedicated to PDF technology use different forms for paramaterization, an example being the CT14 fit, which we encounter in subsequent chapters in calculation, uses 28 free parameters, some of them fixed at reasonable values, or alternatively constrained by sum rules [13]. Broadly speaking, we work to establish a link between the condensate and phenomenology, and we construct sum rules from the information computed via correlation functions. The first application that employed the *QCD* sum rules to the pion wave function $\phi_\pi(x)$ was to calculate its decay constant, which we have seen in 3.3.1. This was the process in which Shifman, Vainschtein, and Zakharov pioneered their initial paper when developing the sum rule where they calculated $\phi_\pi(x)$ within 5% accuracy [109]. The *OPE* is the starting point for *QCD* analysis. An important note for our process is that depending on whether x is large or small, we will need to modify how we proceed with the expansion, and may need some modification.

Integrals over certain combinations of parton distributions hold certain values in the parton model. These integrals additionally go by the name sum rules. We can employ these sum rules up to perturbative corrections, and the limit with which we can access these perturbative methods with respect to the sum rule approach is constrained by the vanishing of the first moment

of the non-singlet anomalous dimensions to all orders when working in perturbation theory [6]. When we need to determine an unknown parameter regarding the hadrons, *QCD* sum rules have become a reliable prediction tool. There lies the issue of unknown structures of the hadronic dispersion integrals and this makes this particular approach difficult. Additionally, the accuracy is limited by approximations in the *OPE* of the correlation function.

Quark and gluon confinement in *QCD* is not attainable via direct experimental measurements of the fundamental *QCD* parameters. We need experimental based measurements since we rely on these to determine the parameters analytically. Once established lattice simulation provide accurate results. This however is still in a "black box" kind of way considering little is still known about their origins [110]. The latter may be obtained from an analytical approach which relying on the relation between Green's function, more specifically, when the *OPE* is carried out beyond perturbation theory and their hadronic counterparts. This relation follows from Cauchys theorem in the complex (squared) energy plane (quark-hadron duality), and is collectively known as the *QCD* sum rule [111]. There had not been analytic proof for confinement, and we are restricted to inference by way of parameterizing quark and gluon propagator corrections from what we can learn about the vacuum condensates [111]. The *OPE* comes in handy when needing to calculate correlation functions. [112]. $g_{\pi N}$ was calculated retaining the first nonperturbative terms in the *OPE*. the calculation was later improved in [78] using higher ordered terms in the *OPE*. The pion two-point correlation function was considered and evaluation of the *OPE* was done in the soft-pion limit $(p_\mu \to 0)$, considered the sum rule beyond the soft-pion limit [87, 113], however it was noted that another source pointed out in reference [114] that there may be a mistake in their calculation, which can invalidate the conclusions based on the sum rule beyond the soft-pion limit. *QCD* sum rules could depend on a specific Dirac structure, as pointed out in reference [114, 115],

where baryon sum rules were investigated. They found the chiral odd sum rule to be more reliable due to partial cancellation of the positive and negative parity excited baryons in the continuum. In the interest of this work, the *QCD* sum rules for the two-point correlation function are used [114], and three different sum rules were constructed starting with the correlation function with a charged pion [87]

$$\Pi(q,p) = i\int d^4x e^{iq.x} < 0|T[J_p(x)\bar{J}_n(0)]|\pi^+(p) > \tag{4.23}$$

The J_p is the proton interpolating field [116]

$$J_p = \epsilon_{abc}[u_a^T C\gamma_\mu u_b]\gamma_5\gamma^\mu d_c \tag{4.24}$$

we obtain the neutron interpolating field J_n by replacing $(ucd) \rightarrow (d,u)$. In the *OPE*, this leaves only the pion wave functions diquark moment [117]. The calculation of the correlator in the coordinate space contains the following diquark component of the pion wave function [117],

$$D^{\beta}_{aa'} \equiv < 0|u^{\alpha}_a(x)d^{-\beta}_{a'}(0)|\pi^+(p) > \tag{4.25}$$

We have Dirac indices denoted by α and β with a and $a^{'}$ taking the range of the color indices. The additional quarks are contracted subsequently forming quark propagators, which is written in the form of the following three Dirac structures

$$D^{\alpha\beta}_{aa'} = \frac{\delta_{aa'}}{12}(\gamma^\mu\gamma_5)^{\alpha\beta} < 0|d(0)\gamma_\mu\gamma_5 u(x)|\pi^+(p) > \ldots \tag{4.26}$$

$$\cdots + \frac{\delta aa^{'}}{12}(i\gamma_5)^{\alpha\beta} < 0|\bar{d}(0)i\gamma_5 u(x)|\pi^+(p) > \ldots$$

$$\cdots - \frac{\delta_{aa'}}{24}(\gamma_5\sigma^{\mu\nu})^{\alpha\beta} < 0|\bar{d}(0)\gamma_5\sigma_{\mu\nu}u(x)|\pi^+(p) >$$

The Dirac structure corresponding to each matrix element is written in terms of relatively well known pion wave functions. The calculation has been carried out up to first order in p_u [64].

4.2.1 The QCD Vacuum with Introduction to the SVZ Method

When introducing the OPE, we needed to incorporate the effects of the *condensate* somehow to account for its contributions being responsible for revealing what was once a missing component in QCD. The color dynamics described by QCD gives rise to complications that needed a solution in a non-abelian gauge theory and higher ordered contributions. The anitscreening phenomenon is generally associated with the counter intuitive coupling strength at long and short distance scales. The gluon starts branching at long distances by way of the Coulomb interaction, which is what causes the antiscreening effects, also known as asymptotic freedom. Within distances that do not permit the coupling expansion to blow up we can apply perturbation theory to quantify this gluon branching. We arrive at the formula for asymptotic freedom

$$\alpha_s = k/ln\frac{r_0}{r} \tag{4.27}$$

r_0 is a scaling parameter of QCD, $r_0 \approx 1fm$. In perturbation theory, the coupling is evaluated order by order, and is known up to three loops. When taken at long distances we now need to think in terms of chromoelectric and chromomagnetic fields, it is conjectured that a specific configuration of the condensate makes dispersed quantities, as they appear in QED energetically and out favoured [118]. We deal with logarithmic gluon exchanges on the perturbative level. In fact it is this gluon branching that is responsible for the logarithmic running of the effective gauge coupling in $pQCD$, in the form of loop diagrams.

The QCD vacuum consists of a variety of condensates, it is stated in [118] that about a half dozen of them are known, being the gluon condensate $G^2_{\mu\nu}$, the quark condensate $q\bar{q}$, the mixed condensate $\bar{q}$, and so on. We use the SVZ sum rules in this situation.

4.2.2 Light Cone Sum Rules

Previously in this chapter we had seen lightcone coordinates in the Bjorken limit, leading to the dispersion relations and showing physical meaning associated with the lightcone momentum fraction. The light cone wave function (LCWF) is a representation of the distribution of LCSR. Insight and use cases for Fock state, light cone wave functions, as well as light front holography are developed for consideration . These serve as one of the tools in our every growing tool box to tackle QCD. By far the simplest and most intuitive representation of relativistic bound state wavefunctions is the light-cone Fock expansion. Light-cone wave functions are the distribution amplitudes of hadrons, and have been introduced in QCD to define the long-distance part of exclusive processes that contain large momentum transfer [62, 77, 119].

This same wave function serves as input in QCD light-cone sum rules that are based on the light-cone operator product expansion, of vacuum-hadron correlators. An example of a simple processes that can be determined in this way is $\gamma^*(q1)\gamma^*(q^2) \rightarrow \pi^0(p)$, where two virtual photons transition into a neutral pion [77]. Recently, the CLEO collaboration has measured the photon-pion transition FF where one of the photons is nearly on-shell and the other highly off-shell [64, 77]. For a more in depth view of Light-cone decomposition, see 6.6.1. The method of QCD sum rules based on two-point correlation function was pioneered for the calculation of Gegenbauer moments [84]. We can reference several available measurements of the $\gamma^*\gamma \rightarrow \pi^0$ process. The Light cone sum rules (LCSR) for the pion e.m. FF is

derived from the correlation function:

$$\mathcal{F}((p-q)^2, Q^2) = \frac{2F_\pi F_\pi(Q^2)}{m_\pi^2 - (p-q)^2} + \int_{(3m_\pi)^2}^{\infty} ds \frac{\rho^h(s, Q^2)}{s - (p-q)^2} \tag{4.28}$$

where the lowest pole corresponds to the intermediate one-pion state interpolated by the axial-vector current. The residue of the pion pole contains a product of the pion decay constant and the FF we are interested in [84].

The most widely studied hadronic distribution amplitude is the twist-2 DA of the pion. This gives the probability amplitude for $q\bar{q}$ Fock state with the $q\bar{q}$ carrying $x(1-x)$ of the total momentum carried by the pion [120].

Chapter 5

Collider Physics: An Overview of Experiment, Procedure, and Results

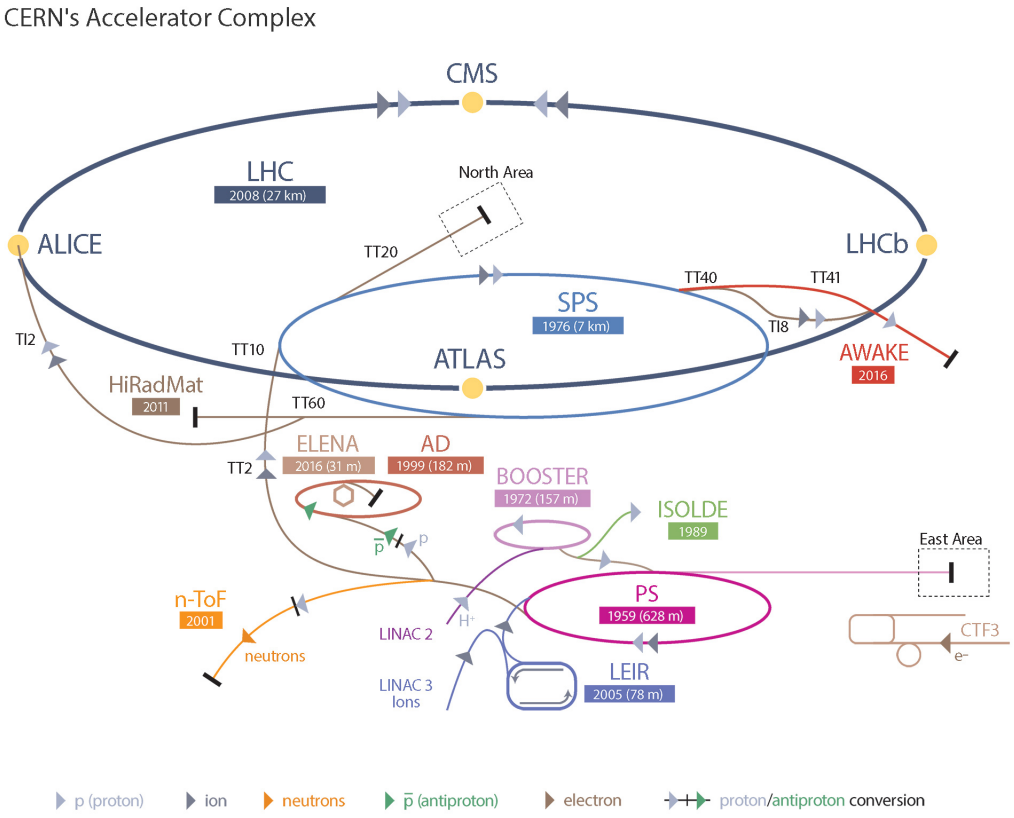

FIGURE 5.1: CERN's accelerator complex showing the production of the proton/ion beam at the LINAC/LEIR and its progressive acceleration towards the LHC. Figure courtesy of the Science and Technology Facilities Council, UK [121, 122].

5.1 Introduction

The goal of this chapter is to examine experimental results of W boson production from ATLAS, CMS and the Tevatron and connect them to our work in *Chapter* 6. At the LHC, the basic idea is to bring together two beams of particles and have them collide at a definite point within the detector, being $\sqrt{s}$. The "particle showers" produced in the collider are detected are by the detector. This information is then processed in such a way that it becomes readable by programs and analysis devices [6,7]. The readout of these events is a subject that deserves a robust study on its own. Most of the photons at the LHC are coming from π^0 decays. When thinking about the collider detectors from the inside out, the center of the apparatus can be thought of as the collision point and the basic idea is that the particles have to go through all the of the layers that have various functions and is discussed later. The center design has to be thought out to where it interferes minimally with the outer layers with some unavoidable interference. Typically, in the center we will have some kind of volume that acts as an ionization detector, which then is set up to detect the path of the tracks post collision. Additionally, a solenoidal magnetic field bends the tracks, and either a gas chamber, or some layers of silicon to trace out space points for these tracks. The curvature of the path in addition to knowing the value of the magnetic field strength, gives read out of the momentum, and that takes care of the charged particles. The next thing we want to do is to measure the electromagnetic component using an electromagnetic calorimeter [19]. More specifically, what is actually detected in particle experiments are the hadrons, leptons, photons as well as weak bosons. No quarks or gluons are readable directly, this is why it is important to leverage jet reconstruction simulation and other numerical methods. The importance of form factors and QCD sum rules has been expressed in abundance. The pion and kaon form factors are of particular interest in hadron

studies, and serves as the cleanest test for the transition from the perturbative regime to the non-perturbative.

5.2 ATLAS

5.2.1 Detector Anatomy

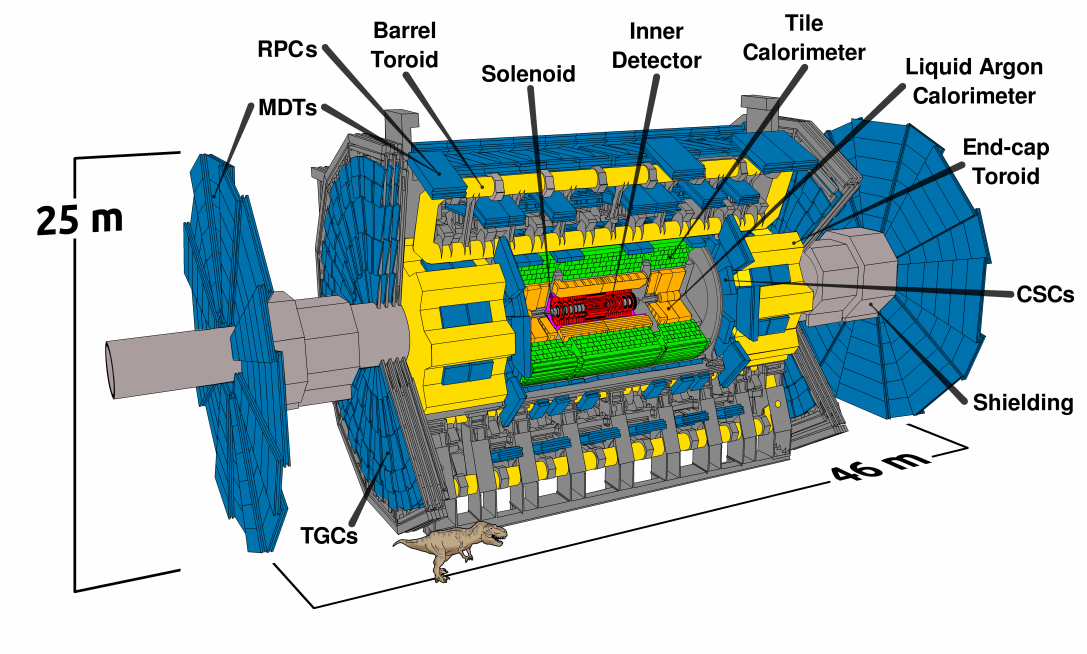

FIGURE 5.2: The ATLAS Detector

Image courtesy of [29].

Information regarding ATLAS detector anatomy is partially paired with Figure 5.2 to supplement our discussion with experimental results and procedure to then follow. The information with respect to detector anatomy is based on *ATLAS* Fact Sheets that can be reviewed in [123]. A beam luminosity of $10^{34} cm^{-2} s^{-1}$ corresponds to about 20 collisions per bunch crossing, with 40 million bunch crossings per second, yields about 1. This gets filtered down to about 75,000 events per second by the trigger filters at level 1, while

level 2 reduces it down to 2,000. Based on the set parameters this gets filtered down to about 200 "interesting" events per second [123].

In a very basic sense, the calorimeters measure the energy carried by the events, a bit more specifically the positions of charged and neutral particles. A liquid argon calorimeter supplies a barrel that is 6.4 m long, and 53 cm thick, with 110,000 channels. The Large end-cap consists of the forward calorimeter, electromagnetic and hadronic end-caps. EM end-caps each have thickness 0.632 m and radius of 2.077 m. The tile calorimeter barrel is made of 64 wedges that are each 5.6 m long and weigh 20 tons, and makes for 500,000 plastic scintillator tiles. The muon system monitor drift tubes (MDTs) in Figure 5.2.1 has gap chambers for triggering and a second measurement system for the coordinates located in the central region. The MDT's measure the curves of the muon tracks and carry a tube resolution of 80 μm [123, 124]. The inner detector consists of the pixel detector, a transition radiation tracker (TRT), and a semiconductor tracker (SCT). The pixel detector is an incredible feat being equipped with 80 million channels, meaning it is capable of picking up and detecting on the order of 80 million pixels as the name suggests. The barrel has 1744 modules with 46080 readout channels per module. Three pixel disks in each end-cap have 6.6 million channels, with 3 disks in each end-cap equipped with 288 modules. The semiconductor tracker has a silicon micro-strip tracker consisting of 4088 two-sided modules and over 6 million implanted readout strips. 60 m^2 of silicon is distributed over 4 cylindrical barrel layers and 18 planar end cap discs. Readout strips every 80 μm on the silicon, we are then able to accurately capture the position of the charged particles at 17 μm per layer which is in the transverse direction to the strips. The TRT has 350,000 readout channels, the basic detector elements are straw tube 4 mm in diameter, and in the center a 0.03 mm diameter gold-plated tungsten wire. Capable of precision measurement of 0.17 mm particle track to wire [125]. This helps us understand better the details of what particle has

been detected [123, 124].

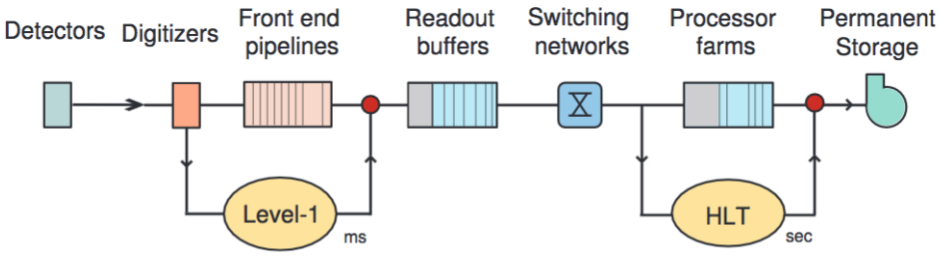

FIGURE 5.3: Flowchart of the CMS trigger systems, both L1 and HLT from detector digitization to permanent storage. Image Courtesy of Roland:2009wc [122, 126]

5.3 The Drell-Yan Cross Section

The primary function of DIS is to study the proton structure in greater detail. The result of electron proton scattering depends strongly on the wavelength $\lambda = \frac{hc}{E}$ and r_p, which denotes the rapidity, with

- $\lambda \gg r_p$ - Very low electron energies. Scattering is equivalent to that from a point like object.
- $\lambda \approx r_p$ - Low electron energies. Scattering with an extended charged object.
- $\lambda < r_p$ - High electron energy. Scattering resolved sub-structure showing the existence of quarks.
- $\lambda \ll r_p$ - Very high energy. Proton appears as a sea of quarks and gluons [13].

In addition to DIS, semi-inclusive-deep inelastic scattering (SDIS) is an alternative providing access to flavor, transverse motion, and transverse spin of the quarks. Inclusive DIS relies on PDF tables that are dependent on and encoded with longitudinal momentum fractions obtained in prior runs. One

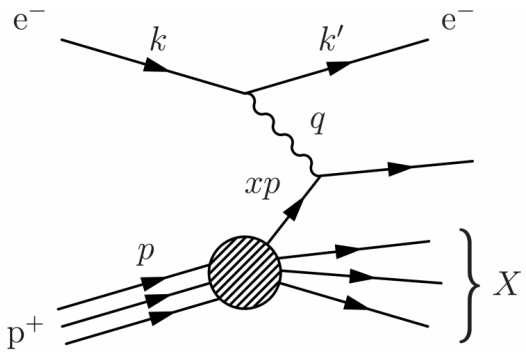

FIGURE 5.4: The simplest tree-level diagram for electron-proton DIS. Including the 4-momentum of the incident lepton, k, with outgoing 4-momentum of the scattered lepton, $k^{'}$. Additionally depicted is the 4-momentum of the exchanged boson denoted here as q, and takes on γ^*, $W^{\pm}$, or Z^0 respectively. The 4-momentum of the incident proton, p, is shown in terms of its three legs representing the uud quark constituent outgoing as parton showers, X. It is worth noting an extra leg branching from the xp q lines that represents jet emission.

notable difference with SDIS is that it probes additional information for transverse distribution in the nucleon. Due to the electromagnetic interactions of electrons being well defined and understood, they become a useful probe of the structure of mesons and baryons. We will look at two very important examples, the production of hadrons in e^+e^- scattering, and deep inelastic scattering of electrons and protons [14, 127]. These two processes have been critical in the development of the color/flavor model for the quarks [127], and DIS lepton scattering plays a central role in factorization. DIS is the first process where point-like partons were "observed" in the hadron in the 1960's era of experimentation. Additionally, high volumes of data determine PDFs that subsequently become extracted from these processes for phenomenological use.

Consider the process $e + A \rightarrow e + X$, which proceeds by exchange of a virtual photon with momentum q^μ. Once the cross section is measured, we

can use it to extract the standard hadronic tensor $W^{\mu\nu}(q^\mu, p^\mu)$,

$$\begin{aligned} W^{\mu\nu} &= \frac{1}{4\pi}\int d^4y e^{iq.y}\sum X < A|j^\mu(y)|X >< X|j^\nu(0)|A > \\ &= F_1(x,Q^2)(-g^{\mu\nu} + \frac{q^\mu q^\nu}{q^2}) \\ &+ F_2(x,Q^2)\frac{(p^\mu - q^\mu p.q/q^2)(p^\nu - q^\nu p.q/q^2)}{p.q} \end{aligned} \tag{5.1}$$

where $Q^2 = -q_\mu q^\mu$, $x = \frac{Q^2}{2q\cdot p}$, and p^μ is the hadron $A's$ incoming momentum, while $j_\mu(x)$ is the electromagnetic current [6,99]. It is important to provide insight regarding the implications of hard and soft QCD processes. Hard QCD takes place in the high Q range, while soft QCD is in connection with low energy fragmentation and jets and associated with soft gluon resummation in soft collinear effective theory (SCET) and hadronization. In hard QCD, we are dealing with perturbation theory and constructing PDFs which includes initial and final state radiation through parton showers resulting in hadronization. The kind of measurements obtained in hard QCD are PDFs and perturbative QCD with jets, measurements of α_s, measurements with photons, and measurements with vector bosons and jets. Soft QCD involves multi-parton scattering as well as fragmentation accompanied by underlying events (UE). A hard proton-proton collision at the LHC carries implications of both center of mass energy $\sqrt{s}$ and its subsequent partons and UE's. The resultant beam-beam remnants along with multiple (soft) parton interactions are not able to be separated out experimentally.

5.3.1 Cross Section

The amplitude corresponding to a basic DIS diagram is

$$\mathcal{A} = e\overline{u}(k^{'})\gamma^\alpha u(k)\frac{1}{q^2}\left\langle X\right|j_\alpha(0)\left|P\right\rangle \tag{5.2}$$

Several structure functions are available to study in the form $F_i(x, Q^2)$ and is carried through various beams and fixed targets at various polarization states. Outgoing electron distributions of the form $e^- + H \rightarrow e^- + X$, where H is a hadron usually consists of a proton, neutron or deuteron. The X in the final state indicates that we do not keep track of the final state. The interaction consists of a photon exchange between the electron and a parton, which is a constituent of a proton. The incoming and outgoing electrons have energy E and E'. We make the choice for the four momentum to orient the incoming electron to propagate in the z direction, $k = E(1, 0, 0, 1)$, with its outgoing direction, $k' = E'$ $(1, sin\theta cos\phi, sin\theta sin\phi, cos\theta)$. A choice of an xy axes ensures the $\phi = 0$ orientation with respect to the hadron rest-frame $P = M(1, 0, 0, 0)$. The photon carries momentum $q = k - k'$. We can define two dimensionless variables

$$x \equiv -\frac{q^2}{2P \cdot q} \qquad y \equiv \frac{2P \cdot q}{2P \cdot k}, \tag{5.3}$$

computing

$$q \cdot P = M(E' - E), q^2 = -2k \cdot k' = -2EE'(1 - \cos\theta). \tag{5.4}$$

5.3.2 Kinematics

Reconstructing the collision kinematics is key. To take a neutral current DIS event into consideration, being those with an electron in the final state we can demonstrate kinematics by reconstruction of the four-momentum transferred to the hadronic system

$$Q^2 = -\overrightarrow{q} \cdot \overrightarrow{q} = -(\overrightarrow{k} - \overrightarrow{k'})^2 \tag{5.5}$$

and Bjorken scaling variable

$$x = \frac{Q^2}{2\,\overrightarrow{P}\cdot\overrightarrow{q}} \tag{5.6}$$

An example using DIS lepton-proton scattering

$$\begin{aligned} M^2 &= p^2 \\ v &= p\cdot q = M(E^{'} - E) \\ x &= \frac{Q^2}{2v} = \frac{Q^2}{2M(E-E^{'})} \\ y &= \frac{q\cdot q}{k\cdot p} = 1 - E^{'}/E, \end{aligned} \tag{5.7}$$

The energy variables are in reference to the rest from of the target with M denoting the proton mass [6].

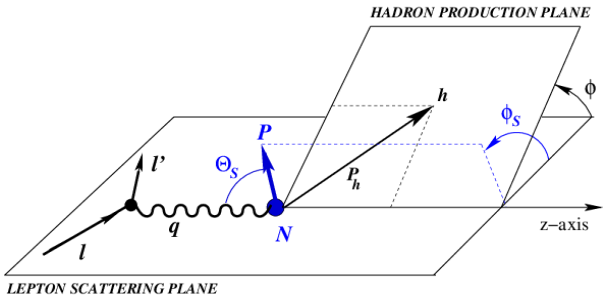

FIGURE 5.5: Kinematics of the SIDIS process $lp \rightarrow l^{'}hX$ and the definitions of the azimuthal angles in the lab frame. The S inclusion in the DIS process is to denote semi-inclusive DIS, which takes into account a hadron interaction with the standard DIS process. In DIS, only the scattered lepton is detected while the remnants of the shattered nucleon are ignored. The "high momentum" hadron is detected in addition to this in the SDIS case, high momentum referring to the leading hadron [53].

Structure Functions

$F_i(x, Q^2)$ parametrize the structure of the target as seen by the virtual photon. We can define this in terms of the lepton scattering cross sections, using

$l_p \to lX$, for example,

$$\frac{d^2\sigma^{em}}{dxdy} = \frac{8\pi\alpha^2 ME}{Q^4}\Big[\Big(\frac{1+(1-y)^2}{2}\Big)\Big]2xF_1^{em} + (1-y)(F_2^{em} - 2xF_1^{em}) - (M/2E)xyF_2^{em}\Big], \tag{5.8}$$

With Bjorken x, the limit noted in eq 5.6, with x fixed, we get the structure functions to obey a scaling law that is approximate allowing it to only depend on the dimensionless variable. We most conveniently formulate the parton model of DIS in the infinite momentum frame, meaning near c, being the speed of light. The proton is moving quickly $p^\mu \approx (P, 0, 0, P)$ with $P >> M$. The Bjorken scaling implies the virtual photon scatters off point like constituent in the process and depend on the ratio Q/Q_0, with $1/Q_0$ characterizing the constituents [6].

5.3.3 Drell-Yan at Fermilab

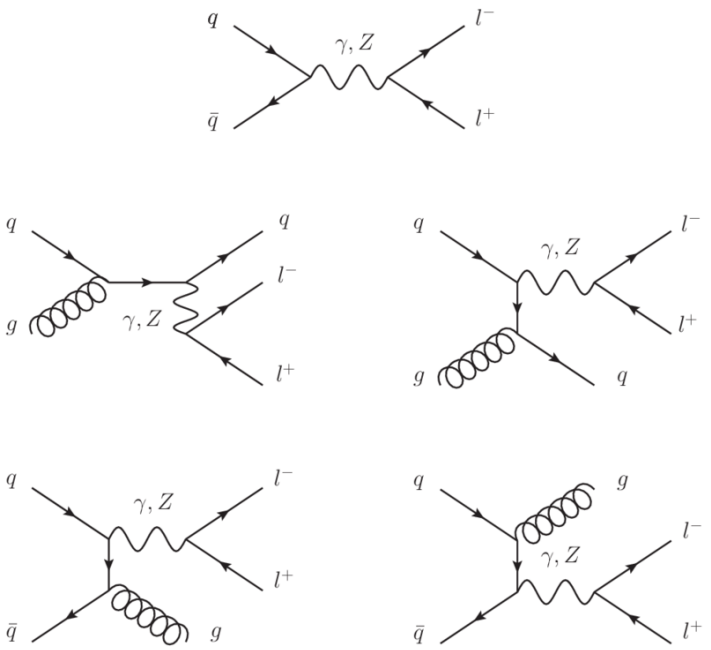

FIGURE 5.6: Feynman diagrams for Drell-Yan pair production at $\mathcal{O}\alpha_s^0$ and $\mathcal{O}\alpha_s^1$

.

Basically after Feynman had introduced the parton model with DIS experiments, it had been said the very next day Drell and Yan exclaimed "lets make this application of it" with what is to referred to as today as Drell-Yan. The Drell-Yan experiment was originally designed to search for intermediate weak bosons, i.e. the $W^{\pm}$ and the Z bosons. The Drell-Yan process became an extended analysis scattering process in reach of DIS experiments. Hadron-hadron inelastic collisions, $s \to \infty, Q^2/s \to 1$, Q^2 with s the the square of its invariant masses with respect to the lepton pair accompanying the hadrons. We will be able to draw distinctions between scaling properties and connections with deep inelastic electron scattering in this discussion [128]. The process below depicts the Drell-Yan mechanism of a dielectron pair showing extra gluon emissions of unintegrated parton distribution functions from incoming beam P_2 and target P_1 [6, 13].

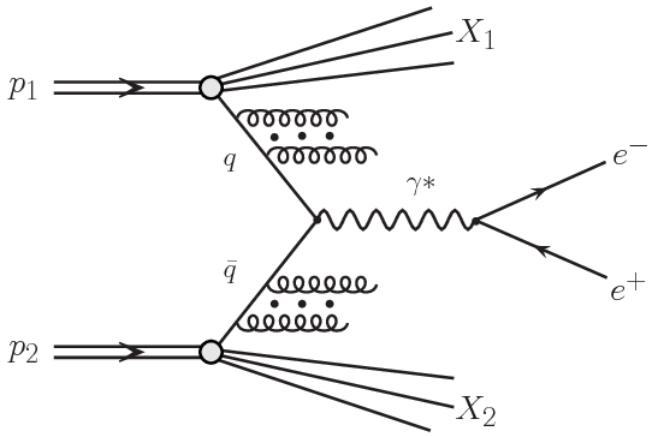

FIGURE 5.7: Drell-Yan mechanism with Z^0 or γ^* exchange proceeding the outgoing dilepton observable. Soft gluon radiation off the quark lines which influence non-perturbatively the final state outcomes are also shown in this depiction
Image courtesy of [129].

5.3.4 Drell-Yan $\to W^{\pm}$ and Z Production

The discovery of the W and Z gauge bosons at CERN with the $p\overline{p}$ collider was a huge triumph for the Electroweak Model. The W and Z widths are not

very big, ($\Gamma_W = 2.08\,GeV$ and $\Gamma_Z = 2.50\,GeV$ in the SM. The production cross sections from the $q\overline{q} \to W, Z$ sub process cross section are obtained from the couplings of these vector bosons to the fermions

$$\hat{\sigma}^{q\overline{q}'} \to W = \frac{\pi}{3}\sqrt{2}G_F M_W^2 |V_{qq'}|^2 \delta(\hat{s} - M_W^2) \tag{5.9}$$

$$\hat{\sigma}^{q\overline{q}} \to Z = \frac{\pi}{3}\sqrt{2}G_F M_Z^2 (V_q^2 + A_q^2)\delta(\hat{s} - M_Z^2),$$

where $V_{qq'}$ is the CKM matrix element. The agreement with experiment and theory is relatively good for these values [6].

5.3.5 $u\overline{d} \to W^+$ Cross section

The coupling of the W^+ to quarks and leptons is

$$\delta L = \frac{g_w}{\sqrt{2}} W_\mu^- (\overline{d}\gamma^\mu P_L u + \overline{l}\gamma^\mu P_L \nu) + h.c. \tag{5.10}$$

with h.c. the hermitian conjugate. where $P_L = (1 - \gamma^5)/2$ is the left-handed projector, and g_w is the weak interaction coupling,

$$\alpha_w = \frac{g_w^2}{4\pi} = \frac{1}{29.6}. \tag{5.11}$$

The W^- field appears due to the field that creates the W^+.

$$i\mathcal{M}(u\overline{d} \to \nu l^+) = i\frac{g^2/2}{s_{12} - m_W^2 + im_W\Gamma_W}\overline{u}(1)\overline{\sigma}^\mu u(2)\overline{u}(3)\overline{\sigma}_\mu u(4)$$

and we find,

$$= ig_w^2 \frac{1}{s_{12} - m_W^2 + im_W\Gamma_W} \tag{5.12}$$

We can obtain a broad mass distribution for the leptons by integrating over phase space where W^+ appears as a resonance, or we can compute amplitudes for the W^+ for a real W^+ on its mass shell. It is shown in [130] that

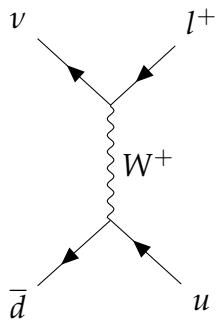

FIGURE 5.8: Feynman Diagram for $u\bar{d} \to \nu l^+$.

we can obtain a formulae if we retain the final-state lepton spinors instead of summing over the W^+ polarization vectors, plus retaining the spinors preserves information regarding the W^+ polarization. The matrix element for W^+ coupling to leptons needs to be squared and integrated over the direction of the leptons in the W^+ rest frame [131].

$$I^{\mu\nu} = \int \frac{d\Omega}{4\pi} < 1\gamma^{\mu}2] < 2\gamma^{\nu}1] \tag{5.13}$$

if q^{μ} is the W^+ momentum, $q = 1 + 2$, then $q_{\mu}I^{\mu\nu}$=$q_{\nu}I^{\mu\nu} = 0$. and

$$I^{\mu}_{\mu} = \int \frac{d\Omega}{4\pi} 2 < 12 > [12] = -2q^2 = -2m_W^2. \tag{5.14}$$

and from this

$$I^{\mu\nu} = -\frac{2}{3}m_W^2(g^{\mu\nu} - \frac{q^{\mu}q^{\nu}}{m_W^2}) \tag{5.15}$$

We can represent the sum over on-shell W^+ polarization vectors as

$$\sum_i \epsilon_i^{\mu}(q)\epsilon_i^{*\nu}(q) = \frac{3}{2m_W^2}\int \frac{d\omega 4}{4\pi} < 1\gamma^{\mu}2] < 2\gamma^{\nu}1] \tag{5.16}$$

This is shown to be a simple procedure to compute cross sections with final on-shell W^+ also seen in We can start the process with the internal W^+ propagator and final state $\nu(1)l^+(2)$. Then remove the factor $(g_w/\sqrt{2})/(s_{12} -$

$m_W^2 + im_W\Gamma_W$) putting the W^+ momentum $(1+2)$ on shell. Next is to evaluate the spinor product amplitude, and then square and integrate over phase space including the on-shell W^+, and integrate over the lepton direction in the W^+ rest frame [130].

$$\int d_{n+W} \equiv \int d\Pi_{n+1} \frac{3}{2m_W^2} \int \frac{d\Omega}{4\pi}. \tag{5.17}$$

We can use the matrix element to show an example of the cross section calculation, we begin with our matrix element [24] in the form of

$$i\mathcal{M}(W^+ d\bar{u}) = \frac{g_w}{\sqrt{2}} < 1\gamma^\mu 2] < 3\gamma^\mu 4] = \sqrt{2} g_w < 31 > [24]. \tag{5.18}$$

where the phase space integral $\int d\Pi_{0+W}$ contains 1-body phase space.

$$\int d\Pi_1 = 2\pi\delta(s - m_W^2). \tag{5.19}$$

we average over initial color and spins

$$\sigma(u\bar{d} \to W^+) = \frac{1}{3 \cdot 4} \cdot \frac{8\pi\alpha_w}{2s} \cdot 2\pi\delta(s - m_W^2) \cdot \frac{3}{2m_W^2} \int \frac{d\Omega}{4\pi} s_{24}^2. \tag{5.20}$$

We implement the angular decay of the lepton with respect to the u quark direction, this lets us know that a W^+ with left-handed polarization is present. When we evaluate this integral we find

$$\sigma(u\bar{d} \to W^+) = \frac{\pi^2 \alpha_w}{3} \delta(s - m_w^2), \tag{5.21}$$

and we arrive at the expression for the Drell-Yan cross section.

We need to be sure that we can compute amplitudes if we wish to compute W^+ production cross sections.

5.3.6 TEVATRON $W^{\pm}$ Mass Measurement

At the Tevatron, W and Z bosons are produced through $q\bar{q}^{'}$ annihilation [132]. The cleanest signatures are involved with high-P_T electrons or muons, $W \rightarrow e\nu, \mu\nu$, and $Z \rightarrow e^+e^-, \mu^+\mu^-$, and this is mostly due to the presence of small background contamination, providing a more distinctive signal analysis and study.

The most accurate measurement of the W boson mass measured by [133] using 200 pb^{-1} of CDF run II data, and as well an improved measurement from 2.4 fb^{-1} CDF run II.

5.3.7 Forward Backward Asymmetry

In proton anti-proton collisions, it has been found that the W^+ and W^- bosons have the same cross-section. One difference noted is that it has been found that the W^+ bosons fly in the direction of the protons during scattering with a higher probability distribution than the W^- bosons, which fly more in the direction of the anti-protons [13]. This has to do with the up and $down$ type quarks influencing the direction in what is referred to as a "kick" into the directions that they have the likelihood to be found. A more important implication that follows this logic is that this is not the case at the LHC, where proton-proton collisions are involved. Here, it is found that the cross-sections for the W^+ production is larger than the cross-section for the W^-. There are higher contributions from additional sea quarks involved with higher ordered gluons that become incident in the process that contribute as well [134]. The measurement of these asymmetries has become an important way to put tighter constraints on high-x valence quark measurements.

Collinear Factorization

The idea of factorization is at the heart of $pQCD$ at hadron colliders. One primary goal is to ensure that the partons are treated as quasi-free particles. Having already reviewed the DGLAP equations in section 4.1.2, the PDFs evolution with the factorization scale is governed by these. This is important for the evaluation of cross sections that rely on the PDFs. The quantum fluctuations that populate the Fock state additionally are governed by the DGLAP equations [13].

We need to to make predictions for hard scattering processes and matrix elements in the IR region, in which carry universal properties available for this purpose. At LO these properties are obtained using factorization formulae for tree level and one loop amplitudes which provide insight into perturbative QCD.Leading logarithmic (LL) parton showers that are simulated in the event generators aid descriptions of exclusive hadronic final states and their structure. Resummation relies on the factorization properties associated with soft and collinear emission, which become improved deeper insight and theoretical understanding is achieved. This requires deeper knowledge regarding infrared factorization at the next order in α_s [135].

5.3.8 CDF Run II $p\overline{p}$ data on W Boson Mass

The Tevatron CDF and $D\emptyset$ have a lot of experience with taking measurements of the W boson mass, which is determined at tree level by the relations to other electroweak parameters. However, it remains as one of the least precisely measured parameters in the electroweak interaction [133]. The published measurements can be seen here based on $Run - I$ data (1992-1996) [136]. The CDF collects $W \rightarrow e\nu$ decays with a trigger that is set to select high-E_T central e^- candidates with specific set parameters and keeps the matched tracks while discarding background sources. QCD dijet events

contribute to the background, many of these events and anticipation of potential background contamination sources are predicted in Monte Carlo simulations [137].

5.3.9 Jet Algorithms

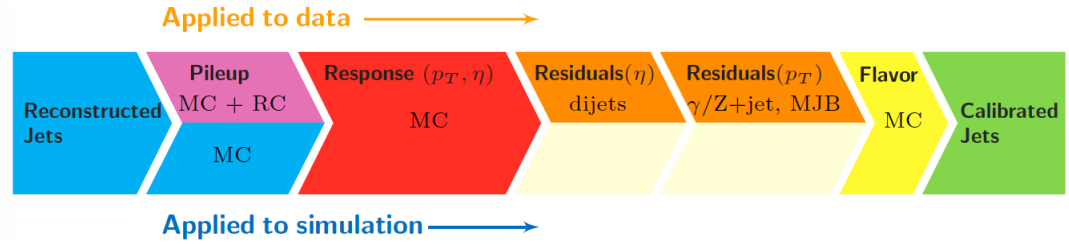

FIGURE 5.9: Schematic representation of the correction factors applied to the jet transverse momenta in data (top row) and MC (bottom row) and their meaning [126].

Most of *QCD* occurs dynamically non-perturbatively via the condensate of high order. When we calculate the cross section for a process, we need to evaluate an integral over phase space and this is usually done through Monte Carlo algorithms. Then, for each phase-space point that represents incoming and outgoing momenta, the square of the matrix element is also evaluated with integration over its phase space. Summing over initial state and averaging over final states allows incorporation of unobserved quantum numbers required for phase space inputs [138].

Monte Carlo Jet Reconstruction

Jets at the CMS detector and determination of their energy scale needs energy corrections to the outgoing jets in the experiments. Using the simulations to correct for detectors and event overlaps is an integral part of the process. As the jets propagate through the CMS detector, they leave small signals behind in the electromagnetic and hadronic calorimeters. These get combined using the jet algorithms to form a reconstructed jet. An important

note is that jet reproduction is to be used as an approximate form. The true particle level energy is independent of the detector response, and so the jet energy corrections will relate these two values. This plays a role in systematic uncertainty calculations to be had and will be discussed in the next chapter.

Chapter 6

Calculation & Procedure

6.1 Setup and Introduction

Many processes at the *LHC* are sensitive to higher order corrections that extend beyond fixed order [20]. Monte Carlo techniques have been developed for the purpose of modeling nonperturbative dynamics, and choice of *PDF* tables to obtain fits for $Wp_{\perp}$ data are crucial in this step. *Pythia* [139], and *MATRIX* [140] are widely employed in the community to run Monte Carlo event generation and parton shower simulations, this requires the input of data sets inclusive of jet production. *PDF*s from *LHAPDF* [141] are integrated into the ManeParse [89, 105] PDF reader for calculating and plotting within the Wolfram Mathematica framework [142]. It contains built=in Mathematica interpolation, and particularly performs well at small x values. Additionally it is leveraged to compute integrated luminosity linking theoretical and experimental cross sections, where the integrated luminosity can be written as a convolution of PDFs for easy calculation within ManeParse [89], as we had seen in subsection 4.1.3. *Madgraph* 5 [143] in conjunction with *Pythia* provides a graphing utility for plotting results. Additionally, *OpenLoops* [144], along with *Sherpa* enables us to generate pure *NLO* results [20]. In a previous chapter we discussed implications of hadronization, taking place just after hard scattering at center of mass collision energy $\sqrt{s}$. What follows is decays into hard jet tails, then jet structure consisting of

soft/collinear bremstrahlung gluon radiation. This proceeds into hadronization as it interacts with the condensate. The final states that interact the detector show as hadron decays to colorless singlets. Event generator programs become important in tandem with clever ways to connect these two regions. The CT10 PDF is of interest [145] as well as fits using the standard CTEQ PDF [146] evolution and $HOPPIT$ α_s running solutions. NNPDF30 NLO from $ATLAS$ runs are considered as well [147], which merges data sets from LHC run II, with production from both $ATLAS$ and CMS, additional vector boson rapidity and $TMDs$ data from $ATLAS$, CMS, $LHCb$, as well as $W + c$ event data from the CMS detector [147]. Merging schemes are important in that many LHC final states benefit from algorithm Reconstruction, as this leads to hard jet identification. Several scales play a role in the determination of the evolution of these events, and we need as accurate as possible inputs to obtain multi scale results [148]. We can compare PDF data with varying transverse momentum, α_s scale evolution and order of soft gluon contributions. The idea is to plot various scenarios tutoring our decision for best fit PDF's.

6.2 Analytic Resummation Technique

Large logarithms are a consequence of of multiple scales present. Resummation of the large logs as we've discussed occur in the perturbative coupling expansion, and when done correctly, enhances sensitivity to small gluon momenta. TMD's of W bosons require detailed analysis in order to obtain accurate reconstruction, and accurate predictions for both the low and high-p_T realms carry equal importance. The dynamics responsible for generating p_T in the W do not depend heavily on the contribution from the proton momentum interacting amongst the partons and can additionally be generated by gluon radiation in the process [30, 38, 149]. Recent estimates show

experimental data being consistent with Gaussian distributions with a p_T width at about 0.6 GeV at energy scale 2 GeV. And it is thought that roughly half comes from primordial p_T of quarks and the other half generated by quark gluon radiation. Moreover, flavor mixing in the process is not known in terms of the distributions in processes that have varying flavors, the best present estimates come from $LQCD$ with insights on down quark distributions a bit larger than the up quark. This plays a role when averaging over nucleon spin orientation, for instance [17, 150].

W-boson decay distributions are sensitive to the order of resummation in these calculations [151]. Kinematics become addressed where p_T values are considerably less than that of the invariant mass scale of bosons. The fraction of transverse momentum $Q_\perp$ is merely a result of recoil when coming into contact with soft gluons, which have been omitted by incident parton interactions [13, 44]. This necessitates "soft-gluon resummation", and is interchangeably known as "transverse-momentum resummation". An example of resumming double-differential cross-sections including these logarithms $m \geq 2n-2$ is what is referred to as next-to-leading logarithmic (NLL) accuracy. With this it follows that all terms with $m \geq 2n-3$ will be next-to-next-to-next-to-leading logarithmic (NNLL) accuracy. The Collins-Soper kernal relating TMDPDFs is used in this context, and is as follows,

$$\frac{d\sigma_{AB}}{dydQ_\perp^2} = \sum_{ij} \pi \hat{\sigma}_{ij}^{(LO)} \left[\int \frac{d^2b_\perp}{(2\pi)^2} \left[exp(ib_\perp \cdot Q_\perp) \tilde{W}_{ij}(b_\perp; Q, x_A, x_B) \right] \right] \tag{6.1}$$

$$+ Y_{ij}(Q_\perp, Q, x_A, x_B) \Big]$$

Two Bjorken parameters x_A and x_B are fixed by the invariant mass of the hadrons, Q^2, with rapidity y. W_{ij} denotes resummation while Y_{ij} is the hard remainder in the process at factorization scale μ_F [13]. The result of the functions with respect to the resummed quantities are then expanded in α_s. The

dependence of the first terms in the function generated are incoming particles that are not exclusive to the original system, this is a consequence of condensate interaction. It is to be noted that the initial hard terms in this process are considered process dependent. The calculation involves the impact parameter going to infinity, contributing to the $Q_\perp, X$ spectrum at all values. The remedy is to employ a nonperturbative FF in order to dampen $b_\perp$. This is the impact parameter's influence on the transverse plane. The exponential in the integrand in Equation 6.1 is responsible for oscillations, which become problematic with numerical calculation techniques due to producing Bessel functions of the form $j_0(b_\perp Q_\perp)$. The Bessel functions are addressed by reducing them to Hankel functions, thus rendering the system finite at all finite values of v, as well as z. This then allows for the deformation of two contours in complex space, one for each of the hadrons, rendering us free of the Landau pole. This procedure yields the same result as the original integral at all finite orders in normal perturbation theory. This solution often is used in Q_T resummation, where the numerical results can now be carried forward for additional consideration, now that we have available newly 'tamed' expansions in α_s [13]. It is to be noted that resummation takes place using Mellin transforms as well. Packages in Wolfram's Mathematica are well equipped to handle this once carried out to a form ready for numerical input.

6.3 *TMD* Plotting and *PDF* Selection for Analysis

We are attempting to use a TMD plotting tool with the use of CT14-NL [152], which is a 2-loop *PDF* evolution using DGLAP, and CT14-NNLO *PDF* [153], being a 3-loop *PDF* evolution with HOPPET α_s running solutions. We are to consider CTEQ6 *PDF*'s [146]. We choose soft gluon contributions as a function of k_T, as well as vs. X and Vs. overall P. The first scenario is to compare soft gluon contribution accuracy as preliminary consideration. We

are free to choose *PDF* inputs from the library built on site with this plotting tool, or import *PDF*'s from various other libraries available. We additionally have parameters to evolve the energy scale akin to that of the DGLAP evolution formalism to run up the coupling scale and consider various outcomes. This was intended to be used as a benchmark tool to plot various situations against one another serving the purpose of tutoring our decision to use one *PDF* over another. The contribution of these processes depend on outcome and available data [154]. Here is an example of *Pythia*, *Herwig* and *Sherpa* jet reconstruction data plotted against *CMS* data. We aim to generate our own jet reconstruction outputs in the same way, using data from CERN open data based on *ATLAS* 8 *TeV* and 13 *TeV* runs, to then plot against *ATLAS* runs after error analysis and large logarithmic summation analysis.

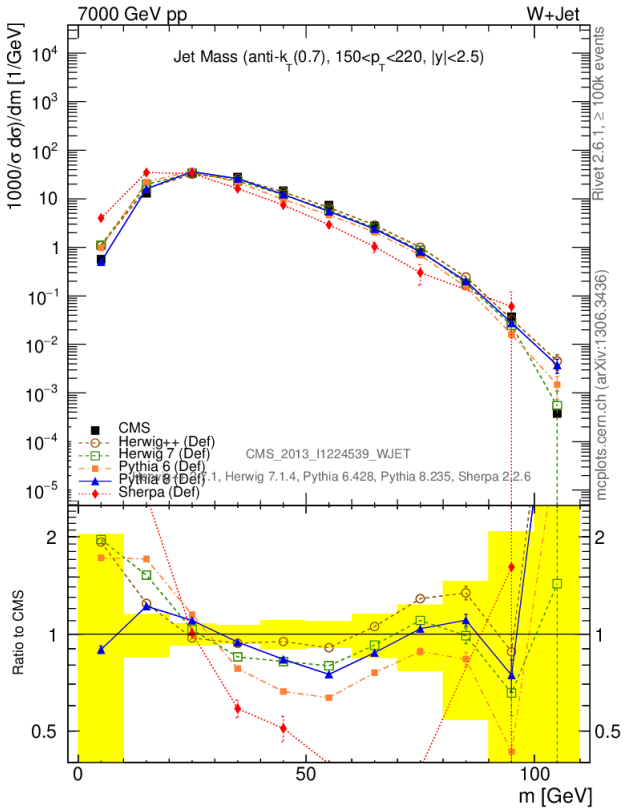

FIGURE 6.1: Jet mass with *anti-k_T* reconstructed from *Herwig* 7.1.4, *Pythia* 6.428, *Pythia*.235, and Sherpa comparing corrections to *CMS* data for $W + jet$ production **[?]**.

6.3.1 Probing PDF Uncertainty

Meta PDF's are a great way in certain cases to reduce total uncertainty for processes at certain energies. An example of this is to re-paramaterize the error PDF's from multiple PDF groups. The uncertainty error becomes transformed into a Hessian basis, and one can choose to retain a number of eigenvectors, thus reducing the ensemble to a range of PDF and $+\alpha_s$ of interest, making it easier to calculate the desired $PDF(+\alpha_s)$ for any observable at the LHC. It is known that parton uncertainties decrease in general as the factorization scales increases along the energy scale, namely DGLAP evolution. A working example is the implementation of data sets to decrease the number of error PDFs required for accurate descriptions of uncertainties. This process is used for all Higgs production processes for all LHC energies [13, 155].

The PDF error master equations read as

$$\Delta X^{+}_{max} = \sqrt{\sum_{i}^{N} = 1[max(X_i^{+} - X_0, X_i^{-} - X_0, 0)]^2} \tag{6.2}$$

$$\Delta X^{-}_{max} = \sqrt{\sum_{i}^{N} = 1[max(X_0 - X_i^{+}, X_0 - X_i^{-}, 0)]^2}$$

ΔX^{+} adds the PDF error that lead to an increase in the observable X and ΔX^{-} the PDF error that lead to the decrease in the observable X [13]. When introducing new PDF'S certain parameter space directions can change leading to higher sensitivity in certain cross-sections [156].

6.4 Calculation Pipeline and Event Generators

We are set up to run the CERN Root [157] framework in a Jupyter notebook, and integrates both C++ and Python libraries in a combined environment. The *Pythia* directory is an interface to the C++ version of *Pythia*.1 event generators, written by T.Sjostrand [158]. Interfacing its functions and classes with direct calls from a compiled C++ script in a straight forward way is very valuable [139]. Additionally it supports embedding these jet algorithm and MC event generators to run directly in the script as subroutines while still maintaining the robust capabilities needed by the HEP community. In figure 6.2 we demonstrate how this is done from the beginning of a new session, and includes relevant particle databases with the graphing utility *TCanvas*. We have parameter control over pseudorapidity, as well as transverse momentum parameters, Figure 6.2 provides a basic example.

```
root > .x pythia8.C
```

```
#include "TSystem.h"
#include "TH1F.h"
#include "TClonesArray.h"
#include "TPythia8.h"
#include "TParticle.h"
#include "TDatabasePDG.h"
#include "TCanvas.h"

void pythia8(Int_t nev  = 100, Int_t ndeb = 1)
{
// Load libraries
   gSystem->Load("libEG");
   gSystem->Load("libEGPythia8");
// Histograms
   TH1F* etaH = new TH1F("etaH", "Pseudorapidity", 120, -12., 12.);
   TH1F* ptH  = new TH1F("ptH",  "pt",              50,   0., 10.);


// Array of particles
   TClonesArray* particles = new TClonesArray("TParticle", 1000);
// Create pythia8 object
   TPythia8* pythia8 = new TPythia8();
```

FIGURE 6.2: Calling Pythia from Root. Packages and libraries are called and graphing utilities implemented for processing once the data crunch has completed [139, 157].

General run settings are set up first in Figure 6.3

```
process_class      =  pp-emmumepmup+X  #  process id
E                  =  6500.   #  energy per beam
coll_choice        =  1       #  (1) PP collider; (2) PPbar collider
photon_induced     =  1       #  switch to turn on (1) and off (0) photon-induced contributions
switch_off_shell   =  0       #  switch for effective integration for off-shell Z bosons (eg, Higgs analysis)
enhance_tails      =  0       #  switch to improve statistics in tail of distributions (factor of two slower)
```

FIGURE 6.3: Input parameters for the general run settings before proceeding to the scale setting step [157].

6.4.1 MadGraph 5

*MadGraph*5 is a framework containing all the elements necessary for *SM* and *BSM* phenomenology. We are able to utilize its resources to compute relevant cross sections, with the additional ability to generate hard events to then match the results with other event generators in the pipeline. *Pythia* and *Herwig* along with *Sherpa* are the main Monte Carlo based event generators for this work, with *Pythia* thus far as the primary. We are setting up *MATRIX* to run processes can be simulated to LO as well as NLO accuracy for any user-defined Lagrangian. See for example a portion of the code given in Figure 6.3. *QCD* and EW corrections to the events and *PDF* analysis are the main feature for these generators, being that this is not detectable as final states in the colliders but still need to be accounted for to obtain accurate fits.

6.4.2 Scale Setting and Order-Dependent Run Settings

We have a range of parameters available to make changes to the code to the desired scale. This acts as one parameter available for "tuning" or modeling efforts. In Figure 6.4 an example of an options menu is available for beginning the initial set up.

4.1.1.2 Scale settings

```
scale_ren          =  91.1876   #  renormalization (muR) scale
scale_fact         =  91.1876   #  factorization (muF) scale
dynamic_scale      =  0         #  dynamic ren./fac. scale
                                #  0: fixed scale above
                                #  1: invariant mass (Q) of system (of colourless final states)
                                #  2: transverse mass (mT^2=Q^2+pT^2) of system (of colourless final states)
                                #  3: geometric average of Z-boson transverse masses:
                                #     sqrt(mT_Z1 * mT_Z2)
                                #  4: sum of Z-boson transverse masses computed with their pole masses:
                                #     sqrt(M_Z^2+pT_ee^2)+sqrt(M_Z^2+pT_mumu^2)
                                #  5: sum of Z-boson transverse masses:
                                #     sqrt(M_Z1^2+pT_Z1^2)+sqrt(M_Z1^2+pT_Z2^2)
factor_central_scale = 1        #  relative factor for central scale (important for dynamic scales)
scale_variation    =  1         #  switch for muR/muF variation (0) off; (1) 7-point (default); (2) 9-point
variation_factor   =  2         #  symmetric variation factor; usually a factor of 2 up and down (default)
```

FIGURE 6.4: [
Scale setting in the *MATRIX* event generator program. This allows the parameters of our model simulation to be tuned dependent on experimental data used, *PDF* choice, as well as the renormalization and factorization scales.]Scale setting in the *MATRIX* event generator program. This allows the parameters of our model simulation to be tuned dependent on experimental data used, *PDF* choice, as well as the renormalization and factorization scales [159].

6.4.3 ResBos

The *ResBos* program fully computes the differential cross section

$$\frac{d(\sigma)}{dQdydQ_T d(\Omega)} \tag{6.3}$$

for processes

$$\frac{h1}{h2} \rightarrow (V) \rightarrow \frac{l1}{l2} X \tag{6.4}$$

$h1$ and $h2$ are the hadrons respectively (primarily decaying to pions or nucleons), V is a virtual electroweak boson in this case, with $l1$ and $l2$ on shell becoming the observed electroweak particles (leptons, prompt photons, or Z bosons). Q, Q_T, and y are invariant mass terms being transverse momentum and rapidity of the intermediate state V respectively. Omega being the solid angle of the $3-momentum$ associated with $l1$ in the Collins-Soper rest frame.

```
LHAPDF_LO          =  NNPDF31_nlo_as_0118_luxqed  #  LO LHAPDF set
PDFsubset_LO       =  0        #  member of LO PDF set
precision_LO       =  1.e-2    #  precision of LO cross section

# NLO-run
run_NLO_QCD        =  0        #  switch for NLO QCD cross section (1) on; (0) off
run_NLO_EW         =  0        #  switch for NLO EW cross section (1) on; (0) off
LHAPDF_NLO         =  NNPDF31_nlo_as_0118_luxqed  #  NLO LHAPDF set
PDFsubset_NLO      =  0        #  member of NLO PDF set
precision_NLO_QCD  =  1.e-2    #  precision of NLO QCD cross section
precision_NLO_EW   =  1.e-2    #  precision of NLO EW correction
NLO_subtraction_method = 1     #  switch to use (2) qT subtraction (1) Catani-Seymour at NLO

# NNLO-run
run_NNLO_QCD       =  0        #  switch for NNLO QCD cross section (1) on; (0) off
add_NLO_EW         =  0        #  switch to add NLO EW cross section to NNLO run (1) on; (0) off
                               #  note: can be added only if also running NNLO
LHAPDF_NNLO        =  NNPDF31_nnlo_as_0118_luxqed  #  NNLO LHAPDF set
PDFsubset_NNLO     =  0        #  member of NNLO PDF set
precision_NNLO_QCD =  1.e-2    #  precision of NNLO QCD cross section
precision_added_EW =  1.e-2    #  precision of NLO EW correction in NNLO run
loop_induced       =  2        #  switch for loop-induced gg (with NNLO settings): (0) off;
                               #   (1) LO [NNLO contribution];   (2) NLO [N3LO contribution]
                               #  (-1) only loop-induced gg LO; (-2) only loop-induced gg NLO
```

FIGURE 6.5: This is an order of execution as the program runs. We are able to have control over EW corrections as well as the subtraction methods called. The calls are sent to pre-build libraries and ran as subroutines. [141].

The production and subsequent decay's of are evaluated with the use of exact matrix elements. Electroweak corrections to the width of V and calculated spin correlation between initial and final-state observables become introduced ad-hoc. *ResBos* is ran through *HepForge*, which additionally hosts a variety of tools and calculation packages. Code was obtained from *FastJet* on the *HepForge* page to run jet clustering algorithms that allow the variation in angular distribution as well as energy range using p_T data, specifically longitudinally invariant k_T algorithms for simulations of the beam direction, including parameters constraining the rapidity and azimuth of transversely distributed shower particles, as well as including jet-radius parameters. The idea is that for every parton i, we should be equipped to make calculations regarding appropriate beam distance. For this we take into consideration $d_{iB} = p_{ti}^2$, which reveals the minimum d_{min} of all the d_{ij}, d_{iB}. If d_{min} is a d_{ij}, then i and j become merged into a single particle. A technique by the name E-Scheme Recombination is then employed. Summation of states is done considering the individual parton four momentum taken into consideration.

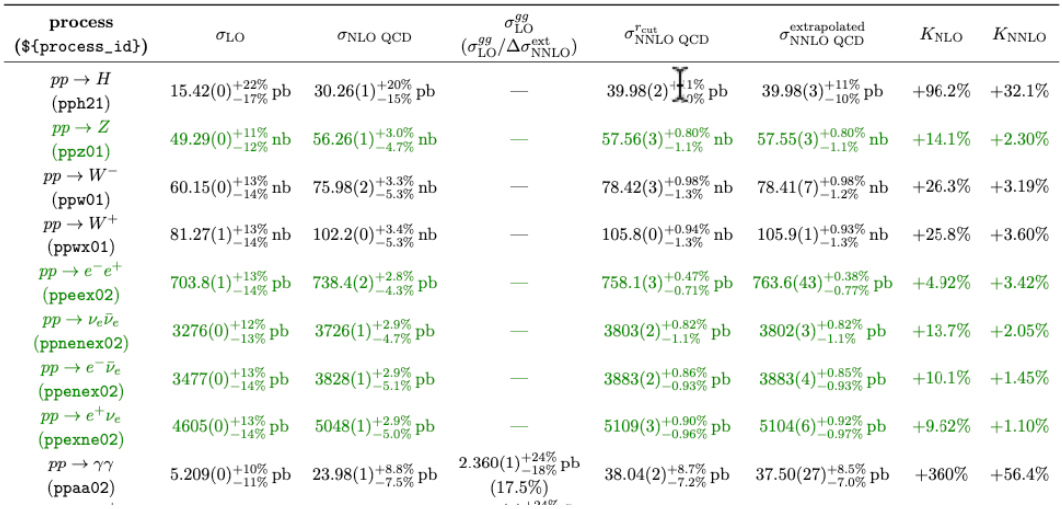

process (${process_id})	σ_{LO}	$\sigma_{\text{NLO QCD}}$	σ^{gg}_{LO} ($\sigma^{gg}_{\text{LO}}/\Delta\sigma^{\text{ext}}_{\text{NNLO}}$)	$\sigma^{r_{\text{cut}}}_{\text{NNLO QCD}}$	$\sigma^{\text{extrapolated}}_{\text{NNLO QCD}}$	K_{NLO}	K_{NNLO}
$pp \to H$ (pph21)	$15.42(0)^{+22\%}_{-17\%}$ pb	$30.26(1)^{+20\%}_{-15\%}$ pb	—	$39.98(2)^{+1\%}_{0\%}$ pb	$39.98(3)^{+11\%}_{-10\%}$ pb	+96.2%	+32.1%
$pp \to Z$ (ppz01)	$49.29(0)^{+11\%}_{-12\%}$ nb	$56.26(1)^{+3.0\%}_{-4.7\%}$ nb	—	$57.56(3)^{+0.80\%}_{-1.1\%}$ nb	$57.55(3)^{+0.80\%}_{-1.1\%}$ nb	+14.1%	+2.30%
$pp \to W^-$ (ppw01)	$60.15(0)^{+13\%}_{-14\%}$ nb	$75.98(2)^{+3.3\%}_{-5.3\%}$ nb	—	$78.42(3)^{+0.98\%}_{-1.3\%}$ nb	$78.41(7)^{+0.98\%}_{-1.2\%}$ nb	+26.3%	+3.19%
$pp \to W^+$ (ppwx01)	$81.27(1)^{+13\%}_{-14\%}$ nb	$102.2(0)^{+3.4\%}_{-5.3\%}$ nb	—	$105.8(0)^{+0.94\%}_{-1.3\%}$ nb	$105.9(1)^{+0.93\%}_{-1.3\%}$ nb	+25.8%	+3.60%
$pp \to e^-e^+$ (ppeex02)	$703.8(1)^{+13\%}_{-14\%}$ pb	$738.4(2)^{+2.8\%}_{-4.3\%}$ pb	—	$758.1(3)^{+0.47\%}_{-0.71\%}$ pb	$763.6(43)^{+0.38\%}_{-0.77\%}$ pb	+4.92%	+3.42%
$pp \to \nu_e\bar{\nu}_e$ (ppnenex02)	$3276(0)^{+12\%}_{-13\%}$ pb	$3726(1)^{+2.9\%}_{-4.7\%}$ pb	—	$3803(2)^{+0.82\%}_{-1.1\%}$ pb	$3802(3)^{+0.82\%}_{-1.1\%}$ pb	+13.7%	+2.05%
$pp \to e^-\bar{\nu}_e$ (ppenex02)	$3477(0)^{+13\%}_{-14\%}$ pb	$3828(1)^{+2.9\%}_{-5.1\%}$ pb	—	$3883(2)^{+0.86\%}_{-0.93\%}$ pb	$3883(4)^{+0.85\%}_{-0.93\%}$ pb	+10.1%	+1.45%
$pp \to e^+\nu_e$ (ppexne02)	$4605(0)^{+13\%}_{-14\%}$ pb	$5048(1)^{+2.9\%}_{-5.0\%}$ pb	—	$5109(3)^{+0.90\%}_{-0.96\%}$ pb	$5104(6)^{+0.92\%}_{-0.97\%}$ pb	+9.62%	+1.10%
$pp \to \gamma\gamma$ (ppaa02)	$5.209(0)^{+10\%}_{-11\%}$ pb	$23.98(1)^{+8.8\%}_{-7.5\%}$ pb	$2.360(1)^{+24\%}_{-18\%}$ pb (17.5%)	$38.04(2)^{+8.7\%}_{-7.2\%}$ pb	$37.50(27)^{+8.5\%}_{-7.0\%}$ pb	+360%	+56.4%

FIGURE 6.6: *MATRIX* provides built in integrated cross sections for various processes, this is a variety of the available values, including those of interest to our calculations [159].

Furthermore, if it is a d_{iB} particle, then declare particle i to be a final jet, and we can now remove it from the list [160].

6.5 Data Acquisition

We are using data from CERN Open Data, and data sets from *HepData* [161], which is intended for photoproduction results that will correspond to future light cone gauge calculations that become mandatory when considering production from highly virtual photons interaction with partons and effecting the outcome of final state observables. The hadronization "*epoch*" consist of mainly pions and kaons, and the pions have a high branching ratio for decay into $\gamma\gamma$. These photons incidentally come into contact with partons x at momentum p. We have to make the simulations as accurate as possible. There is not a scenario where a single generator is able to describe all observed distributions. We have to consider what is referred to as the interface to the parton shower.

For this step, we start from a *MATRIX* and *Pythia* combination and apply the corrections using the jet simulation software generators. We refer to ancillary measurements of Drell-Yan production to validate (and tune) the model and assess systematic uncertainties.

6.6 Conclusion

Resummation serves as a powerful tool for both theory and phenomenological interest that takes place in the perturbative expansion of the strong coupling. Non-perturbative correlations and interactions are modeled both from available data and theoretical predictions in combination with MC simulators at various energy scale and *PDF* choices. The large logarithmic correction and soft gluon resummation has been referred to as a mandatory tool for the era of precision phenomenology. It relies heavily on the factorization theorems as well as evolution equations. Soft-gluon resummation is mainly treated as a soft collinear effective theory, (SCET), to be applied to *QCD* processes. A primary goal in our approach of resummation via radiative corrections is to better understand the all-order structure of the perturbative exponent in the running coupling α_s. Top quark production is not discussed in our work, however it is worth mentioning that large log resummation methods are valuable in regard to top resonance distributions via computational tools. The approach lends unprecedented theoretical precision, and will be saved for future work consideration. A lot of progress is made up to $\mathcal{O}\alpha_s^2$ and NNLL accuracy, however, once beyond three and four loop calculations, many *PDF*'s do not work correctly, and a lot research and data is required to accurately compute the higher order corrections. Moreover, the strong coupling can be precisely determined from the resummed event shapes, and phenomenologically speaking, electroweak annihilation

processes can be known to high logarithmic accuracy as well with more precise knowledge from these corrections when successful. We have presented a proposal to generate our own jet reconstruction outputs using the methods and tools outlined in this chapter, as well as the theoretical background provided in the rest of the thesis along the way. Data sets from CERN open data based on $ATLAS$ at 8 TeV and 13 TeV runs, are stored and ready to be called. ManeParse as a PDF reader in the Mathematica framework serves as a valuable tool for plotting and computing cross-sections. We will plot our calculations against $ATLAS$ and Tevatron runs following our error analysis along with large logarithmic correction and soft gluon resummation analysis. The master equations are ready to be called up for these various logarithmic correction along with the graphing utilities provided both in Root, and the callable *Madgraph* 5 for charting these results once executed. All of this to take place in the Root framework, ManeParse, as well as various parton shower generators running as subroutines for various tasks as inputs.

6.6.1 Existing Results and Future Calculation

The graphs in 6.7, 6.9, 6.10, and 6.8 for W, W $+1$ jet, $W+$ 2 $Jets$, and W, with missing transverse energy distributions, due to the physical limitations of the calorimeter detectors in $ATLAS$, are for the comparisons to our calculations of interest when carried out with the proposed process elucidated in this chapter. The example in figure 6.7 shows predictions for the differential cross sections as a function of the boson transverse momentum for $n-jets$ greater or equal to 0, $(left)$ and $n-jets$ greater or equal to 1, $(right)$ from *Sherpa* 2.2 (red) and $MG5-aMC$ at NLO with *Pythia* using $CKKW-L$ $(blue)$. The orange band includes PDF and scale uncertainties estimated with *Sherpa* 2.2, while the size of the statistical uncertainty components are indicated by the size of the error bars. Figure 6.9 shows predictions for the

differential cross sections as a function of the lepton transverse momentum and the missing transverse energy from *Sherpa* 2.2 (red) and $4MG5 - aMC$ at NLO, plus *Pythia* using $CKKW - L$ $(blue)$. The orange band includes PDF and scale uncertainties estimated with *Sherpa* 2.2, while the size of the statistical uncertainty components are indicated by the size of the error bars. In figure 6.10, we show predictions for the differential cross sections as a function of the leading and sub-leading jet transverse momentum from *Sherpa* 2.2 (red) and $MG5 - aMC$ at NLO plus *Pythia* using $CKKW - L$ $(blue)$. The orange band includes PDF and scale uncertainties estimated with*Sherpa* 2.2, while the size of the statistical uncertainty components are indicated by the size of the error bars. Figure 6.8, is a prediction for the differential cross sections as a function of the leading and sub-leading jet transverse momentum from *Sherpa* 2.2 (red) and $MG5 - aMC$ at NLO plus *Pythia* using $CKKW - L$ $(blue)$. The orange band includes PDF and scale uncertainties estimated with *Sherpa* 2.2, while the size of the statistical uncertainty components are indicated by the size of the error bars. When we analyze this data, we will be using simulations from *Pythia* using *Madgraph* 5, along with our choice of PDF's for fitting, and compare against these runs as well. Approaching towards the above mentioned direction, we expect to find a better fit between experimental data and theoretical calculation. We expect to improve the current results.

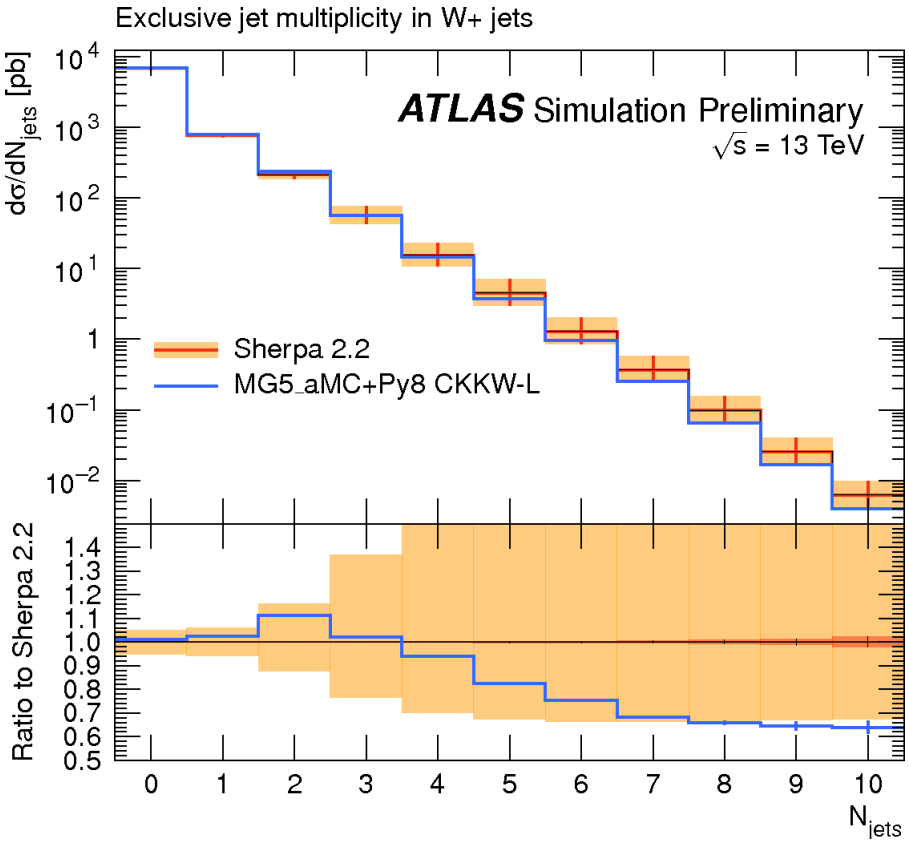

FIGURE 6.7: Predictions for the differential cross sections as a function of the boson transverse momentum. This is plotted using *MG*5 Monte Carlo plus inputs from *Pythia* and plotted against uncertainty results from *Sherpa* 2.2. As the number of jet contributions are considered, we notice a slight divergence in the ratio comparison between the generated uncertainty [162].

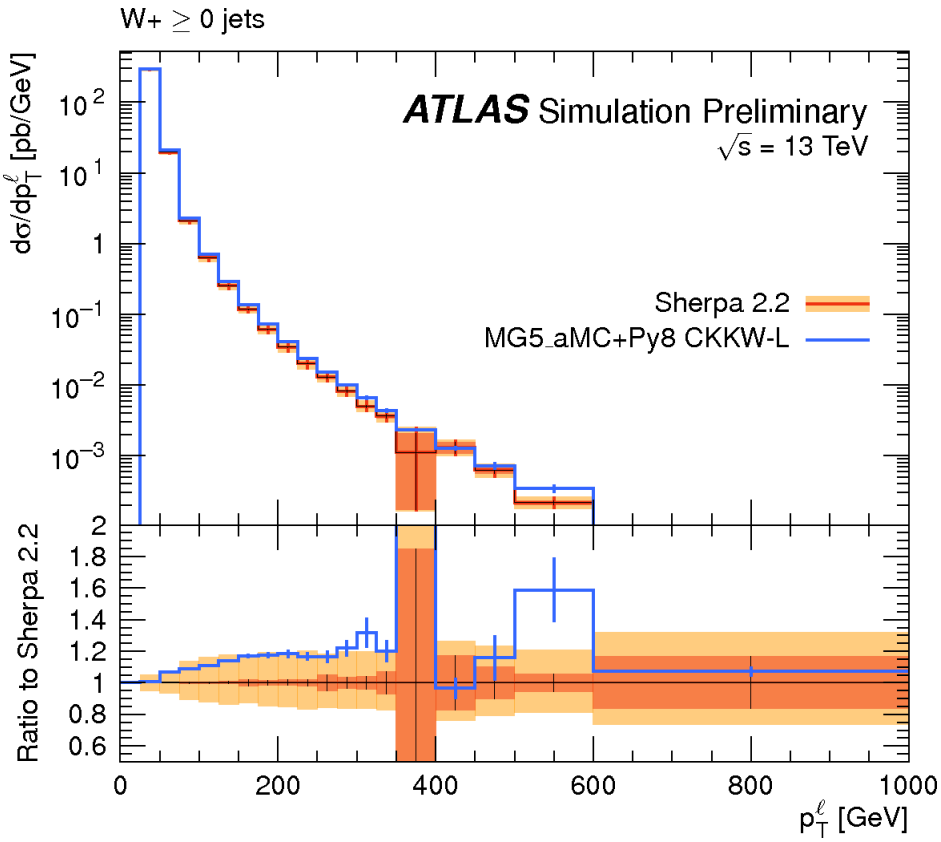

FIGURE 6.8: Differential cross sections as function of boson transverse momentum for the W boson with EW corrections on a growing p_T scale [162].

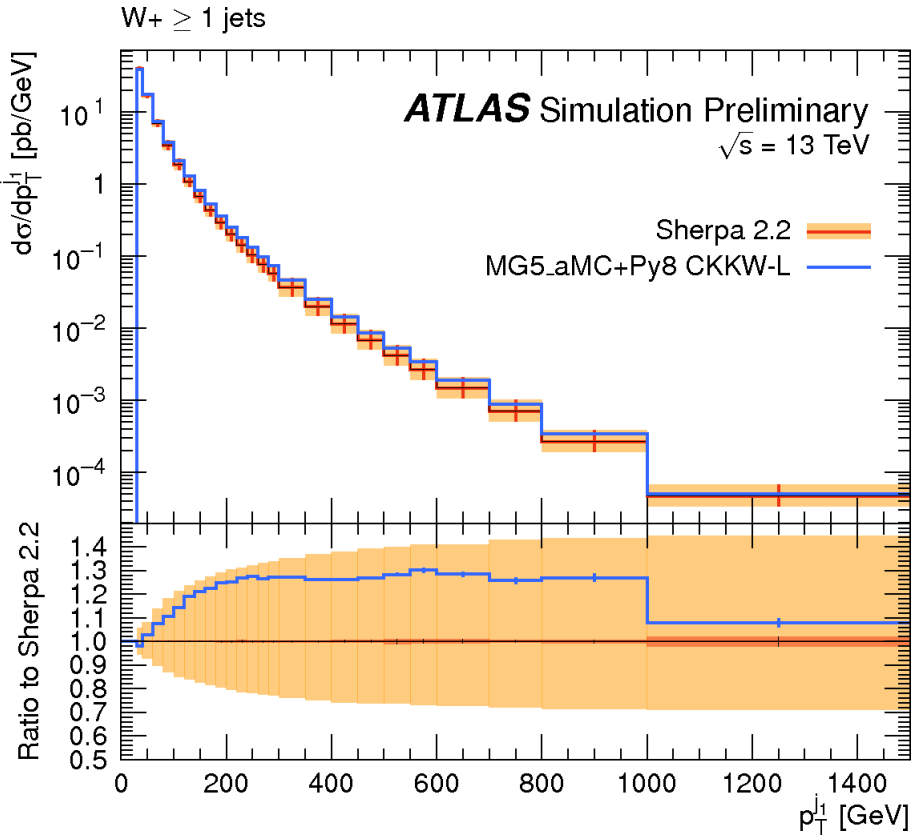

FIGURE 6.9: W^+ production taken into consideration with a minimum of $1 - jet$ correction, we see the contributions at the higher p_T energy scales versus figure 6.7 [162].

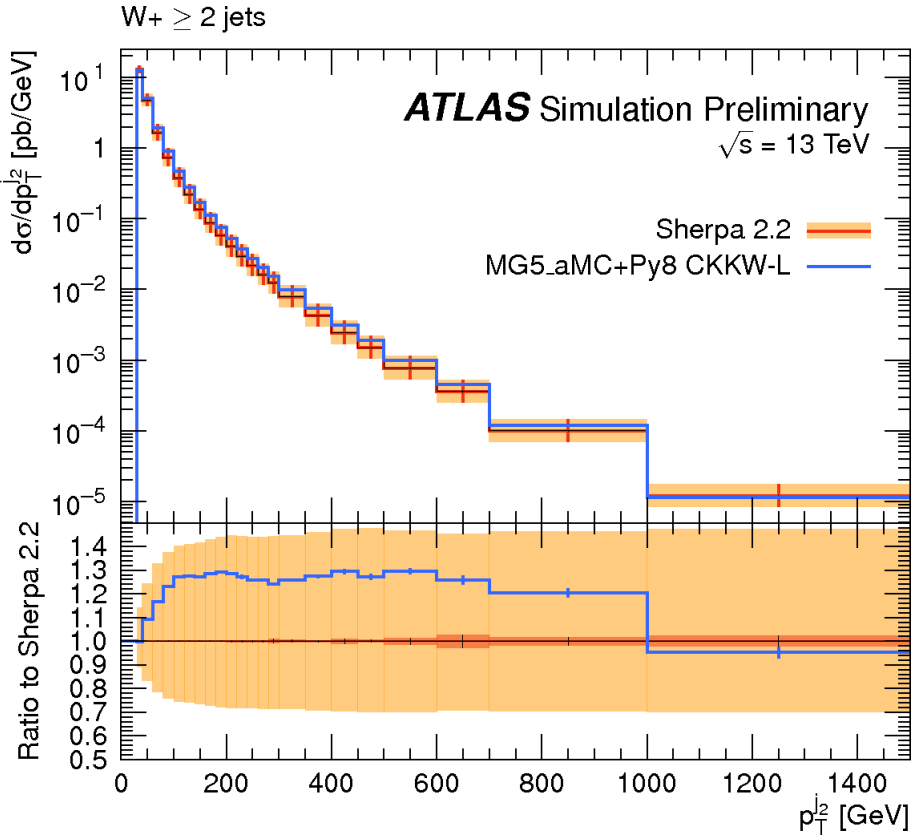

FIGURE 6.10: In this greater than or equal to 2-jet correction case, and with the same W^+ process considered, we continue to notice additional information becoming relevant on the plot at larger p_T considerations in the *Sherpa*, *Madgraph*5 and *Pythia* simulation runs, providing more accurate representations of the actual process between collision and detector readout to final state production
[162].

Bibliography

[1] Yoichiro Nambu. Axial vector current conservation in weak interactions. *Phys. Rev. Lett.*, 4:380–382, Apr 1960.

[2] Y. Nambu and G. Jona-Lasinio. Dynamical model of elementary particles based on an analogy with superconductivity. i. *Phys. Rev.*, 122:345–358, Apr 1961.

[3] Jeffrey Goldstone, Abdus Salam, and Steven Weinberg. Broken symmetries. *Phys. Rev.*, 127:965–970, Aug 1962.

[4] Alexander Khodjamirian. *Hadron Form Factor, From Basic Phenomenology to QCD Sum Rules*. CRC Press - Taylor Francis Group, 2020.

[5] T Binoth, M Ciccolini, N Kauer, and M Krämer. Gluon-induced WW background to higgs boson searches at the LHC. *Journal of High Energy Physics*, 2005(03):065–065, mar 2005.

[6] Richard Keith Ellis, William James Stirling, and Bryan R Webber. *QCD and collider physics*. Cambridge monographs on particle physics, nuclear physics, and cosmology. Cambridge University Press, Cambridge, 2003. Photography by S. Vascotto.

[7] Hey Anothony J.G Aitchison, Ian J.R. *Gauge Theories in Particle Physics*, volume 1-2. Taylor and Francis Group, 2-013.

[8] P.A. Zyla et al. Review of Particle Physics. *PTEP*, 2020(8):083C01, 2020.

[9] Steven Weinberg. *The Quantum Theory of Fields*, volume $I - II$. Cambridge University Press, 1995.

[10] M. Göckeler, R. Horsley, E.-M. Ilgenfritz, H. Oelrich, H. Perlt, P.E.L. Rakow, G. Schierholz, A. Schiller, and P. Stephenson. The drell-yan process and deep inelastic scattering from the lattice. *Nuclear Physics B - Proceedings Supplements*, 53(13):315317, Feb 1997.

[11] Peng Sun and Feng Yuan. Transverse momentum dependent evolution: Matching semi-inclusive deep inelastic scattering processes to drell-yan andw/zboson production. *Physical Review D*, 88(11), Dec 2013.

[12] Jian Liang, Terrence Draper, Keh-Fei Liu, Alexander Rothkopf, and Yi-Bo Yang. Towards the nucleon hadronic tensor from lattice qcd. *Physical Review D*, 101(11), Jun 2020.

[13] John Campbell. *The black book of quantum chromodynamics*, volume 1. Oxford, 2020.

[14] Joey Huston* Stephen Kuhlmann4 Sanjib Mishra5; Jorge G. Morfins Fredrick Olnesss Joseph Owens Jon Pumplin* Jian-Wei Qiug John Smith Davison E. SoperO Wu-Ki Tung* Hendrik Weerts2 James Whitmore3 Chien-Peng Yuan2 George Sterman Editor Raymond Brock*, John C. Collins3. *Handbook of Perturbative QCD*, volume 1. CTEQ Collaboration, 1993., 1993.

[15] Richard J. Gonsalves, Jerzy Pawłowski, and Chung-Fai Wai. Qcd radiative corrections to electroweak-boson production at large transverse momentum in hadron collisions. *Phys. Rev. D*, 40:2245–2268, Oct 1989.

[16] J Smith. Nlo distributions for higgs production at the lhc. *Nuclear Physics B - Proceedings Supplements*, 116:164–167, 2003. Proceedings of the 6th International Symposium on Radiative Corrections and the 6th Zeuthen Workshop on Elementary Particle Theory.

[17] Alessandro Bacchetta. Transverse momentum distributions. 2012.

[18] Jakob Schwichtenberg. *No Nonsense Quantum Field Theory*, volume 1. No nonsense books, 2020.

[19] Herwig Schopper. *Particle Physics Reference Library: Volume 1: Theory and Experiments*. Springer Nature, 2020.

[20] Emmet P. Byrne. Logarithmic corrections for jet production at the lhc, 2021.

[21] Geoffrey C. Fox and Stephen Wolfram. Observables for the analysis of event shapes in e^+e^- annihilation and other processes. *Phys. Rev. Lett.*, 41:1581–1585, Dec 1978.

[22] C. Louis Basham, Lowell S. Brown, Stephen D. Ellis, and Sherwin T. Love. Energy correlations in electron-positron annihilation: Testing quantum chromodynamics. *Phys. Rev. Lett.*, 41:1585–1588, Dec 1978.

[23] C. Louis Basham, Lowell S. Brown, Stephen D. Ellis, and Sherwin T. Love. Energy correlations in electron-positron annihilation in quantum chromodynamics: Asymptotically free perturbation theory. *Phys. Rev. D*, 19:2018–2045, Apr 1979.

[24] Wikipedia contributors. Asymptotic freedom — Wikipedia, the free encyclopedia, 2022. [Online; accessed 12-May-2022].

[25] Wikipedia contributors. Color confinement — Wikipedia, the free encyclopedia, 2022. [Online; accessed 12-May-2022].

[26] John C. Collins, L. Frankfurt, and M. Strikman. Proof of factorization for exclusive deep-inelastic processes. *Low x Physics*, Jun 1998.

[27] G. Peter Lepage and Stanley J. Brodsky. Exclusive processes in perturbative quantum chromodynamics. *Phys. Rev. D*, 22:2157–2198, Nov 1980.

[28] Andreas Schäfer. The chernyak-zhitnitsky wave function and the elastic proton form factor. *Physics Letters B*, 217(4):545–550, 1989.

[29] J.J. Goodson. *Search for Supersymmetry in States with Large Missing Transverse Momentum and Three Leptons including a Z-Boson*. PhD thesis, Stony Brook University, May 2012. Presented 17 Apr 2012.

[30] Thomas Becher, Christian Lorentzen, and Matthew D. Schwartz. Resummation for w and z at large p_T. *Physical Review Letters*, 108(1), jan 2012.

[31] Thomas Becher, Christian Lorentzen, and Matthew D. Schwartz. Precision direct photon and w-boson spectra at high p_T and comparison to lhc data. *Phys. Rev. D*, 86:054026, Sep 2012.

[32] G. 't Hooft and M. Veltman. Regularization and renormalization of gauge fields. *Nuclear Physics B*, 44(1):189–213, July 1972.

[33] Wikipedia contributors. Yangmills theory — Wikipedia, the free encyclopedia, 2022. [Online; accessed 12-May-2022].

[34] C. N. Yang and R. L. Mills. Conservation of isotopic spin and isotopic gauge invariance. *Phys. Rev.*, 96:191–195, Oct 1954.

[35] Anthony Zee. *Quantum field theory in a nutshell*, volume 1. Princeton university press, 2010.

[36] Guilherme Telo R Catumba. Gluon correlation functions from lattice quantum chromodynamics. [arXiv preprint arXiv:2101.06074].

[37] Olesandr Kubelskyi.

[38] Michael Peskin. Collider physics, lecture 4/6.

[39] Unknown lecture. *Higher order corrections to jet observables*. PhD thesis, University of Zurich, 2010.

[40] CERN. Open data portal.

[41] Roger Penrose. *The Road to Reality*, volume 1. First Vintage books, 2004.

[42] Peter Collier. *Beginners guide to differential forms*, volume 1. Incomprehensible books, 2021.

[43] Christian Brouder. The structure of green functions in quantum field theory with a general state. Jul 2007.

[44] John Collins. *Handbook of Perturbative QCD*, volume 1. Cambridge University Press, 2011.

[45] Gionata Luisoni. Chapter ii - the qcd lagrangian, 2010.

[46] Benjamín Grinstein. Introductory lectures on qcd. 2006.

[47] nscl.msu.edu. Qcd, 2016. [Online; accessed 14-April-2022].

[48] Anthony Zee. *Group theory in a nutshell for physicists*, volume 1. Princeton University Press, 2016.

[49] Guilherme Telo R. Catumba. Gluon correlation functions from lattice quantum chromodynamics, 2021.

[50] Roland. Renormalization — CERN, Document Server. http://cftp.ist.utl.pt/~gernot.eichmann/2020-QCDHP/QCD-renormalization.pdf, 2022. [Online; accessed 07-March-2022].

[51] Joseph Polchinski. Renormalization and effective lagrangians. *Nuclear Physics B*, 231(2):269–295, 1984.

[52] Renormalizability UT Lecture Notes and Dimensional Analysis.

[53] John C. Collins. Renormalization: general theory, 2006.

[54] Julian Schwinger. Gauge invariance and mass. ii. *Phys. Rev.*, 128:2425–2429, Dec 1962.

[55] Kimball A. Milton. In appreciation julian schwinger: From nuclear physics and quantum electrodynamics to source theory and beyond. *Physics in Perspective*, 9(1):70–114, jan 2007.

[56] Joseph Polchinski. Scale and conformal invariance in quantum field theory. *Nuclear Physics*, 303:226–236, 1988.

[57] Steven Weinberg. High-energy behavior in quantum field theory. *Phys. Rev.*, 118:838–849, May 1960.

[58] Alexandre Deur, Stanley J. Brodsky, and Guy F. de Téramond. On the interface between perturbative and nonperturbative qcd. *Physics Letters B*, 757:275281, Jun 2016.

[59] Alexandre Deur, Stanley J. Brodsky, and Guy F. de Téramond. The qcd running coupling. *Progress in Particle and Nuclear Physics*, 90:174, Sep 2016.

[60] A. Zichichi. Murray gell-mann and the last frontier of lhc physics: The qgcw project. *International Journal of Modern Physics A - IJMPA*, 25:2619–2630, 05 2010.

[61] Oluseyi Latunde-Dada. ttherwig /ttmonte carlo at next-to-leading order for i e /i sup /sup i e /i sup-/sup annihilation and lepton pair production. *Journal of High Energy Physics*, 2007(11):040–040, nov 2007.

[62] Stanley Brodsky. Qcd on the light cone. Sep 1992.

[63] Patricia Ball and V. M. Braun. Handbook of higher twist distribution amplitudes of vector mesons in qcd, 1998.

[64] Hungchong Kim, Su Houng Lee, and Makoto Oka. Two-point correlation function with a pion in QCD sum rules. *Physical Review D*, 60(3), jun 1999.

[65] V. M. Braun, S. Collins, M. Göckeler, P. Pérez-Rubio, A. Schäfer, R. W. Schiel, and A. Sternbeck. Pion distribution amplitude from lattice qcd, 2015.

[66] S Brodsky. Quantum chromodynamics and other field theories on the light cone. *Physics Reports*, 301(4-6):299486, Aug 1998.

[67] Anatoly Radyushkin. Photon-pion transition form factor and pion distribution amplitude. In *APS Meeting Abstracts*, volume 3 of *APS Meeting Abstracts*, page CF.001, October 2009.

[68] Xiangdong Ji, Jian-Ping Ma, and Feng Yuan. Generalized counting rule for hard exclusive processes. *Physical Review Letters*, 90(24), Jun 2003.

[69] N. G. Stefanis. The physics of exclusive reactions in qcd: Theory and phenomenology, 1999.

[70] Gunnar S. Bali, Vladimir M. Braun, Meinulf Göckeler, Michael Gruber, Fabian Hutzler, Piotr Korcyl, Andreas Schäfer, and Philipp Wein. Pion and kaon distribution amplitudes from lattice qcd: towards the continuum limit, 2018.

[71] V. M. Braun, M. Göckeler, R. Horsley, H. Perlt, D. Pleiter, P. E. L. Rakow, G. Schierholz, A. Schiller, W. Schroers, H. Stüben, and et al. Moments of pseudoscalar meson distribution amplitudes from the lattice. *Physical Review D*, 74(7), Oct 2006.

[72] Cé sar Ayala, S. V. Mikhailov, and N. G. Stefanis. Calculation of the pion-photon transition form factor using dispersion relations and renormalization-group summation. *Physical Review D*, 98(9), nov 2018.

[73] A. P. Bakulev, S. V. Mikhailov, A. V. Pimikov, and N. G. Stefanis. Comparing antithetic trends of data for the pion-photon transition form factor. *Physical Review D*, 86(3), Aug 2012.

[74] Alexander P. Bakulev. Pion distribution amplitude – from theory to data (cello, cleo, e-791, jlab f(pi)), 2004.

[75] A. V. Radyushkin and R. Ruskov. The asymptotics of the transition form factor $\gamma\gamma^*$ -> π^0 and qcd sum rules, 1997.

[76] Alexander P. Bakulev. Pion distribution amplitude – from theory to data (cello, cleo, e-791, jlab f(pi)), 2004.

[77] A. Khodjamirian. Form factors of $\gamma^*\ \rho \to \pi$ and $\gamma^*\ \gamma \to \pi^0$ transitions and light cone sum rules. *The European Physical Journal C*, 6(3):477484, Jan 1999.

[78] H. Shiomi. Second class current in *QCD* Sum Rules. *Nuclear Physics A*, 603(3):281–302, 1996. [https://doi.org/10.1016/0375-9474(96)80003-A].

[79] Sergey Alekhin, Simone Alioli, Richard D. Ball, Valerio Bertone, Johannes Blumlein, Michiel Botje, Jon Butterworth, Francesco Cerutti, Amanda Cooper-Sarkar, Albert de Roeck, Luigi Del Debbio, Joel Feltesse, Stefano Forte, Alexander Glazov, Alberto Guffanti, Claire Gwenlan, Joey Huston, Pedro Jimenez-Delgado, Hung-Liang Lai, Jose I. Latorre, Ronan McNulty, Pavel Nadolsky, Sven-Olaf Moch, Jon Pumplin, Voica Radescu, Juan Rojo, Torbjorn Sjostrand, W. J. Stirling, Daniel Stump, Robert S. Thorne, Maria Ubiali, Alessandro Vicini,

Graeme Watt, and C. P. Yuan. The pdf4lhc working group interim report, 2011.

[80] Alejandro Garcia and Ernest M Henley. *Subatomic Physics*. World Scientific Publishing Company, 2007.

[81] Huey-Wen Lin, Emanuele R. Nocera, Fred Olness, Kostas Orginos, Juan Rojo, Alberto Accardi, Constantia Alexandrou, Alessandro Bacchetta, Giuseppe Bozzi, Jiunn-Wei Chen, and et al. Parton distributions and lattice qcd calculations: A community white paper. *Progress in Particle and Nuclear Physics*, 100:107160, May 2018.

[82] A. V. NESTERENKO and I. L. SOLOVTSOV. New analytic running coupling in qcd: Higher loop levels. *Modern Physics Letters A*, 16(39):25172528, Dec 2001.

[83] D. V. Shirkov and I. L. Solovtsov. Analytic model for the qcd running coupling with universal $\overline{\alpha}_s(0)$ value. *Phys. Rev. Lett.*, 79:1209–1212, Aug 1997.

[84] Shan Cheng, Alexander Khodjamirian, and Aleksey V. Rusov. Pion light-cone distribution amplitude from the pion electromagnetic form factor. *Phys. Rev. D*, 102:074022, Oct 2020.

[85] Enrique Ruiz Arriola and Wojciech Broniowski. Pion transition form factor and distribution amplitudes in large-ncregge models. *Physical Review D*, 74(3), Aug 2006.

[86] N. Nasrallah. Form factor of the transition $\gamma\gamma^* \to \pi^0$. 04 2000.

[87] Hungchong Kim, Su Houng Lee, and Makoto Oka. Two-point correlation function with a pion in qcd sum rules. *Physical Review D*, 60(3), Jun 1999.

[88] Th. Feldmann. Phenomenology of and transition form factors at large momentum transfer. *Nuclear Physics B - Proceedings Supplements*, 82:331–336, 2000. Proceedings of the International Conference on the Structure and Interactions of the Photon, including the 12th International Workshop on Photon-Photon Collisions.

[89] D.B. Clark, E. Godat, and F.I. Olness. ManeParse : A mathematica reader for parton distribution functions. *Computer Physics Communications*, 216:126–137, jul 2017.

[90] A. Kulesza, G. Sterman, and W. Vogelsang. Phenomenological studies in qcd resummation. *Nuclear Physics A*, 721:C591–C596, 2003.

[91] On low energy tests of qcd. *Physics Letters B*, 94(1):51–53, 1980.

[92] R. Odorico. Exclusive calculations for qcd jets in a monte carlo approach. *Nuclear Physics B*, 172:157–200, 1980.

[93] John C. Collins, Davison E. Soper, and George Sterman. Does the drell-yan cross section factorize? *Physics Letters B*, 109(5):388–392, 1982.

[94] M. Gluck, E. Reya, and A. Vogt. Pionic parton distributions. *Z. Phys. C*, 53:651–656, 1992.

[95] M. Glück, E. Reya, and I. Schienbein. Pionic parton distributions revisited. *The European Physical Journal C*, 10(2):313317, Sep 1999.

[96] M. Glück, E. Reya, and M. Stratmann. Mesonic parton densities derived from constituent quark model constraints. *The European Physical Journal C*, 2(1):159163, Mar 1998.

[97] J. F. Owens. Q^2-dependent parametrizations of pion parton distribution functions. *Phys. Rev. D*, 30:943–946, Sep 1984.

[98] P. J. Sutton, A. D. Martin, R. G. Roberts, and W. J. Stirling. Parton distributions for the pion extracted from drell-yan and prompt photon experiments. *Phys. Rev. D*, 45:2349–2359, Apr 1992.

[99] John C. Collins, Davison E. Soper, and George Sterman. Factorization of hard processes in qcd, 2004.

[100] Ian Cloët. Hadron phenomenology and qcds dses, pdfs, July 2012.

[101] Minghui Ding, Khé pani Raya, Daniele Binosi, Lei Chang, Craig D. Roberts, and Sebastian M. Schmidt. Symmetry, symmetry breaking, and pion parton distributions. *Physical Review D*, 101(5), mar 2020.

[102] Guido Altarelli and G. Parisi. Asymptotic Freedom in Parton Language. *Nucl. Phys. B*, 126:298–318, 1977.

[103] Yuri L. Dokshitzer. Calculation of the Structure Functions for Deep Inelastic Scattering and e+ e- Annihilation by Perturbation Theory in Quantum Chromodynamics. *Sov. Phys. JETP*, 46:641–653, 1977.

[104] V. N. Gribov and L. N. Lipatov. Deep inelastic e p scattering in perturbation theory. *Sov. J. Nucl. Phys.*, 15:438–450, 1972.

[105] Eric Godat. Maneparse: Mathematica toolbox for pdf uncertainties and application to new physics searches, 2015.

[106] Michael H. Seymour. Jets in qcd. *AIP Conference Proceedings*, 1996.

[107] Raghav Kunnawalkam Elayavalli and Korinna Christine Zapp. Simulating v+jet processes in heavy ion collisions with jewel. *The European Physical Journal C*, 76(12), Dec 2016.

[108] Redamy Pérez-Ramos and David d'Enterria. a_s from soft qcd jet fragmentation functions. page 005, 07 2019.

[109] S. Mikhailov and Anatoly Radyushkin. Nonlocal condensates and qcd sum rules for the pion wave function. *Physical review D: Particles and fields*, 45:1754–1759, 04 1992.

[110] H. Fritzsch and M. Gell-Mann. *50 Years of Quarks*. Number v. 1 in International journal of modern physics / A. World Scientific, 2015.

[111] C. A. DOMINGUEZ. Introduction to qcd sum rules. *Modern Physics Letters A*, 28(24):1360002, Aug 2013.

[112] L.J Reinders, H Rubinstein, and S Yazaki. Hadron properties from qcd sum rules. *Physics Reports*, 127(1):1–97, 1985.

[113] Michael C. Birse and Boris Krippa. Determination of pion-baryon coupling constants from qcd sum rules. *Phys. Rev. C*, 54:3240–3246, Dec 1996.

[114] Hungchong Kim, Su Houng Lee, and Makoto Oka. Two-point correlation function with a pion in qcd sum rules. *Physical Review D*, 60(3), Jun 1999.

[115] Xuemin Jin and Jian Tang. Chirality and reliability of baryon qcd sum rules. *Phys. Rev. D*, 56:515–518, Jul 1997.

[116] B.I. Ioffe and A.V. Smilga. Hyperon magnetic moments in qcd. *Physics Letters B*, 133(6):436–440, 1983.

[117] Hungchong Kim. About qcd sum rules for pion-nucleon coupling, 1999.

[118] Mikhail Shifman. Snapshots of hadrons. *Progress of Theoretical Physics Supplement*, 131:171, 1998.

[119] Stanley J. Brodsky. The light-cone fock representation in QCD. *Nuclear Physics B - Proceedings Supplements*, 90:3–13, dec 2000.

[120] Jian-Hui Zhang, Jiunn-Wei Chen, Xiangdong Ji, Luchang Jin, and Huey-Wen Lin. Pion distribution amplitude from lattice QCD. *Physical Review D*, 95(9), may 2017.

[121] Esma Mobs. The CERN accelerator complex - August 2018. Complexe des accélérateurs du CERN - Août 2018. Aug 2018. General Photo.

[122] Raghav Kunnawalkam Elayavalli. Jetting through the primordial universe. 2017.

[123] CERN. ATLAS Fact Sheet — Wikipedia, the free encyclopedia. 2022. [Online; accessed 05-April-2022].

[124] Ana Elena Dumitriu. *Study of the Higgs production in association with tt quarks*. Theses, University of Bucharest ; Aix Marseille University, September 2018.

[125] Atlas: Detector physics and physical design report.

[126] Roland. CERN Document Server — CERN, Document Server. https://cds.cern.ch/record/2645860/plots, 2022. [Online; accessed 04-April-2022].

[127] David Griffiths. *Introduction to Elementary Particles:*, volume 1. Wiley, 1987.

[128] Sidney D. Drell and Tung-Mow Yan. Massive lepton-pair production in hadron-hadron collisions at high energies. *Phys. Rev. Lett.*, 25:316–320, Aug 1970.

[129] R. Maciua, A. Szczurek, and G. lipek. Kinematical correlations of dielectrons from semileptonic decays of heavy mesons and drell-yan processes at bnl rhic. *Phys. Rev. D*, 83, 03 2011.

[130] Michael E. Peskin. Simplifying multi-jet qcd computation, 2011.

[131] R. Kleiss and W.J. Stirling. Cross sections for the production of an arbitrary number of photons in electron-positron annihilation. *Physics Letters B*, 179(1):159–163, 1986.

[132] Tommaso Dorigo. W and z cross sections at the tevatron, 2003.

[133] I. Bizjak. W boson mass measurement at the tevatron, 2008.

[134] Seyed Yaser Ayazi, Sara Khatibi, and Mojtaba Mohammadi Najafabadi. Top quark forward-backward asymmetry and w'-boson with general couplings. 2012.

[135] Stefano Catani and Massimiliano Grazzini. Collinear factorization and splitting functions for next-to-next-to-leading order qcd calculations. *Physics Letters B*, 446(2):143152, Jan 1999.

[136] The Tevatron Electroweak Working Group. Combination of cdf and d0 results on the w-boson width, 2005.

[137] Tommaso Dorigo. W and z cross sections at the tevatron, 2003.

[138] Andy Buckley, Jonathan Butterworth, Stefan Gieseke, David Grellscheid, Stefan Höche, Hendrik Hoeth, Frank Krauss, Leif Lönnblad, Emily Nurse, Peter Richardson, Steffen Schumann, Michael H. Seymour, Torbjörn Sjöstrand, Peter Skands, and Bryan Webber. General-purpose event generators for lhc physics. *Physics Reports*, 504(5):145233, Jul 2011.

[139] Torbjörn Sjöstrand, Stefan Ask, Jesper R. Christiansen, Richard Corke, Nishita Desai, Philip Ilten, Stephen Mrenna, Stefan Prestel, Christine O. Rasmussen, and Peter Z. Skands. An introduction to PYTHIA 8.2. *Computer Physics Communications*, 191:159–177, jun 2015.

[140] Massimiliano Grazzini, Stefan Kallweit, and Marius Wiesemann. Fully differential NNLO computations with MATRIX. *The European Physical Journal C*, 78(7), jun 2018.

[141] Andy Buckley, James Ferrando, Stephen Lloyd, Karl Nordström, Ben Page, Martin Rüfenacht, Marek Schönherr, and Graeme Watt. LHAPDF6: parton density access in the LHC precision era. *The European Physical Journal C*, 75(3), mar 2015.

[142] Wolfram Research, Inc. Mathematica, Version 13.0.0. Champaign, IL, 2021.

[143] J. Alwall, R. Frederix, S. Frixione, V. Hirschi, F. Maltoni, O. Mattelaer, H.-S. Shao, T. Stelzer, P. Torrielli, and M. Zaro. The automated computation of tree-level and next-to-leading order differential cross sections, and their matching to parton shower simulations. *Journal of High Energy Physics*, 2014(7), jul 2014.

[144] Federico Buccioni, Jean-Nicolas Lang, Stefano Pozzorini, Hantian Zhang, and Max Zoller. On-the-fly reduction of open loops, 07 2018.

[145] Hung-Liang Lai, Marco Guzzi, Joey Huston, Zhao Li, Pavel M. Nadolsky, Jon Pumplin, and C.-P. Yuan. New parton distributions for collider physics. *Physical Review D*, 82(7), oct 2010.

[146] Pavel M. Nadolsky, Hung-Liang Lai, Qing-Hong Cao, Joey Huston, Jon Pumplin, Daniel Stump, Wu-Ki Tung, and C.-P. Yuan. Implications of CTEQ global analysis for collider observables. *Physical Review D*, 78(1), jul 2008.

[147] Richard D. Ball, , Valerio Bertone, Stefano Carrazza, Christopher S. Deans, Luigi Del Debbio, Stefano Forte, Alberto Guffanti, Nathan P.

Hartland, José I. Latorre, Juan Rojo, and Maria Ubiali. Parton distributions for the LHC run II. *Journal of High Energy Physics*, 2015(4), apr 2015.

[148] Federico Buccioni, Jean-Nicolas Lang, Stefano Pozzorini, Hantian Zhang, and Max Zoller. On-the-fly reduction of open loops, 07 2018.

[149] Prerit Jaiswal, Patrick Meade, and Harikrishnan Ramani. Precision diboson measurements and the interplay of and jet-veto resummations. *Physical Review D*, 93(9), may 2016.

[150] H. Mkrtchyan, P.E. Bosted, G.S. Adams, A. Ahmidouch, T. Angelescu, J. Arrington, R. Asaturyan, O.K. Baker, N. Benmouna, C. Bertoncini, H.P. Blok, W.U. Boeglin, H. Breuer, M.E. Christy, S.H. Connell, Y. Cui, M.M. Dalton, S. Danagoulian, D. Day, T. Dodario, J.A. Dunne, D. Dutta, N. El Khayari, R. Ent, H.C. Fenker, V.V. Frolov, L. Gan, D. Gaskell, K. Hafidi, W. Hinton, R.J. Holt, T. Horn, G.M. Huber, E. Hungerford, X. Jiang, M. Jones, K. Joo, N. Kalantarians, J.J. Kelly, C.E. Keppel, V. Kubarovsky, Y. Li, Y. Liang, S. Malace, P. Markowitz, E. McGrath, P. McKee, D.G. Meekins, B. Moziak, T. Navasardyan, G. Niculescu, I. Niculescu, A.K. Opper, T. Ostapenko, P.E. Reimer, J. Reinhold, J. Roche, S.E. Rock, E. Schulte, E. Segbefia, C. Smith, G.R. Smith, P. Stoler, V. Tadevosyan, L. Tang, M. Ungaro, A. Uzzle, S. Vidakovic, A. Villano, W.F. Vulcan, M. Wang, G. Warren, F. Wesselmann, B. Wojtsekhowski, S.A. Wood, C. Xu, L. Yuan, X. Zheng, and H. Zhu. Transverse momentum dependence of semi-inclusive pion production. *Physics Letters B*, 665(1):20–25, jul 2008.

[151] Moh'd Hussein, Joshua Isaacson, and Joey Huston. A study of the role of the PDF uncertainty on the LHC *w*-boson mass measurement. *Journal of Physics G: Nuclear and Particle Physics*, 46(9):095002, aug 2019.

[152] A. Accardi, L. T. Brady, W. Melnitchouk, J. F. Owens, and N. Sato. Constraints on large parton distributions from new weak boson production and deep-inelastic scattering data. *Physical Review D*, 93(11), jun 2016.

[153] Jun Gao, Marco Guzzi, Joey Huston, Hung-Liang Lai, Zhao Li, Pavel Nadolsky, Jon Pumplin, Daniel Stump, and C.-P. Yuan. CT10 next-to-next-to-leading order global analysis of QCD. *Physical Review D*, 89(3), feb 2014.

[154] Sayipjamal Dulat, Tie-Jiun Hou, Jun Gao, Marco Guzzi, Joey Huston, Pavel Nadolsky, Jon Pumplin, Carl Schmidt, Daniel Stump, and C. P. Yuan. New parton distribution functions from a global analysis of quantum chromodynamics. *Phys. Rev. D*, 93(3):033006, 2016.

[155] Juan Rojo and Alessandro Vicini. Pdf uncertainties in the extraction of the w mass at lhc: a snowmass whitepaper, 2013.

[156] Sergey Alekhin, Simone Alioli, Richard D. Ball, Valerio Bertone, Johannes Blumlein, Michiel Botje, Jon Butterworth, Francesco Cerutti, Amanda Cooper-Sarkar, Albert de Roeck, Luigi Del Debbio, Joel Feltesse, Stefano Forte, Alexander Glazov, Alberto Guffanti, Claire Gwenlan, Joey Huston, Pedro Jimenez-Delgado, Hung-Liang Lai, Jose I. Latorre, Ronan McNulty, Pavel Nadolsky, Sven Olaf Moch, Jon Pumplin, Voica Radescu, Juan Rojo, Torbjorn Sjostrand, W.J. Stirling, Daniel Stump, Robert S. Thorne, Maria Ubiali, Alessandro Vicini, Graeme Watt, and C.-P. Yuan. The PDF4LHC Working Group Interim Report. Technical report, Jan 2011. Comments: 35 pages.

[157] Rene Brun, Fons Rademakers, Philippe Canal, Axel Naumann, Olivier Couet, Lorenzo Moneta, Vassil Vassilev, Sergey Linev, Danilo Piparo,

Gerardo GANIS, Bertrand Bellenot, Enrico Guiraud, Guilherme Amadio, wverkerke, Pere Mato, TimurP, Matev Tadel, wlav, Enric Tejedor, Jakob Blomer, Andrei Gheata, Stephan Hageboeck, Stefan Roiser, marsupial, Stefan Wunsch, Oksana Shadura, Anirudha Bose, CristinaCristescu, Xavier Valls, and Raphael Isemann. root-project/root: v6.18/02, August 2019.

[158] T. Sjostrand. Class tpythia8: Public tgenerator.

[159] M. Grazzini, S. Kallweit, J.M. Lindert, S. Pozzorini, and M. Wiesemann. NNLO QCD NLO EW with matrixOpenLoops: precise predictions for vector-boson pair production. *Journal of High Energy Physics*, 2020(2), feb 2020.

[160] Gavin P. Salam Matteo Cacciari and Gregory Soyez. Fastjet user manual.

[161] Eamonn Maguire, Lukas Heinrich, and Graeme Watt. HEPData: a repository for high energy physics data. *Journal of Physics: Conference Series*, 898:102006, oct 2017.

[162] ATLAS simulation of boson plus jets processes in Run 2. Technical report, CERN, Geneva, May 2017. All figures including auxiliary figures are available at https://atlas.web.cern.ch/Atlas/GROUPS/PHYSICS/PUBNOTES/ATL-PHYS-PUB-2017-006.

[163] Jan Pieczkowski. Compton scattering sum rules for massive vector bosons. 10 2009.

Appendix A

Appendices

A.1 Mandelstam Variables

s, u, and t are related to three different reaction channels. s represents the invariant mass related to initial and final particles, t is the momentum transfer, and u is the crossed momentum transfer.

These variables describe scattering kinematics in an invariant way due to the development of these invariant variables, for Compton scattering we define them by

$$\begin{aligned} s &= (p+q)^2 = (p^{'}+q^{'})^2, \\ t &= (p-p^{'})^2 = (q-q^{'})^2, \\ u &= (p-q^{'}) = (q-p^{'})^2. \end{aligned} \tag{A.1}$$

A general paramaterization of the 4-momenta is

$$\begin{aligned} p &= (E,p), \\ p^{'} &= (E^{'},p^{'}), \\ q &= (\omega,q), \\ q^{'} &= (\omega^{'},q^{'}), \end{aligned} \tag{A.2}$$

where $E^{'}$ and $\omega^{'}$ are the initial-(final) state target particle and photon energies in a given frame. In all frames, the energy-momentum conservation is

$$p^{\mu}+q^{\mu} = p^{'\mu}+q^{'\mu}. \tag{A.3}$$

Due to on shell condition for external particles, the Mandelstam variables are constrained by the relation

$$s + t + u = \sum_i m_i^2 = 2M^2 \tag{A.4}$$

[163]

A.2 Light-cone decomposition

Showing the transition to light-cone variables, we begin by defining two momenta P^+ and P^- in hadronic collisions, this is given by the incoming beams. We work with z-axis orientation and assume symmetric collisions [13]

$$P_\pm = (E, 0, 0, \pm E), \tag{A.5}$$

we are neglecting the projectiles mass. Total hadronic centre-of-mass energy squared can now be expressed as

$$S = 2P_+P_-. \tag{A.6}$$

Then any momentum p^μ can be decomposed as

$$p^\mu = \alpha P_+^\mu + \beta P_+^\mu + \overrightarrow{p}_\perp^{\,\mu}, \tag{A.7}$$

where α and β are the plus and minus components of the momentum. The rapidity of p is given by

$$y = \frac{1}{2} log \frac{E + p_z}{E - p_z} = \frac{1}{2} log \frac{p_+}{p^-} = \frac{1}{2} log \frac{\alpha}{\beta}. \tag{A.8}$$

In addition,

$$p^2 = \alpha\beta S - p_\perp^2, \tag{A.9}$$

together with $p^2 = m^2$ allows α or β to be eliminated through

$$\alpha = \frac{m^2 + p_\perp^2}{\beta S} = \frac{m^2 + p_\perp^2}{S} e^{+y} \quad \text{or} \quad \beta = \beta = \frac{m^2 + p_\perp^2}{\alpha S} = \frac{m^2 + p_\perp^2}{S} e^{-y} \tag{A.10}$$

In a scattering process $p_1 + p_2 \rightarrow p_3 + ... + p_n$, four-momenta conservation then translates into

$$\begin{aligned} \alpha_1 + \alpha_2 = \alpha_1 &= \sum_{i=3}^{n} \alpha_i \\ \beta_1 + \beta_2 = \beta_2 &= \sum_{i=3}^{n} \beta_i \\ \overrightarrow{p}_{\perp,1} + \overrightarrow{p}_{\perp,2} = 0 &= \sum_{i=3}^{n} \overrightarrow{p}_{\perp,i}, \end{aligned} \tag{A.11}$$

where it has been assumed the two incident partons $p_{q,2}$ move along the positive and negative z axis, this implies they have zero transverse momentum and that $\alpha_2 = \beta_1 = 0$. This allows the identification of α_1 and β_2 as the light-cone momentum fractions the partons carry with respect to the incoming hadrons. We can identify these with $Bjorken - x$,

$$x_1 \equiv \alpha_1 \text{and} x_2 \equiv \beta_2. \tag{A.12}$$

A.3 Gell-Mann Matrices

$$t^A = \frac{1}{2}\lambda^A \tag{A.13}$$

The normalization over two was done by Gell-Mann as it incorporates the Pauli matrices within the 3x3 Gell-Mann matrices [6],

$$\lambda^1 = \begin{pmatrix} 0 & 1 & 0 \\ 1 & 0 & 0 \\ 0 & 0 & 0 \end{pmatrix} \lambda^2 = \begin{pmatrix} 0 & -i & 0 \\ i & 0 & 0 \\ 0 & 0 & 0 \end{pmatrix} \lambda^3 = \begin{pmatrix} 1 & 0 & 0 \\ 0 & -1 & 0 \\ 0 & 0 & 0 \end{pmatrix}$$

$$\lambda^4 = \begin{pmatrix} 0 & 1 & 1 \\ 0 & 0 & 0 \\ 1 & 0 & 0 \end{pmatrix} \lambda^5 = \begin{pmatrix} 0 & 0 & -i \\ 0 & 0 & 0 \\ i & 0 & 0 \end{pmatrix} \lambda^6 = \begin{pmatrix} 0 & 0 & 0 \\ 0 & 0 & 1 \\ 0 & 1 & 0 \end{pmatrix} \tag{A.14}$$

$$\lambda^7 = \begin{pmatrix} 0 & 0 & 0 \\ 0 & 0 & -i \\ 0 & i & 0 \end{pmatrix} \lambda^8 = \frac{1}{\sqrt{3}} \begin{pmatrix} 1 & 0 & 0 \\ 0 & 1 & 0 \\ 0 & 0 & -2 \end{pmatrix}$$